

Regulation of the Nicotinic Acetylcholine Receptor ACR-16 in *C. elegans*

BY

ASHLEY ANNE MARTIN
B.S., University of Illinois at Chicago, 2008

THESIS

Submitted as partial fulfillment of the requirements
for the degree of Doctor of Philosophy in Biological Sciences
in the Graduate College of the
University of Illinois at Chicago, 2016

Chicago, Illinois

Defense Committee:

John Leonard, Chair
Janet Richmond, Advisor
Liang-Wei Gong
Simon Alford, Anatomy and Cell Biology
Hongkyun Kim, The Chicago Medical School

ACKNOWLEDGMENTS

I would like to thank my advisor, Dr. Janet Richmond, for her guidance, knowledge, and time. This work was possible because of her vision and her help has molded me into an independent scientist. I am very proud to be a member of her scientific family tree. I would also like to thank the members of my committee: Dr. John Leonard, Dr. Simon Alford, Dr. Liang-Wei Gong, and Dr. Hongkyun Kim. Their questions, critiques, and conversations were invaluable in making my thesis project – and myself – stronger in both scientific merit and experimental creativity. A thank you also goes to Dr. Dave Featherstone, whose off the wall conversations and ideas, as well as persistent questioning, has helped me to become confident in my work and my understanding of material.

A multitude of thanks goes to all the past and present members of both the Richmond and Featherstone labs. All of the conversations I've had with them, scientifically driven and other, has enriched my time in graduate school. A special thanks goes to Dr. Julie Minbiole who helped me feel welcomed and valued when I first joined the lab and continues to do so, Dr. Susan Klosterman who navigated the sometimes rough waters of graduate school with me, Sarah Zinn for her unwavering support, both scientifically and emotionally, and friendship, and Dina Beeler for understanding and appreciating an icy exterior, and pushing past it to become a valued friend and colleague. I am honored to know them all and my time at UIC was made better by their presence.

Thank you to my parents, Terrence and Cheryl, for teaching me from the start that with hard work I could be whoever I wanted and achieve whatever I set out to do. It was with their endless love, support, and encouragement, along with the dedicated support and love of my sister Alyssa and other family and friends, that I was able to achieve this goal. I feel extremely lucky to have them behind me and am beyond grateful for all they have done to help me succeed.

Finally I would like to thank my partner in science, my partner in crime, and my partner in life, Andy. It has been said that living with me is like standing in the eye of the storm and I am forever grateful that he has chosen to stand in the middle. I am calmer, stronger, and quantifiably better at math because of him. He is my anchor and I know that I will be able to continue to achieve great success with him by my side – and I look forward to pursuing our next great adventure together.

-AAM

TABLE OF CONTENTS

| | |
|--|-----------|
| I. INTRODUCTION..... | 1 |
| I.a. nAChRs structure and function in vertebrates..... | 1 |
| I.b. Role of nAChRs in disease..... | 4 |
| I.c. Clustering mechanism of nAChRs in vertebrates..... | 6 |
| I.d. <i>Caenorhabditis elegans</i> as a model system..... | 12 |
| I.e. nAChRs structure and function in <i>C. elegans</i> | 13 |
| I.f. ACh receptor assembly, trafficking, and membrane targeting in <i>C. elegans</i> | 17 |
| I.g. LACHR clustering in <i>C. elegans</i> | 27 |
| II. Screen to identify NACHR regulators and characterization of candidates... 33 | 33 |
| II.a. Introduction..... | 33 |
| II.b. Materials and Methods..... | 34 |
| II.c. Results..... | 39 |
| II.c.1 Forward mutagenesis screen using jaSi4 [pmyo-3::acr-16::GFP]..... | 39 |
| II.c.2 Quantification of ACR-16::GFP fluorescence levels in candidate <i>EMS</i> mutations..... | 41 |
| II.c.3 Behavioral analysis of <i>EMS</i> mutations..... | 44 |
| II.c.4 Evaluations of LACHR levels and localization in <i>EMS</i> mutants..... | 46 |
| II.c.5 Electrophysiological analysis of <i>EMS</i> mutants..... | 48 |
| II.c.6 Whole genome sequencing to determine the identity of <i>EMS</i> mutants. | 52 |
| II.c.7 Quantification of ACR-16::GFP fluorescence intensity in candidate gene mutant backgrounds..... | 54 |

TABLE OF CONTENTS (continued)

II.c.8 Confirmation of candidate gene identity.....59

II.d Discussion.....62

III. The *C. elegans* sarcoplasmic reticulum calcium-ATPase regulates nicotinic acetylcholine receptor ACR-16 expression.....63

III.a Introduction.....63

III.b Materials and Methods.....64

III.c Results.....71

III.c.1 SCA-1 is a SERCA present in *C. elegans*.....71

III.c.2 *sca-1* causes a reduction in ACR-16 levels.....74

III.c.3 Localization and levels of the two other *C. elegans* NMJ receptor types are unchanged in *sca-1* mutants.....77

III.c.4 Behavioral analysis of *sca-1* mutants.....79

III.c.5 Synapse abundance and muscle integrity appear unaltered in *sca-1* mutants.....81

III.c.6 A mutation in *sca-1* does not affect levels of *acr-16* mRNA.....83

III.c.7 *sca-1* mutants have a significant reduction in evoked response amplitude.....85

III.c.8 Expression of *Pmyo-3::SCA-1::mCherry* in *sca-1* mutants rescues ACR-16::GFP reduction.....89

III.d Discussion and Future Directions.....92

IV. *C. elegans* VAB-1 and F59D12.1 regulate nicotinic acetylcholine receptor ACR-16 expression.....96

TABLE OF CONTENTS (continued)

| | |
|--|------------|
| IV.a Introduction..... | 96 |
| IV.b Materials and Methods..... | 98 |
| IV.c Results..... | 100 |
| IV.c.1 <i>C. elegans</i> VAB-1 is an ephrin RTK and F59D12.1 is a GPCR-like protein | 100 |
| IV.c.2 <i>vab-1</i> and <i>f59d12.1</i> cause a reduction in ACR-16::GFP and ACR-16::RFP levels..... | 103 |
| IV.c.3 Behavioral analysis of <i>vab-1</i> and <i>f59d12.1</i> mutants..... | 107 |
| IV.c.4 Synapse abundance and muscle integrity in <i>vab-1</i> and <i>f59d12.1</i> mutants..... | 111 |
| IV.c.5 Localization and levels of the LAChR in <i>vab-1</i> and <i>f59d12.1</i> mutants. | 115 |
| IV.c.6 Electrophysiological analysis of <i>vab-1</i> and <i>f59d12.1</i> | 117 |
| IV.c.7 Relative <i>acr-16</i> mRNA levels in <i>vab-1</i> and <i>f59d12.1</i> mutants is increased..... | 119 |
| IV.d Discussion and Future Directions..... | 121 |
| CITED LITERATURE..... | 124 |
| VITA..... | 141 |

LIST OF FIGURES

| | |
|--|----|
| Figure 1. Schematic of vertebrate nAChR subunit conformations..... | 3 |
| Figure 2. Schematic of nAChR clustering in vertebrates..... | 10 |
| Figure 3. Schematic of the two classes of NACHRs found at the NMJ of <i>C. elegans</i> | 15 |
| Figure 4. The NACHR and LACHR make up the total cholinergic current at the <i>C. elegans</i> NMJ..... | 16 |
| Figure 5. Schematic of the assembly and trafficking proteins RIC-3, UNC-50, and UNC-74 acting on the LACHR at the <i>C. elegans</i> NMJ..... | 20 |
| Figure 6. Schematic of the CAM-1 and the WNT-signaling protein pathway..... | 23 |
| Figure 7. MADD-4 is a master organizer of both excitatory and inhibitory..... | 25 |
| Figure 8. Components of the LACHR clustering mechanism act specifically on the LACHRs at the NMJ..... | 29 |
| Figure 9. Schematic of the LACHR clustering complex in <i>C. elegans</i> | 31 |
| Figure 10. A forward genetic screen using EMS was done to identify regulators of the nAChR ACR-16..... | 40 |
| Figure 11. All three <i>EMS</i> mutations cause a reduction in ACR-16::GFP fluorescence levels at the NMJ of <i>C. elegans</i> | 42 |
| Figure 12. The <i>EMS</i> mutants alone do not have any locomotory defects, but LACHR double mutants have a severe motility defect..... | 45 |
| Figure 13. Expression and localization of the LACHRs was unchanged in the <i>EMS</i> mutants..... | 47 |
| Figure 14. Changes in synaptic transmission were observed in the <i>EMS</i> mutants.... | 50 |

LIST OF FIGURES (continued)

| | |
|---|-----|
| Figure 15. Whole genome sequencing and analysis with CloudMap was done to determine the mutated loci in the <i>EMS</i> mutants..... | 53 |
| Figure 16. Evaluation of ACR-16::GFP in candidate mutants..... | 57 |
| Figure 17. <i>EMS</i> mutants and candidate genes are non-complimentary..... | 60 |
| Figure 18. Gene structure and expression pattern of <i>sca-1</i> | 72 |
| Figure 19. The mutant <i>sca-1(tm5339)</i> causes a reduction in ACR-16 receptor levels at the NMJ..... | 76 |
| Figure 20. The LACHR and GABA receptor levels and localization are unchanged in a <i>sca-1</i> mutant..... | 78 |
| Figure 21. Similar to <i>acr-16</i> mutants, <i>sca-1</i> worsens the motility deficits of LACHR mutants..... | 80 |
| Figure 22. ACR-16 deficits in <i>sca-1</i> mutants are not due to a mispatterning of the NMJ..... | 82 |
| Figure 23. <i>sca-1</i> mutants do not affect transcription of <i>acr-16</i> | 84 |
| Figure 24. Evoked response amplitudes are decreased in <i>sca-1</i> mutants..... | 86 |
| Figure 25. Pressure-ejected nicotine responses are unchanged in the <i>sca-1</i> mutant..... | 88 |
| Figure 26. Rescue of ACR-16::GFP expression by <i>Pmyo-3::SCA-1::mCherry</i> is cell autonomous and dose dependent..... | 90 |
| Figure 27. Gene structure and expression of <i>vab-1</i> and <i>f59d12.1</i> | 102 |

LIST OF FIGURES (continued)

Figure 28. Both *vab-1* and *f59d12.1* mutants decrease expression levels of ACR-16 receptors at the NMJ.....105

Figure 29. *vab-1* and *f59d12.1* mutants cause an increase in locomotory deficits in a LACHR mutant background.....109

Figure 30. Evaluation of *vab-1* and *f59d12.1* mutants roles in NMJ patterning.....113

Figure 31. Change in LACHR levels and localization in *vab-1* and *f59d12.1* mutants116

Figure 32. Electrophysiological evaluation of synaptic transmission in *vab-1* and *f59d12.1* mutants.....118

Figure 33. *vab-1* and *f59d12.1* mutants are affecting transcription of *acr-16*.....120

|

LIST OF ABBREVIATIONS

| | |
|-------------|--|
| nAChR/NACHR | nicotinic acetylcholine receptor |
| GABA | <u>γ-aminobutyric acid</u> |
| ACh | acetylcholine |
| CNS | central nervous system |
| NMJ | neuromuscular junction |
| MuSK | muscle specific kinase |
| LACHR | levamisole sensitive acetylcholine receptor |
| CICR | calcium induced calcium release |
| IP3 | inositol (1,4,5)-triphosphate |
| SERCA | sarco(endo)plasmic reticulum calcium ATPases |
| CAMK | calcium/calmodulin-dependent protein kinase |
| Eph | ephrin tyrosine kinase receptor |
| GPCR | G-protein coupled receptor |
| GPI | glycosylphosphatidylinositol |
| CCK-B/CCKR2 | cholecystokinin type B receptor |
| PLC | phospholipase C |
| PKC | protein kinase C |

SUMMARY

Nicotinic acetylcholine receptors (nAChR) are present in many excitable tissues and are found both pre and post-synaptically (1). Through their non-specific cationic permeability, these nAChRs have excitatory roles in neurotransmission, neuromodulation, synaptic plasticity, and neuroprotection (2, 3). Thus, nAChR mislocalization or functional deficits are associated with many neurological disease states (4). Therefore identifying the mechanisms that regulate nAChR expression and function will inform our understanding of normal as well as pathological conditions and offer avenues for potential therapeutic advances.

Taking advantage of the genetic tractability of the soil nematode *C. elegans*, a forward screen was done to isolate regulators of the vertebrate $\alpha 7$ nAChR homologue ACR-16. From this screen three novel regulators of the ACR-16 receptor were identified: *sca-1*, *vab-1*, and *f59d12.1*. Further examination of these three genes promises to shed light on previously uncharacterized pathways of regulation of the ACR-16 receptor.

I. INTRODUCTION

I.a nAChRs structure and function in vertebrates

In mammals nAChRs belong to the Cys-loop ligand-gated ion channel superfamily, which also includes GABA ([γ-aminobutyric acid](#)), glycine, and 5-HT₃ receptors (5). nAChRs are responsible for all skeletal muscle excitability, and function in both the peripheral and central nervous systems as well as other non-neuronal tissues. The human genome encodes for seventeen nAChR subunits, found in several unique pentameric combinations, providing a rich variety of receptor types. In skeletal muscles the receptor subunit composition varies based on developmental stage. In fetal skeletal muscles the receptors have a subunit composition of two α 1 subunits and one β 1, γ , and δ subunit, while in the adult skeletal muscle an ϵ subunit replaces the γ subunit. These heteropentamers form two acetylcholine (ACh) ligand-binding sites: the first between an α subunit and either the γ subunit in fetal skeletal muscles or the ϵ subunits in adult skeletal muscles, the second between the α and δ subunits, regardless of developmental stage (Fig. 1A). When both ACh binding sites are occupied, a conformational change in the receptor results in the opening of the receptor channel. These receptors are located on postsynaptic folds in the muscle membrane and control excitation-contraction coupling (6, 7).

In neurons, nAChRs are constituted from a larger population of subunits with receptors forming either hetero- or homomeric pentamers. In the case of heteromeric receptors there is generally an $\alpha\beta$ -based pattern. The subunits involved

in this patterning are $\alpha 2$ - $\alpha 6$ and $\beta 2$ - $\beta 4$ and normally have a stoichiometry of two α and three β subunits. Functional receptors can also form from homomeric pentamers involving $\alpha 7$ - $\alpha 9$ subunits, or alternatively, $\alpha 9$ forms heteromeric receptors with the $\alpha 10$ subunit. Similar to skeletal muscle nAChRs, the neuronal heteromeric receptors have two ACh binding sites found between the α and β subunits. The ACh binding sites in the homomeric receptors are found at the interface of each of the $\alpha 7$ subunits (Fig. 1B). The subunit composition of nAChRs dictates their localization, ligand binding affinities, kinetics and permeability (6, 8).

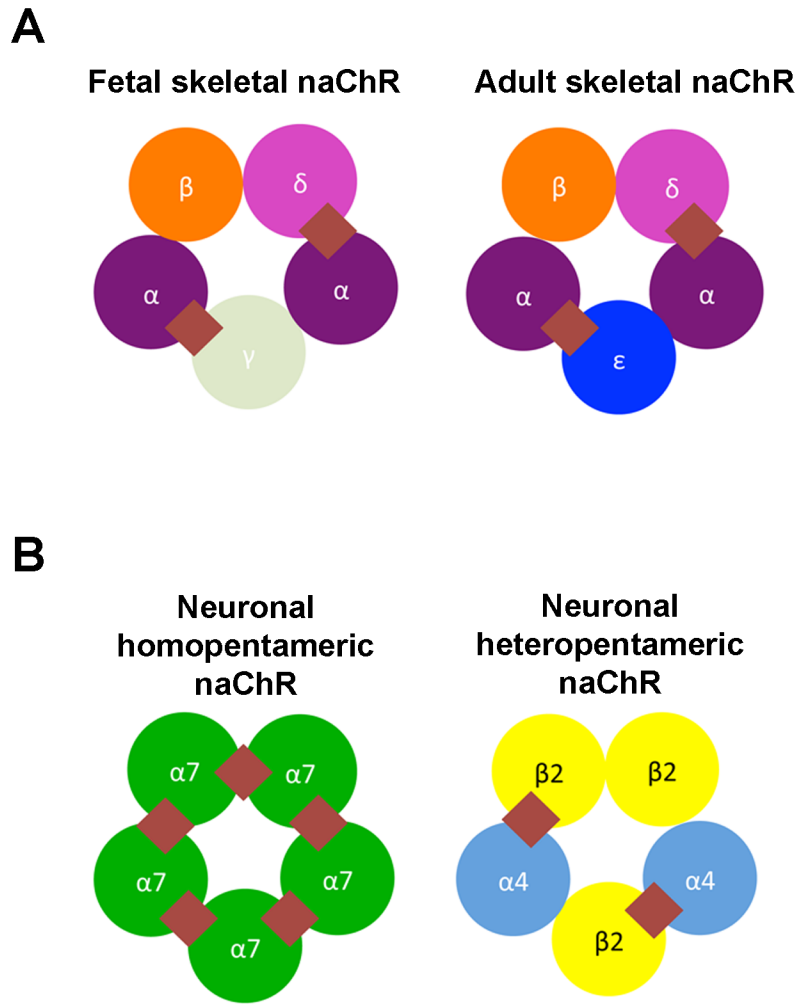


Figure 1. Schematic of vertebrate nAChR subunit conformations. A. nAChR subunit structure in both embryonic and adult vertebrate skeletal muscles, ACh binding sites shown with red diamonds. B. nAChR subunit structure in vertebrate neurons, ACh binding sites shown with red diamonds.

Given that nAChRs regulate both movement and cognitive processing, their proper expression, localization, and function are critical for normal behavior and survival. Furthermore, nAChRs have also been implicated in the pathology of several debilitating neurological diseases. By uncovering the molecular pathways regulating nAChRs it is anticipated that novel therapeutic approaches will [help patients](#) who suffer from conditions including those discussed below.

I.b Role of nAChRs in disease

Alzheimer's disease is a progressive neurological disorder characterized by dementia with declines in memory, attention, and orientation (9). This disease state is associated with an increase in the abundance of misfolded β -amyloid leading to the formation of amyloid plaques and hyperphosphorylation of tau protein that [results in](#) neurofibrillary tangles, both hallmarks of Alzheimer pathology (10). [Studies have](#) shown that in the brain, β -amyloid protein binds to α -7 nAChRs with high-affinity and the colocalization of these two proteins [with](#) amyloid plaques has implicated nAChRs in Alzheimer's pathology (11). Evidence suggests that acute exposure of nAChRs to moderate doses of β -amyloid can [actually](#) lead to nAChR receptor activation and downstream neuroprotective affects. [In contrast](#), exposure of nAChRs to either higher concentrations of β -amyloid or exposure for long periods of time causes receptor inactivation, possibly through desensitization, which can be detrimental (12, 13). Although these studies imply that β -amyloid interactions with α 7 nAChRs play roles in the development of Alzheimer's disease, [the](#) opposing

effects on receptor function and downstream signaling, relative to amyloid levels makes it difficult to develop obvious therapeutic strategies.

Parkinson's is considered to be neurodegenerative, movement disease that presents with loss of dopaminergic neurons and damage to the nigrostriatal brain region (6, 14). In addition, a decrease in levels of $\alpha 7$ nAChRs has been demonstrated in the brains of Parkinson's patients, which may contribute to the cognitive [impairments](#) seen in some patients (15). Work has shown that $\alpha 7$ receptor agonists reduce the nigrostriatal damage seen in various animal models through an increase in calcium signaling, which suggests a possible role by which nAChR activation may slow the disease progression. Studies have also demonstrated that treatment with nicotine can help reduce instances of L-dopa induced dyskinesias (LIDS), which are random, involuntary muscle movements. In rodent and nonhuman primate studies, as much as a 50-60% reduction in LIDS was seen when Parkinson's animal models when treated with nAChR agonists. Thus, $\alpha 7$ nAChRs are an important target in slowing Parkinson's disease [progression](#) and managing negative side effects (14)

nAChRs have also been shown to play a role in various psychiatric illnesses, including schizophrenia. In both *in vivo* and post mortem imaging studies of patients diagnosed with schizophrenia a significant decrease in levels of nAChRs in the brain was reported (9, 6, 16). [Evidence further indicates](#) that mutations affecting the human $\alpha 7$ gene seen in some schizophrenia patients cause reduced inhibition of the P50 evoked response, which controls auditory sensory gating (9). This impairment is thought to be associated with auditory hallucinations in a subset of schizophrenics. The application of nicotine has been shown to attenuate some

deficits seen with this disease (17). This has led to speculation that schizophrenia patients may smoke to self-medicate.

Based on the body of research demonstrating a strong correlation between the regulation of nAChRs and crippling [neurological](#) disease states, a complete understanding of the mechanisms involved in nAChR receptor modulation and function is necessary for the development of effective treatments. Further study of the individual components involved in these pathways has shed considerable light on the molecular machinery involved at the neuromuscular junction, however nAChR targeting and stabilization in the CNS is less [well understood](#).

I.c Clustering mechanism of nAChRs in vertebrates

Progress in the identification of nAChR clustering mechanisms has advanced further at neuromuscular junctions (NMJ). In vertebrates there are four key proteins that are required for nAChRs to be properly clustered [at NMJs](#), namely agrin, MuSK (Muscle-Specific Kinase), Lrp4 and Dok7.

Agrin is a presynaptic proteoglycan that is secreted from motor neurons. It has many structural domains that are common to basal lamina proteins and has alternate splice sites at the N-terminus that give rise to two isoforms of agrin, one short and one long. The short agrin isoform is an integral plasma membrane protein expressed in the brain where as the long isoform is secreted from motor neurons at NMJs. In agrin mutant mice there are significant synaptogenesis defects and a reduction of nAChR clusters at the NMJ. This supports roles for agrin in both synaptic development and nAChR localization (18). The C-terminal of agrin is

composed of three laminin G-like modules, which have been shown to play a critical role in nAChR clustering (19). Extracellular calcium is also necessary for the function of agrin. In rats that have [mutations in](#) either of the two calcium coordinating residues found in the third laminin G-like domain, agrin is no longer able to cluster nAChRs at the NMJ (20). Studies have also demonstrated that agrin can trigger upregulation of nAChR gene expression at the NMJ. Studies performed on cultured myotubes have uncovered the molecular events leading to [this](#) increase [in](#) nAChR transcription. Specifically, agrin has been shown to act synergistically with neuron secreted neuroregulin-1 (NRG-1) to induce clustering of NRG-1 receptor kinase (ErbB2), leading to the activation of ets transcription factors that enhance nAChR transcription (21). Additionally secreted agrin and neuregulin converge in a separate pathway to induce nAChR clustering through the activation of the tyrosine kinase receptor MuSK (Fig.2).

Mice lacking MuSK [exhibit](#) a significant disruption of their postsynaptic development, leading to a complete abolishment of nAChR clustering (22). MuSK contains an extracellular ligand binding domain, a transmembrane domain, and an intracellular kinase domain. Once activated by agrin, MuSK autophosphorylation signals via a positive feedback loop, causing increased clustering of MuSK at the neuromuscular junction (20). MuSK contains a Frizzled-like CRD (cysteine-rich domain) in its extracellular domain. Although this CRD is not necessary for agrin-mediated nAChR clustering, research has shown that it is through this domain that MuSK interacts with WNT signaling proteins to cluster nAChRs. Mice with the CRD region deleted show defects in neuromuscular junction patterning. This results in

significant decreases in nAChR clusters and overgrowth of motor axons (23).

Though it is widely accepted that agrin is an activating ligand of MuSK, it has been shown that the two do not interact directly. The interaction between Agrin and MuSK takes place through a myotube-associated specificity component (MASC), which has been identified as LRP4 (24, 25, 26) (Fig.2).

LRP4 belongs to the LDLR family of transmembrane proteins. It has an intracellular C-terminal domain and an extracellular domain with eight LDLa repeats. In *LRP4* null mice nAChRs are no longer clustered at the neuromuscular junction (27). LRP4 binds directly to agrin in a 2:2 stoichiometry, this dimerization causing the activation of MuSK and nAChR clustering (20), thus LRP4 is the agrin receptor. The direct constitutive interaction between LRP4 and MuSK is strengthened in the presence of agrin (28) (Fig.2).

Another essential component of the nAChR clustering machinery is the cytoplasmic adaptor protein Dok7 (downstream of kinase or docking protein 7), which can activate MuSK in the absence of agrin. Like MuSk mutants, Dok7 mutant mice lack all nAChR clustering (29, 30) and Dok7 mutations have been found to underlie a human congenital myasthenic condition characterized by a “limb girdle” pattern of muscle weakness (31). Dok7 is also phosphorylated by MuSK and this phosphorylation causes the recruitment of two noncatalytic adapter proteins Crk and Crk-L. These proteins seem to play a redundant role in NMJ differentiation, mice deficient in both Crk and Crk-L show mistargeting of motor axons, a reduction in synapse number, and a decrease in nAChR clusters. This suggests that Dok7 works

both as an activator and substrate of MuSK to help pattern the neuromuscular junction (32) (Fig.2).

Tid1, a member of the heat shock protein 40 family, is then necessary for MuSK-Dok7 downstream signaling (33). This protein regulates Rac and Rho GTPases that play a role in the tyrosine phosphorylation necessary for the β nAChR subunit to interact with the synaptic anchoring protein rapsyn (20) (Fig.2).

Rapsyn is a peripheral, cytoplasmic, non-integral membrane protein that colocalizes with both synaptic and cytosolic nAChRs *in vivo*, and mutant mice lacking rapsyn have no nAChR clusters (34, 35, 36). Single-receptor tracking has shown that when rapsyn is present at the synapse nAChRs are more stable, as the number of mobile receptors decreases (37). There is also evidence that nAChRs facilitate the transport of rapsyn to the synapse; in the absence of nAChRs rapsyn clusters remain in the Golgi complex (38) (Fig.2).

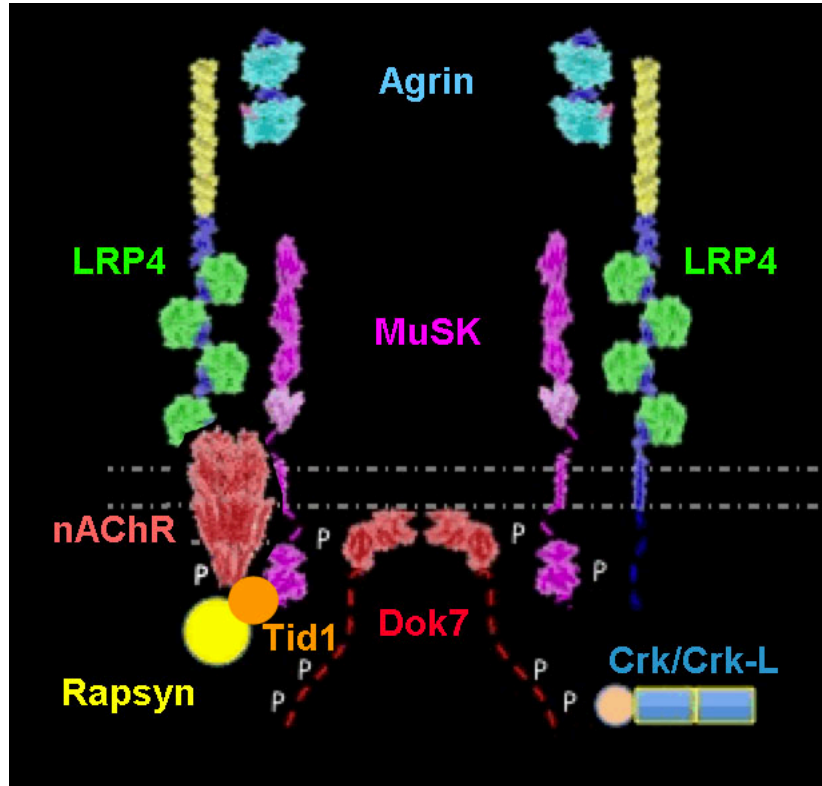


Figure 2. Schematic of nAChR clustering in vertebrates. Modified from Burden Lab Website (<http://www.med.nyu.edu/skirball-lab/burdenlab/research/synapse.html>)

The extent to which agrin, MuSK, and LRP4 are involved in nAChR localization in the CNS is less well understood. In part because nAChRs are predominantly presynaptic in the CNS, are less abundant, have a diverse composition and are often activated through paracrine signaling. Adding to this complexity is the fact that vertebrate agrin null mutants are embryonic lethal. Despite these drawbacks, several studies do suggest that the agrin/MuSK, LRP4 machinery may function in the CNS. Specifically, the long isoform of agrin isolated from avian brain was shown to be able to cluster nAChRs in myotube cultures (39). The synaptogenesis role of agrin may also be conserved in the CNS, as neuronal cultures derived from agrin-deficient mice exhibit reduced synapse formation between cultured spinal cord and sympathetic ganglion neurons (40). Similarly, in viable mosaic mice expressing agrin only in motor neurons, a 30% reduction was observed in the number of cortical pyramidal neuron excitatory synapses (40, 41). These data suggest that the long, brain specific agrin isoform may have similar roles in synapse formation/maintenance and nAChR clustering in the brain and NMJ.

Both MuSK and LRP4 are also expressed in the vertebrate brain and have been implicated in memory consolidation (41, 42, 43). Furthermore, in brain slices inhibition of MuSK disrupts cholinergic activity in the hippocampus (44). Although this supports a role for MuSK and LRP4 in brain function, evidence of LRP/MuSK activation by agrin at central synapses has yet to be established (45).

In summary, while the regulation of nAChRs at the vertebrate NMJ has been well documented, there remains a paucity of information regarding the localization and function of the diverse population of CNS nAChR subtypes. However, in the last

decade, genetic screens looking for defects in nAChR function in the soil nematode *Caenorhabditis elegans* (*C. elegans*) have identified components of a completely novel nAChR clustering mechanism. Furthermore, these elements are highly conserved, although [many of](#) the vertebrate homologs [that are enriched in the CNS](#) have yet to be characterized.

I.d *Caenorhabditis elegans* as a model system

Like vertebrates, *C. elegans* NMJs are cholinergic; therefore mutants that are defective in ACh signaling can be readily identified in screens on the basis of movement defects, pharmacological assays, or by receptor mislocalization. Despite the importance of nAChRs for locomotion, another advantage is that mutants lacking NACHRs receptors remain viable under laboratory conditions. The fact that *C. elegans* is self-fertilizing and can produce a brood of ~300 offspring that reach adulthood in a short 3 day life cycle, facilitates the performance of large scale forward and reverse genetic screens (46). Additionally, the entire genome has been sequenced providing annotated information for many *C. elegans* genes (47). There are 302 neurons in *C. elegans*, each of which is identifiable based on known cell lineage, morphology, and position (48). Importantly, many proteins, including those that make up NACHRs expressed at the worm NMJ are homologous to those in the vertebrate [nervous](#) system. These NACHRs also have similar subunit structure to those found in vertebrates. In the worm, there are currently twenty-seven [known](#) NACHR subunits, which are classified and divided into five groups based on homology. Each group is named after the first unique subunit that was discovered

i.e. DEG-3, ACR-16, UNC-38, ACR-8, and UNC-29 (49). The assembly of subunits from the latter four groups account for the two functional receptors at the *C. elegans* NMJ (50).

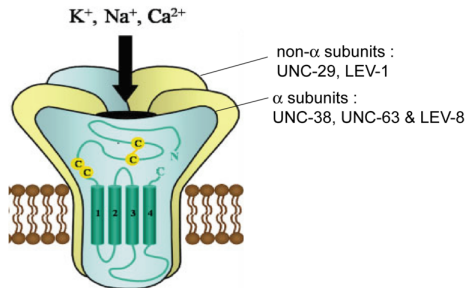
I.e nAChRs structure and function in *C. elegans*

The two classes of *C. elegans* NMJ nAChRs differ **not only in** their subunit composition **but also** pharmacology. Components of the first and best-characterized nAChR receptor was identified in screens looking for mutants resistant to the worm nematocide levamisole, and so named the Levamisole-sensitive nAChR (LACHR). This pentameric receptor is made up of three α -subunits (UNC-38, UNC-63, and LEV-8) and two non- α subunits (UNC-29 and LEV-1). Three of these subunits are essential **for** receptor function: UNC-29, UNC-63, and UNC-38. Null mutants **of** any of these subunits exhibit strong levamisole-resistance. Null mutations in LEV-1 and LEV-8 cause a weaker resistance to levamisole, making these subunits non-essential (51, 52, 50, 53, 54) (Fig.3). The LACHR receptor can be reconstituted by combining all five subunits in *Xenopus laevis* oocytes along with several *C. elegans* trafficking and assembly genes (UNC-50, RIC-3 and UNC-74). When **all eight genes are** expressed the subunits form functional receptors **on the oocyte plasma membrane** that produce currents with similar pharmacology to endogenously expressed **LACHRs at the NMJ**. Work has also shown that this receptor contributes to the slowly desensitizing component of the **NMJ evoked postsynaptic** current (50, 55).

ACR-16 was subsequently identified as an essential subunit of the second *C. elegans* NMJ nAChR (56, 57). This subunit is homologous to human $\alpha 7$. In

vertebrates $\alpha 7$ nAChRs form homopentamers (6). Similarly, expression of ACR-16 in *Xenopus laevis* oocytes is able to form functional nAChRs (58, 55). Unlike the LACHR, the ACR-16 receptors are activated by nicotine and are therefore, referred to as the NACHRs at *C. elegans* NMJ (Fig.3). This receptor has been shown to contribute to the large quickly desensitizing component of the NMJ postsynaptic current, demonstrating unique kinetics between NACHRs and LACHRs (50,56, 57, 55). Surprisingly, although the NACHR at the *C. elegans* NMJ accounts for ~80% of the evoked cholinergic postsynaptic current amplitude, *acr-16* null mutants have no obvious locomotory phenotype. However, when crossed into a LACHR mutant background (*unc-63*) there is substantial worsening of the *unc-63* mutant uncoordinated phenotype, indicating that both receptors function in locomotion. Consequently, in worm strains that are null for both *unc-63* and *acr-16*, the cholinergic postsynaptic current is completely abolished, suggesting these are the only ionotropic AChRs at the NMJ (56) (Fig.4). The homology between *C. elegans* NACHRs and the $\alpha 7$ receptors in vertebrate brain suggest that screens for NACHR disregulation in worms may uncover conserved machinery.

- **Heteropentameric lev-sensitive**



- **Homopentameric lev-insensitive**

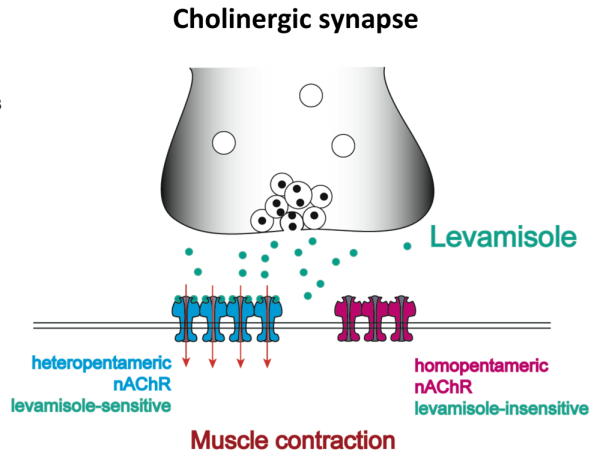
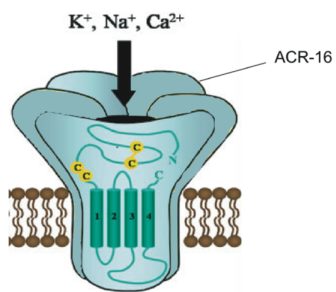


Figure 3. Schematic of the two classes of NACHRs found at the NMJ of *C. elegans*

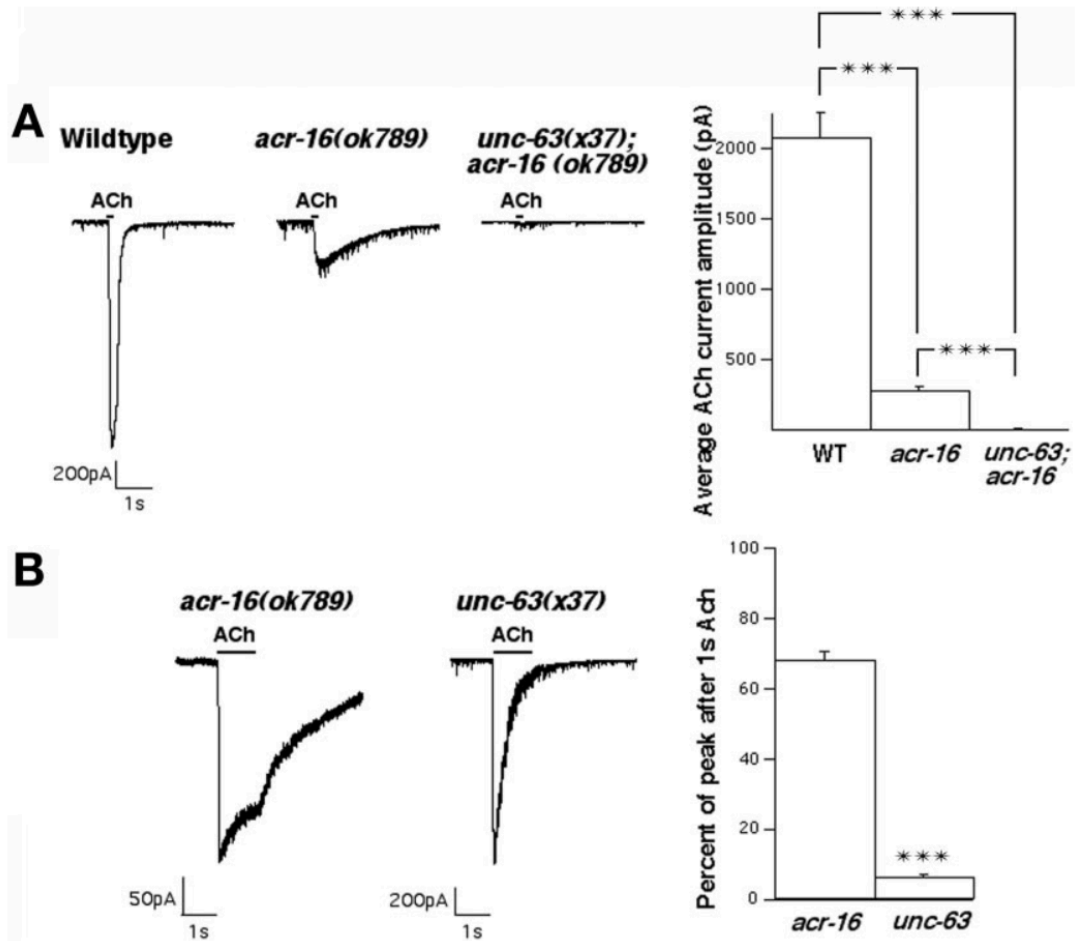


Figure 4. The NACHR and LACHR make up the total cholinergic current at the *C. elegans* NMJ. A. Postsynaptic responses to pressure-ejected exogenous ACh demonstrated a significant decrease in current amplitude in NACHR mutants *acr-16(ok789)* and a complete abolishment of cholinergic current in the NACHR and LACHR double mutants. 100ms bar. B. In a NACHR *acr-16(ok789)* mutant the slowly desensitizing portion of the current remains. In a LACHR *unc-63(x37)* mutant the quickly desensitizing portion of the current remains, suggesting that the two receptor classes have differing kinetics. 1000ms bar. Figure adapted from (56).

If ACh receptor assembly, trafficking, and membrane targeting in

C.elegans

Due to the ease of screening for locomotory defects and levamisole-resistance, forward genetic screens for mutants affecting LACHRs has been very successful in identifying relevant genes as briefly summarized below.

Mutants in *ric-3* were first identified in pharmacological screens (resistance to inhibitors of cholinesterase hence RIC mutants) for mutants defective in cholinergic transmission (59, 60). RIC-3 is a protein necessary for both NACHR and LACHR function. Its structure predicts two transmembrane domains and three coiled-coiled regions, suggesting that it is an integral membrane protein thought to be located at the endoplasmic reticulum. RIC-3 is expressed in pharyngeal and body wall muscles as well as many neurons. Electrophysiological recordings revealed that *ric-3* null mutants fail to respond to pressure-ejected ACh onto body wall muscles, which suggests that the receptors are affected. When either levamisole, to activate the LACHRs, or nicotine, to specifically activate the NACHRs, was pressure-ejected the postsynaptic response amplitudes were also abolished, again suggesting that in *ric-3* mutants both ACh receptors types were affected at the NMJs (Fig.5). In contrast, responses to pressure-ejected GABA in the *ric-3* mutant were not significantly changed at the NMJ, suggesting that RIC-3 is not necessary for the localization of worm GABA receptors encoded by the *unc-49* gene (61, 62). These findings are consistent with the requirement for RIC-3 in expressing functional receptors in *Xenopus* oocytes, along with two other proteins: UNC-50 and UNC-74 (55).

unc-50 mutants were isolated in screens for uncoordinated phenotypes as well as levamisole-resistance (51). UNC-50 contains five transmembrane domains and its structure and sequence is highly conserved across many organisms. UNC-50 localizes to the Golgi system and may play a role in COPI-dependent transport, specifically Arf activated mobilization of the COPI coat protein, which has been found to be necessary for both anterograde and retrograde trafficking between the endoplasmic reticulum and Golgi (63, 64, 65). In *unc-50* mutants the levamisole receptor is no longer localized to the neuromuscular junction **based on** antibody staining against **the** LACHR subunit UNC-29. There is **also** no response to pressure-ejected levamisole in *unc-50* mutants, **whereas** wild-type amplitudes in response to pressure-ejected nicotine and GABA are **normal**, suggesting that UNC-50 specifically regulates LACHRs. It has subsequently been reported that UNC-50 is required to traffic LACHRs, post-assembly from the Golgi to the muscle membrane (65) (Fig.5).

unc-74 was also isolated by Lewis et al., in 1980 as a levamisole-resistant mutant. The UNC-74 protein is predicted to encode a thioredoxin protein similar to the human TMX3 protein and **is** thought to localize at the endoplasmic reticulum (66, 55). The LACHR reconstitution experiments in *Xenopus* oocytes helped to establish the role of UNC-74 as necessary for LACHR membrane expression. Expression of the five LACHR subunits along with RIC-3, UNC-50, and UNC-74 produced functional receptors with robust responses to pressure-ejected ACh and levamisole. However when the UNC-74 subunit was removed from the injection there was a 10% decrease in response amplitudes, suggesting that UNC-74 is a necessary protein for proper expression and function of the LACHR. As was seen

with UNC-50, oocyte expression of NACHRs was unaffected in *unc-74* mutants, again suggesting that UNC-74 is a specific regulator of LACHRs (55) (Fig.5).

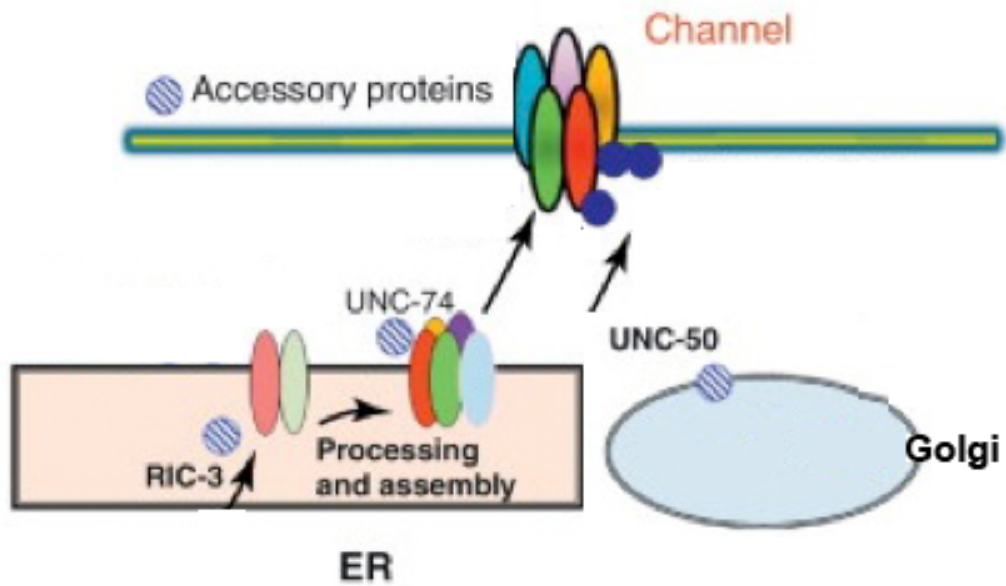


Figure 5. Schematic of the assembly and trafficking proteins RIC-3, UNC-50, and UNC-74 acting on the LACHR at the *C. elegans* NMJ. Adapted from (67).

A different cohort of proteins has been reported to specifically regulate *C. elegans* NACHRs. The first protein in this category is the Ror receptor tyrosine kinase CAM-1, which shares strong sequence identity with the vertebrate receptor kinase MuSK, implicated in the clustering mechanism of vertebrate nAChRs. CAM-1 is specifically expressed at the distal tips of *C. elegans* body wall muscle arms, as well as the cell membrane of cholinergic motor neurons. In *cam-1* mutants the expression of a GFP-tagged ACR-16 clusters accumulates in the muscle arms distal to the NMJs, while expression of LAChRs and GABA receptors seem to be unchanged in this mutant background. This mislocalization is also reflected electrophysiologically, as *cam-1* mutants have significantly reduced responses to pressure-ejected ACh as well as to nicotine. Responses to pressure-ejected levamisole and GABA were unaffected, suggesting that CAM-1 is acting specifically on ACR-16 receptors. Structure-function analysis of CAM-1 determined that the extracellular and transmembrane domains were necessary for this function, arguing that proper membrane localization of CAM-1 is needed for CAM-1 function (57) (Fig.6).

CAM-1 possesses a cysteine rich region that is predicted to bind a class of glycoproteins called Wnts. In mammals Wnts have been shown to work with MuSK to stabilize and cluster AChRs through a well defined molecular pathway involving Wnt binding to the Frizzled receptor (Fzd), which acts through the intracellular signaling molecule termed dishevelled (Dvl). Thus, Jensen et al, undertook a candidate gene approach to examine whether this pathway was conserved in *C. elegans*, evaluating the corresponding mutants *lin-17* (Fzd), *cwn-2* (Wnt), and *dsh-1*

(Dvl). In all three mutant backgrounds ACR-16::GFP clusters were mislocalized, similar to the phenotype seen in *cam-1* mutants. There was also a decrease in the number of surface expressed receptors, as measured with fluorescently labeled alpha-bungarotoxin injected into the pseudocoelomic space and a corresponding reduction in electrophysiological responses to pressure-ejected ACh and nicotine (Fig. 6) (68).

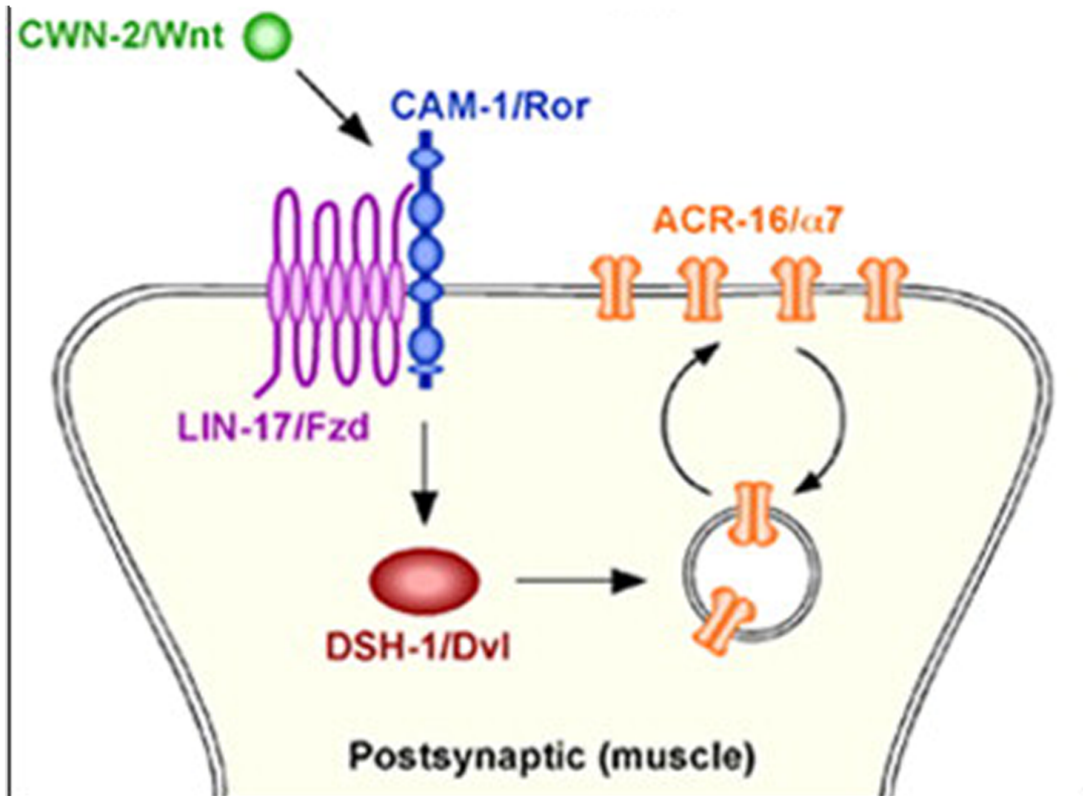


Figure 6. Schematic of the CAM-1 and the WNT-signaling protein pathway.

These proteins play a role in targeting ACR-16 receptors to the surface of the body wall muscle at the NMJ. Adapted from (68).

Given *C. elegans* NMJs have discrete GABA and ACh synapses it is critical that GABA and ACh receptors are targeted to the appropriate subcellular domains corresponding to ACh and GABA release sites. Recent evidence suggests that *C. elegans* MADD-4 serves this role. Three isoforms of MADD-4 are present in the worm, two long isoforms, MADD-4A and MADD-4C, and one short isoform, MADD-4B. MADD-4 is orthologous to mammalian punctin-1/ADAMTS-like1 and punctin-2/ADAMTS-like2. In *madd-4* mutants LACHR, NACHR, and GABA receptor clusters are all mislocalized. The fact that the receptors remain clustered, although mislocalized, suggests that MADD-4 is necessary for recruitment of receptors to their cognate postsynaptic sites. Further analysis demonstrated that the long MADD-4A/MADD-4C isoforms were localized to cholinergic terminals only, but the short MADD-4B isoform was present at both cholinergic and GABAergic terminals (Fig. 7A). Further work determined that the long MADD-4 isoforms specifically localize LACHRs and NACHRs while the presence of the short MADD-4 isoform excludes GABA receptor clusters from cholinergic NMJs while promoting GABA receptor clustering at GABA NMJs (Fig. 7B) (69). Thus MADD-4 is a master organizer of receptor clusters, but is not required to establish or maintain clusters. How then are receptor subtypes clustered together?

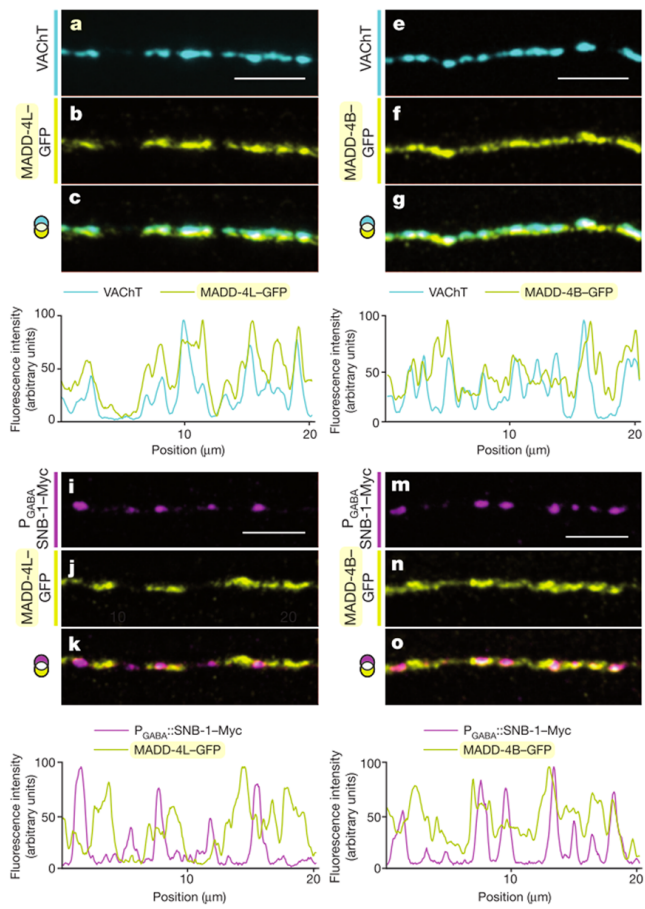
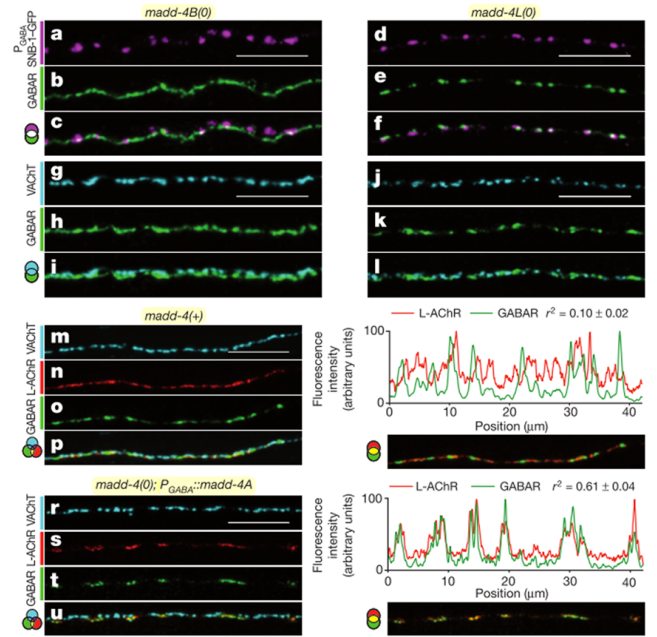
A**B**

Figure 7. MADD-4 is a master organizer of both excitatory and inhibitory receptors at the *C. elegans* NMJ. A. Immunostaining demonstrating that both the MADD-4L (long) isoform and the MADD-4B (short) isoform colocalize with the cholinergic synaptic marker VACHT, but only the short MADD-4B isoform colocalizes with the GABA specific promoter driven synaptic marker SNB-1. B. In mutants of the MADD-4 short isoform the GABA receptor clusters are now present at the cholinergic synapses, however GABA clusters were properly located in the MADD-4L isoform mutants, demonstrating a role for the short isoform in GABA receptor patterning. When MADD-4A (the long isoform) was expressed at GABAergic synapses there was an increase in LACHR present and colocalized with the GABA receptors, suggesting that the long isoform can cluster both receptor types. Adapted from (69).

I.g LACHR clustering in *C. elegans*

Screens for mutants that have a mild resistance to levamisole have been very powerful in identifying LACHR clustering machinery. The first component discovered was LEV-10, which contains five predicted CUB domains and one predicted LDLa domain in its extracellular region. These domains show the highest similarity to mouse NETO2 and its paralog NETO1. The NETO proteins in mammalian systems have subsequently been shown to stabilize NMDA and kainate receptors (70). In *lev-10* mutant worms immunostaining of the LACHRs was greatly reduced while NACHR and GABA receptor localization were unchanged. Western blots established that the LACHR plasma membrane level was unchanged in *lev-10*, suggesting that in this mutant background the LACHRs are dispersed. This was confirmed by electrophysiology. In *lev-10* mutants, although the evoked amplitude of the synaptic current was significantly decreased, the amplitude in response to pressure-ejected levamisole was unchanged, again indicating that the LACHR receptors are present and functional but simply dispersed. Based on these results it was concluded that LEV-10 is part of the LACHR clustering machinery (71).

The second component of the LACHR clustering machinery is LEV-9, mutants of *lev-9* exhibiting mild resistance to levamisole. LEV-9 encodes a muscle-secreted protein that contains eight CCP, or sushi domain, modules and a whey acidic protein (WAP) domain. The WAP domain, previously implicated in cell adhesion and migration, is not necessary for LEV-9 function. However the string of CCP domains may play a role in protein-protein interactions. LEV-9 colocalized with LACHR clusters and, similar to *lev-10* mutants, in *lev-9* mutants LACHR antibody staining

was no longer visible at the NMJ, but again NACHR and GABA receptors were unaffected (Fig. 8A). Both the overall amount of LACHR protein and the electrophysiological phenotypes were similar to those seen in *lev-10* mutants, suggesting that *lev-10* and *lev-9* work in the same pathway. This was verified by demonstrating a physical interaction between LEV-9 and LEV-10, and observing colocalization of the two proteins. From this study it was proposed that LEV-10 interacts directly with LEV-9 to form an extracellular scaffold required to cluster LACHRs at the NMJ (72).

The final component of this LACHR clustering complex, *OIG-4*, was also isolated in a screen for mutants with mild resistance to levamisole. The *C. elegans oig-4* gene is predicted to encode a protein with a single immunoglobulin domain. *OIG-4* is expressed in body wall muscles and immunostaining showed discrete expression along the nerve cords where it colocalized with LACHRs. *OIG-4::GFP* was also seen in coelomocytes, suggesting that this protein is secreted. Although *oig-4* mutants specifically affect LACHRs clustering at NMJs (Fig. 8B), the level of LACHR declustering in *oig-4* mutants was not as severe as in *lev-9* and *lev-10* mutants. Thus although the amplitude of the LACHR evoked synaptic current was not lower, the response had slower kinetics, consistent with local LACHR dispersal. As expected, in *oig-4* mutants LEV-9 and LEV-10 were no longer synaptically localized. Co-immunoprecipitation studies confirmed that *OIG-4* and LEV-10 interact only in the presence of LACHRs and in *oig-4* mutants LEV-10 no longer interacts with LACHRs. Based on these results it was proposed that *OIG-4* functions in a physical complex with LEV-9 and LEV-10 to cluster LACHRs at the NMJ (73).

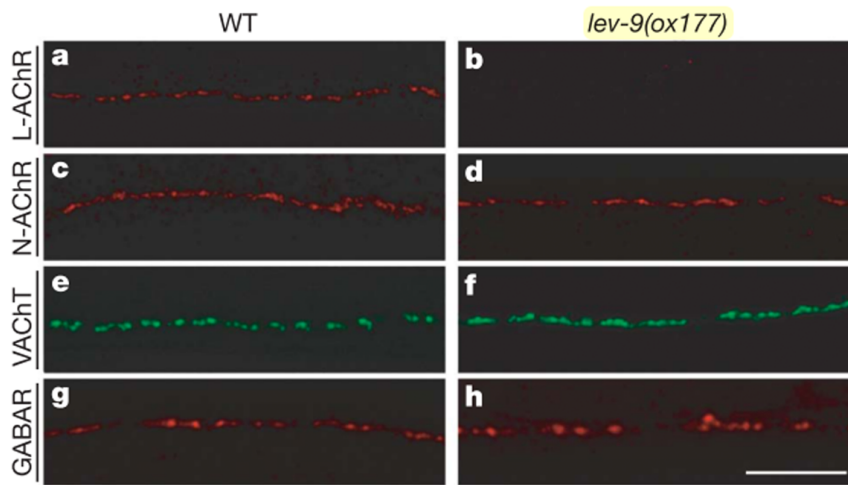
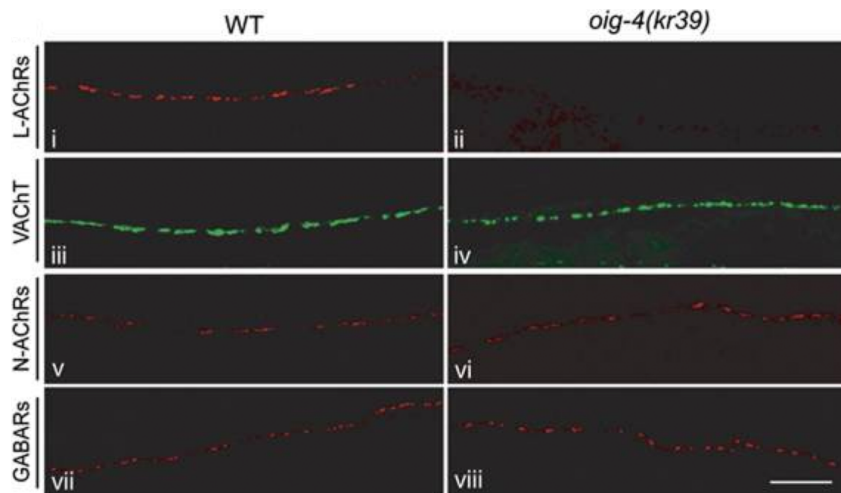
A**B**

Figure 8. Components of the LACHR clustering mechanism act specifically on the LACHRs at the NMJ. A. Immunostaining shows that *lev-9* mutants specifically affect localization of the LACHRs at the NMJ while both the NACHRs and GABA receptors are unaffected. Also staining of a cholinergic specific synaptic marker is unchanged suggesting this reduction in LACHRs is not due to a synaptogenesis defect. Adapted from (72). B. Immunostaining demonstrates that *oig-4* mutants specifically affect the localization of the LACHRs, while the NACHRs and GABA receptors remain unchanged. Again immunostaining of the cholinergic synaptic marker VACHT is unchanged in the *oig-4* mutant, which implies these changes in LACHR localization are not due to a defect in synaptogenesis. Adapted from (73).

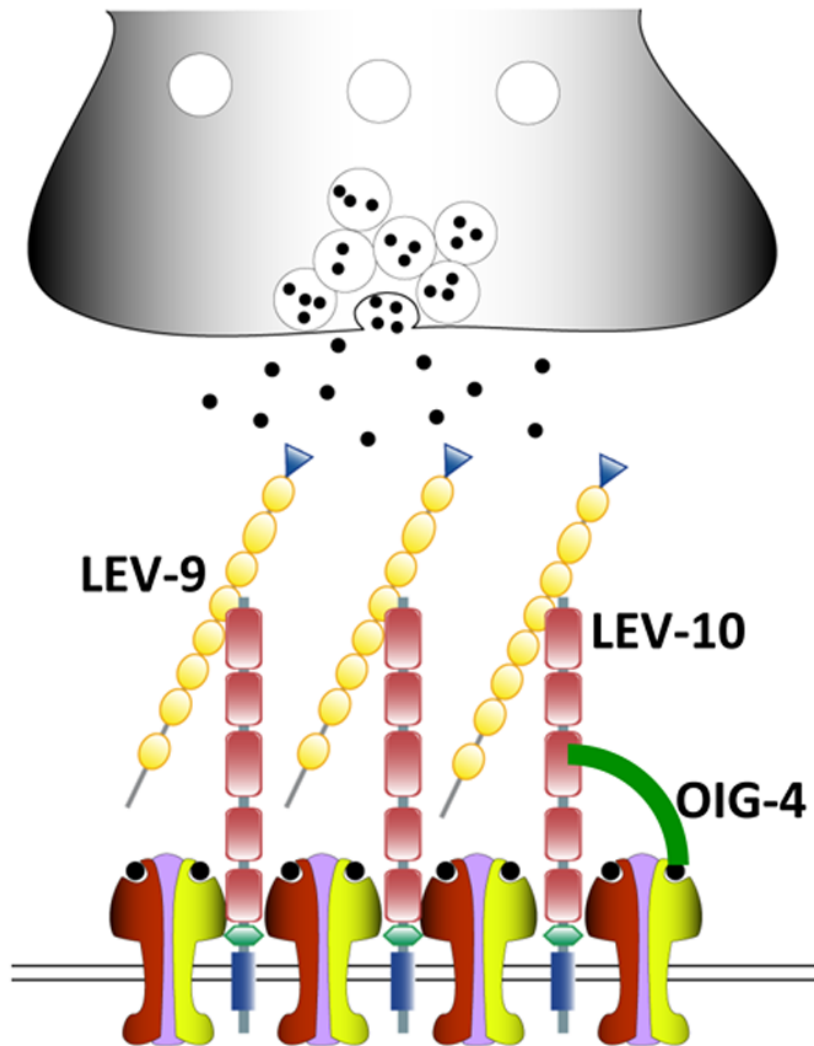


Figure 9. Schematic of the LACHR clustering complex in *C. elegans*

Although this body of work has uncovered a novel *C. elegans* LAcHR clustering complex (Fig. 9), with the tantalizing presence of multiple conserved homologs in the Allen Brain Atlas linked to several neurological phenotypes in humans, surprisingly to date no mutants have been uncovered that disrupt *C. elegans* NAcHR receptor clustering. Given the homology of these ACR-16 homomeric receptors to $\alpha 7$ nAcHRs in the human brain, the goal of this thesis was to use the strengths of *C. elegans* genetics and the accessibility of the worm NMJ for imaging and recording of these receptors, to uncover novel components of ACR-16 regulation.

II. Screen to identify NACHR regulators and characterization of candidates

II.a Introduction

Vertebrate $\alpha 7$ nAChRs, expressed in the CNS, have been implicated in a number of neurological diseases such as Alzheimer's, Parkinson's, and schizophrenia, where a hallmark in each is the declustering or misregulation of the receptors (4). Therefore, determining factors that play a role in regulating nAChRs is critical for learning more about and combating these afflictions.

The model system *C. elegans* presents a platform in which to study this regulation as it expresses the NACHR forming subunit ACR-16, a homologue to the vertebrate $\alpha 7$ nAChRs at NMJs (56, 57). *C. elegans* also have a vast genetic toolbox, allowing for the easy manipulation of many genes through screens and the ability to quickly determine the effects and locations of these gene perturbations. Previous studies by Gally (71), Gendrel (72), and Rapti (73) in *C. elegans* have elucidated the clustering mechanism of the second class of cholinergic receptors found at the NMJ, the LACHRs. However, this clustering mechanism is specific to LACHRs, NACHRs remaining unaffected in mutants of *lev-10*, *lev-9* and *oig-4* that encode the LACHR clustering complex. Thus an unknown mechanism must exist to cluster ACR-16 receptors.

In order to determine what genes are involved in the regulation of the ACR-16 receptor, a forward genetic screen was performed using a single copy insertion of ACR-16::GFP. This allowed for even subtle changes in ACR-16 expression to be

found. Once mutants were identified from the screen their effect on ACR-16 receptor function was determined. Whole genome sequencing was then performed to identify potential mutant loci and complementation tests were performed on mutants isolated from the screen using reference alleles. From this screen three new regulators of the ACR-16 receptor were identified.

II.b Materials and Methods

Strains and Culturing Conditions: The genotypes of nematode strains used in this study are: the wild-type Bristol isolate N2, *acr-16(ok789)*, *unc-63(x37)*, *unc-63(x37);acr-16(ok789)*, *jaSi4[Pmyo-3::ACR-16::GFP]* SY1407, *jaSi4;acr-16(ok789)* SY1422, *unc-63(x37); jaSi4;acr-16(ok789)* SY1423, *jaSi4;acr-16(ok789);EMS19* (6x) SY, *unc-63(x37); jaSi4;acr-16(ok789);EMS19* (4x) SY, *jaSi4;acr-16(ok789);EMS27* SY, *unc-63(x37);jaSi4;acr-16(ok789);EMS27* SY, *jaSi4;acr-16(ok789);EMS28* SY, *unc-63(x37);jaSi4;acr-16(ok789);EMS28* SY, *jaSi4;acr-16(ok789);UNC-29::RFP (kr208)* SY1568, *jaSi4;acr-16(ok789);EMS19;UNC-29::RFP(kr208)* SY1569, *jaSi4;acr-16;EMS28;UNC-29::RFP(kr208)* SY1570, *nrx-1(ok149)*, *jaSi4;acr-16(ok789);nrx-1(ok1649)*; SY 1598, *nlg-(ok259)*, *jaSi4;acr-16(ok789);nlg-1(ok259)* SY1596, *sca-1(tm5339)*, *jaSi4;sca-1(tm5339);acr-16(ok789)* SY1615, *ced-7(n1996)*, *jaSi4;ced-7(n1996);acr-16* SY1594, *vab-1(ok1699)*, *vab-1(e2027)*, *vab-1(ju8)*, *jaSi4;vab-1(ok1699);acr-16(ok789)* SY1597, *f59d12.1(gk1000)*, *jaSi4;acr-16(ok789);f59d12.1(gk1000)* SY1620. Animals were grown at 15-20° C on OP50-seeded NGM plates.

Forward Genetic Screen: Ethane methyl sulfonate (EMS) was used at a concentration of 50mM to mutagenize [L4](#) staged *unc-63(x37);jaSi4;acr-16(ok789)* animals. The worms were kept in the EMS solution for four hours. Following the four hour [EMS treatment](#), worms were washed in M9 buffer, placed on a large 2x NGM plate and allowed to recover for one hour. Eight mutagenized animals were picked to three large 2xNGM plates, for a total of 24 animals. These 24 animals served as the P0 generation and were allowed to propagate for three days. From this P0 generation, three F1s were picked to 60 separate plates and allowed to propagate for three days. After three days, approximately 30 F2 worms from each plate were mounted on 2% agarose pads and immobilized with 1mM sodium azide (Sigma, St. Louis, Missouri, United, States) and localization of ACR-16::GFP was examined. Animals showing a reduction in levels of ACR-16::GFP fluorescence levels were rescued off the pad and placed onto an NGM plate and allowed to propagate, creating independent lines.

Microscopy: Fluorescence images were obtained using an Olympus Fluoview™ FV10i laser-scanning confocal microscope with a 60x objective (oil-immersion) or a Fluoview™ laser-scanning confocal microscope with a 40x objective (oil-immersion). Worms were mounted on 2% agarose pads and immobilized with 20mM sodium azide (Sigma, St. Louis, Missouri, United, States) in M9. For analysis of ACR-16::GFP and UNC-29::RFP expression, maximum intensity Z-series stacks were made in the image analysis program ImageJ (imagej.nih.gov/ij).

Fluorescence levels were then measured at three locations along the length of the ventral nerve cord, anterior to the vulva, using a rectangular region of interest 10 μ m in length. For each measurement along the nerve cord, a corresponding measurement of background fluorescence level was taken. The background fluorescence level was then subtracted from the nerve cord fluorescence to control for variations in illumination intensity.

Behavior Analysis: Behavioral analysis was conducted on *jaSi4;acr-16(ok789)*, *unc-63(x37);jaSi4;acr-16(ok789)*, *jaSi4;acr-16(ok789);EMS19* (6x) SY, *unc-63(x37);jaSi4;acr-16(ok789);EMS19*; (4x) SY, *jaSi4;acr-16(ok789);EMS27* SY, *unc-63(x37);jaSi4;acr-16(ok789);EMS27* SY, *jaSi4;acr-16(ok789);EMS28* SY, *unc-63(x37);jaSi4;acr-169(ok789);EMS28* SY. Thrashing motility for individual worms in M9 medium was measured per minute for a total of three minutes. Body bend assays were performed on worms allowed to acclimate for one minute on unseeded agar plates. The number of full body bends completed by the worm in one minute was then counted. A body bend is counted when the head of the worm completes a full sinusoid.

Electrophysiology: The worm dissection and electrophysiological methods were done as previously described (50,74). Briefly, animals were immobilized with Histoacryl Blue glue, and a lateral cuticle incision was made with a borosilicate glass needle, exposing the ventral medial body wall muscles. Body wall muscle recordings were done in the whole-cell voltage-clamp configuration (holding

potential, -60 mV) using an EPC-10 patch-clamp amplifier and digitized at 1 kHz. The 5 mM Ca^{2+} extracellular solution consisted of 150 mM NaCl, 5 mM KCl, 5 mM CaCl_2 , 4 mM MgCl_2 , 10 mM glucose, 5 mM sucrose, and 15 mM HEPES (pH 7.3, ~ 340 mOsm). The patch pipette was filled with 120 mM KCl, 20 mM KOH, 4 mM MgCl_2 , 5 mM (N-tris[Hydroxymethyl] methyl-2-aminoethane-sulfonic acid), 0.25 mM CaCl_2 , 4 mM Na^2ATP , 36 mM sucrose, and 5 mM EGTA (pH 7.2, ~ 315 mOsm). Data were acquired using Pulse software (HEKA, Southboro, Massachusetts, United States) run on a Dell computer. Analysis and graphing was performed using Pulsefit (HEKA), Mini analysis (Synaptosoft Inc., Decatur, Georgia, United States) and Igor Pro (Wavemetrics, Lake Oswego, Oregon, United States).

Whole Genome Sequencing: Whole genome sequencing was done using the Variant Density method (75, 76). Briefly, animals with a phenotype of interest were backcrossed into the original mutagenized strain four times, following the [ACR-16::GFP](#) phenotype. Animals were grown on three to four large plates (150x15mm) until starved. DNA was then extracted using a Genra Puregene Kit (Quiagen, Hilden, Germany). Whole genome sequencing was performed at the University of Kansas Genome Sequencing Core Laboratories (gsc.ku.edu). TruSeq DNA libraries were constructed and used on a Hiseq 2500 platform (Illumina, San Diego, California, United States) with 100bp single reads at 40x coverage. [These](#) data [were](#) then analyzed using the CloudMap platform (76).

RNAi: In order to selectively knock down genes of interest, RNAi was done by

the feeding method (77). Briefly, NGM plates with carbenicillin and IPTG were poured and allowed to dry for approximately five days before seeding. Meanwhile bacteria containing the RNAi constructs of interest were taken from the Ahringer library glycerol stocks and inoculated into LB containing ampicillin and grown, shaking at 37°C, overnight. RNAi plates were then seeded and allowed to dry and induce overnight at room temperature. *jaSi4;acr-16(ok789)* worms were grown on standard NGM plates seeded with OP50 bacteria until there was a large population of adult animals with a sufficient number of eggs. A standard bleaching and washing protocol was used to isolate embryos, which were allowed to hatch in M9 overnight in a 20°C incubator. The starved L1s were then plated onto the prepared RNAi plates and allowed to grow to the desired stage for screening.

Statistical Analysis: Graphed data were plotted as mean and S.E.M, and significance was calculated using either the Mann-Whitney test or a ONE-way ANOVA with a Tukey post test correction. Statistically significant values were as follows: not significant ($p>0.05$), *($p\leq 0.05$), **($p\leq 0.01$), ***($p\leq 0.001$). Sample sizes for each experiment were determined using a type two error rate of 0.80 and a type one error rate of 0.05.

II.c Results

II.c.1 Forward mutagenesis screen using *jaSi4* [*Pmyo-3::acr-16::GFP*]

In order to identify previously unknown regulators of the NACHR ACR-16, a forward genetic screen was performed using the chemical mass mutagen EMS (Fig. 10A). EMS is the most commonly used mutagen in *C. elegans* and generally creates single base pair changes of G/C and A/T (78). A single copy insertion of ACR-16::GFP, generated using the MOSCI protocol, referred to as *jaSi4* (79), was used in an *acr-16(ok789)* mutant background for the mutagenized strain. This line was kept in the *acr-16* null background in order to prevent reduction of the ACR-16::GFP signal due to the presence of endogenous untagged ACR-16 receptors. The use of a single copy transgene should allow for the discovery of mutants with even a subtle reduction phenotype. After animals were mutagenized, their second generation (F2) progeny were screened for a reduction of ACR-16::GFP fluorescence (Fig. 10B). Approximately 5600 haploid genomes were screened and three mutant candidates were found, referred to as *EMS28*, *EMS27*, and *EMS19* based on their generation in an EMS screen.

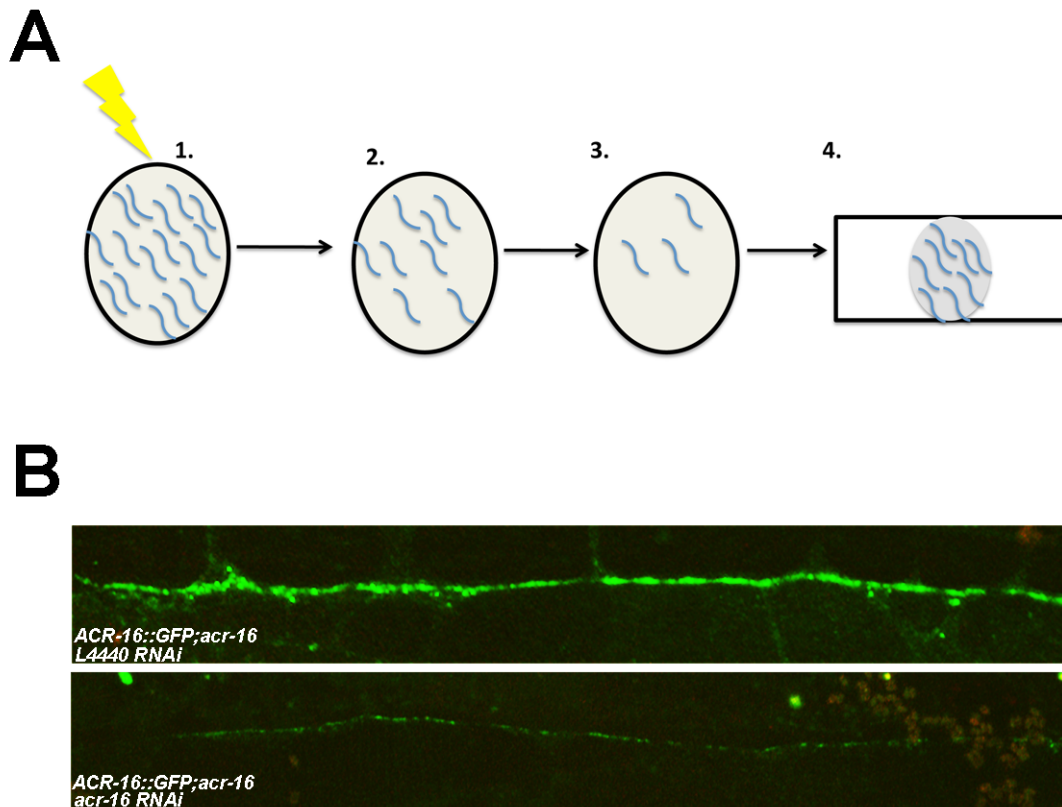
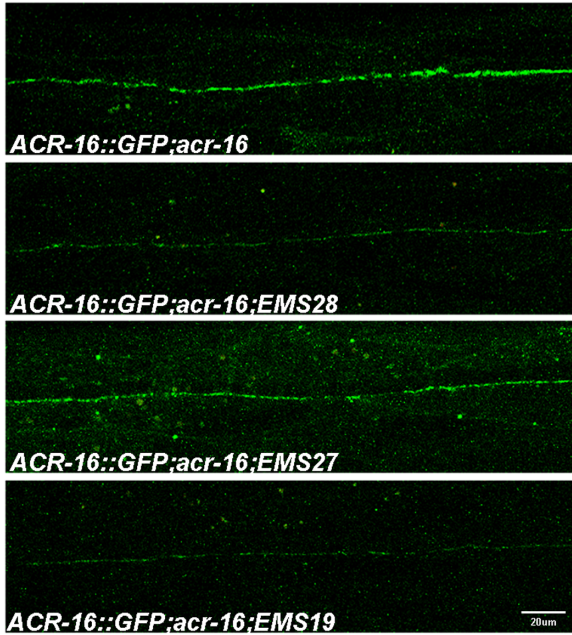


Figure 10. A forward genetic screen using EMS was done to identify regulators of the nAChR ACR-16. A. 1. Mutagenized L4 animals were allowed to recover for 8hrs on a large 2xNGM plate. 2. Eight animals were picked to 3 separate plates to establish the P0 generation. 3. Three F1 animals were picked to 60 separate plates and allowed to propagate. 4. Approximately 30 F2 animals from each of the 60 plates were mounted onto agar pads and ACR-16::GFP localization was examined. B. An example of the reduction in levels of ACR-16::GFP that was screened for. This reduction was generated using an *acr-16* specific RNAi construct.

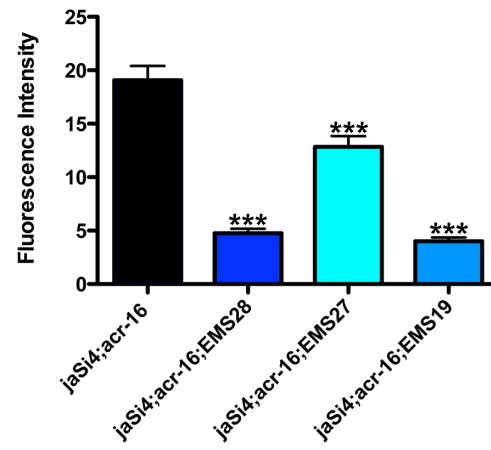
II.c.2 Quantification of ACR-16::GFP fluorescence levels in candidate EMS mutations

To evaluate the reduction in levels of ACR-16 in the *EMS* mutant backgrounds, fluorescence of ACR-16::GFP was quantified. All three mutants, *jaSi4;acr-16(ok789);EMS28*, *jaSi4;acr-16(ok789);EMS27*, and *jaSi4;acr-16(ok789);EMS19*, referred to from here as *EMS28*, *EMS27*, and *EMS19*, had a significant reduction in levels of ACR-16::GFP as compared to [the control strain *jaSi4;acr-16\(ok789\)*](#) (*EMS28*: 4.770 ± 1.857 n=7, *EMS27*: 12.838 ± 5.092 n=8, *EMS19*: 4.020 ± 1.567 n=7, control: 19.065 ± 7.443 n=10) suggesting that there is a significant reduction in expression of the ACR-16 receptor at the NMJ (Fig. 11A,B). The reduction of ACR-16::GFP was also quantified in an LACHR (*unc-63(x37)*) mutant background to verify that the reduction remained in these double mutant strains. Again, all three EMS mutants, *EMS28*, *EMS27*, and *EMS19*, had a significant reduction in levels of ACR-16::GFP fluorescence when compared to the control (*EMS28*: 4.514 ± 2.239 n=7, *EMS27*: 10.422 ± 7.226 n=5, *EMS19*: 4.467 ± 2.441 n=7, control: 26.070 ± 13.551 n=7) (Fig. 11C,D).

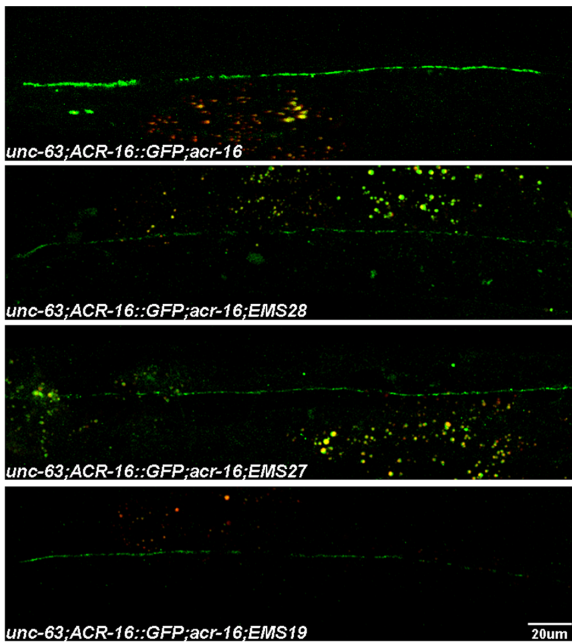
A



B



C



D

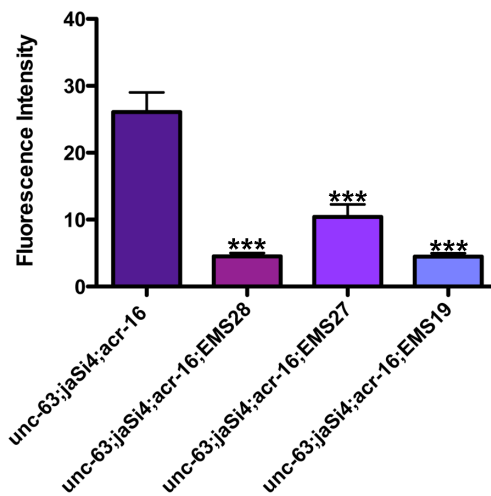


Figure 11. All three *EMS* mutations cause a reduction in ACR-16::GFP fluorescence levels at the NMJ of *C. elegans*. A. Representative images of ACR-16::GFP in *acr-16(ok789);EMS* mutant backgrounds. B. Quantification of ACR-16::GFP fluorescence at the NMJ demonstrated a significant decrease in ACR-16::GFP levels in the *EMS* mutants as compared to the control (*EMS28*: 4.770 ± 1.857 n=7, *EMS27*: 12.838 ± 5.092 n=8, *EMS19*: 4.020 ± 1.567 n=7, control: 19.065 ± 7.443 n=10). C. Representative images of ACR-16::GFP fluorescence in *unc-63(x37);acr-16(ok789);EMS* mutant backgrounds. D. Quantification of ACR-16::GFP shows a significant decrease in ACR-16::GFP levels in the *EMS* mutants as compared to the control (*EMS28*: 4.514 ± 2.239 n=7, *EMS27*: 10.422 ± 7.226 n=5, *EMS19*: 4.467 ± 2.441 n=7, control: 26.070 ± 13.551 n=7).

II.c.3 Behavioral analysis of EMS mutations

Touroutine et. al., (56) have shown that *acr-16(ok789)* mutants do not have any behavioral defects on their own. However, when crossed into the uncoordinated LACHR mutant *unc-63(x37)* to create a double mutant, the resulting worms are extremely uncoordinated and move very little, if at all. This information can be used to test if the *EMS* mutations affect ACR-16 function by evaluating their behavioral phenotypes in the *unc-63(x37)* mutant background. As expected, the *EMS* mutants alone had no significant difference as compared to control in the thrashing assay (Fig. 12A) and body bend assay (*EMS28*: 15.9 ± 4.228 n=10, *EMS27*: 16.7 ± 3.974 n=10, *EMS19*: 15.2 ± 3.910 n=10, control: 18.3 ± 4.029) (Fig. 12B). However, when thrashing and body bend phenotypes were examined in the *EMS* and *unc-63(x37)* double mutant backgrounds, there was a significant reduction in both number of thrashes (Fig. 12A) and body bends as compared to the LACHR mutant *unc-63(x37)* control (*EMS28*: 1.5 ± 1.4 n=10, *EMS27*: 3.8 ± 2.2 n=10, *EMS19*: 2.9 ± 1.4 n=10, control: 7 ± 3.1 n=10) (Fig. 12B). Based on the additivity of the motility defect, this implies that the ACR-16 receptor is affected by these *EMS* mutations, causing a locomotory defect.

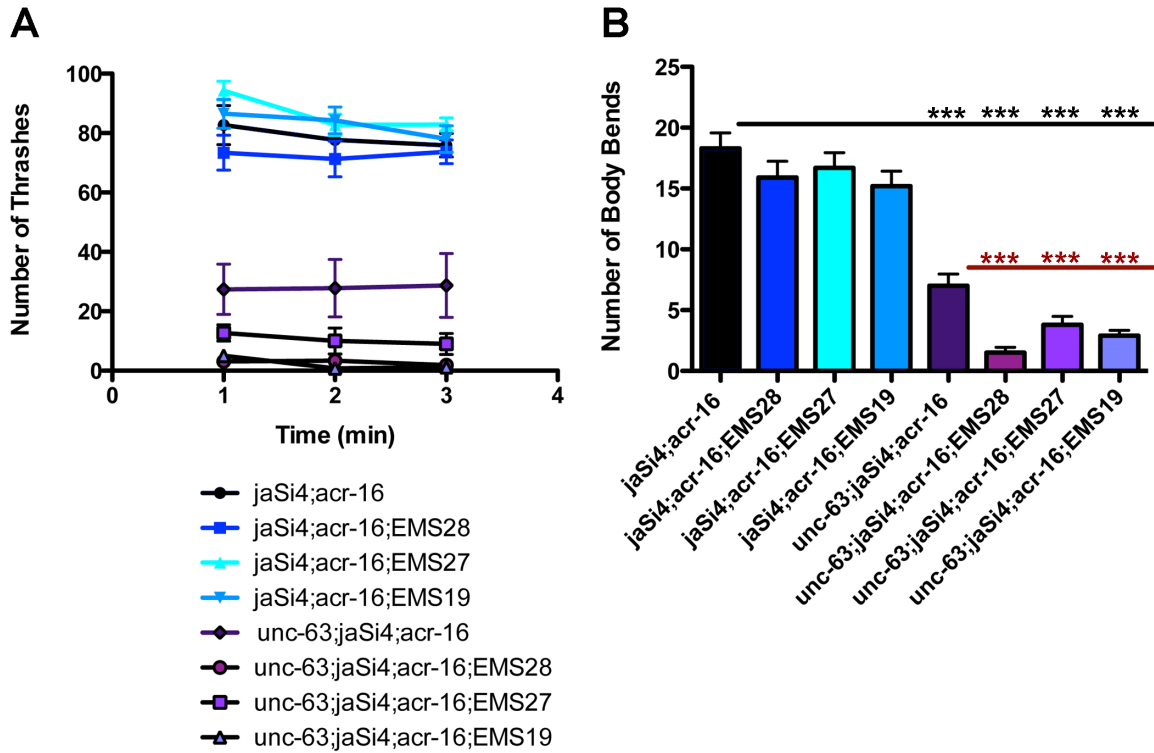


Figure 12. The *EMS* mutants alone do not have any locomotory defects, but *LACHR* double mutants have a severe motility defect. A. Thrashing assay to examine locomotion in the *EMS* mutants. The *EMS* mutants alone do not have any significant change in number of thrashes as compared to the control, however in the *LACHR* mutant background the *EMS* mutants have a significant reduction in number of thrashes as compared to the *LACHR* control. B. Body bend assay to examine locomotion in the *EMS* mutants. Alone, the *EMS* mutants do not have a significant change in the number of body bends as compared to the control (*EMS28*: 15.9 ± 4.228 $n=10$, *EMS27*: 16.7 ± 3.974 $n=10$, *EMS19*: 15.2 ± 3.910 $n=10$, control: 18.3 ± 4.029), however in the *LACHR*;*EMS* double mutant background there is a significant decrease in the number of body bends as compared to the *LACHR* control (*EMS28*: 1.5 ± 1.4 $n=10$, *EMS27*: 3.8 ± 2.2 $n=10$, *EMS19*: 2.9 ± 1.4 $n=10$, control: 7 ± 3.1 $n=10$).

II.c.4 Evaluations of LAChR levels and localization in *EMS* mutants

There are two cholinergic receptor types at the *C. elegans* [NMJ](#), and it is important to examine if the *EMS* mutations are affecting only the ACR-16 receptor type or if they are acting on the LAChR as well. To do this the *EMS* mutants were crossed into a line that expressed a RFP tagged UNC-29 subunit of the LAChR. Levels of RFP fluorescence were quantified and localization was examined in the *EMS* mutant backgrounds. The two mutants that were imaged, *EMS19* and *EMS28*, had no significant difference in RFP fluorescence levels as compared with the control, and there seemed to be no gross change in RFP localization (*EMS19*: 10.7 ± 9.6 n=10, 10.7 ± 3.7 n=6, *EMS28*: 11.8 ± 5.1 n=13) (Fig. 13A,B). This result suggested that the *EMS* mutants were affecting the ACR-16 receptor specifically.

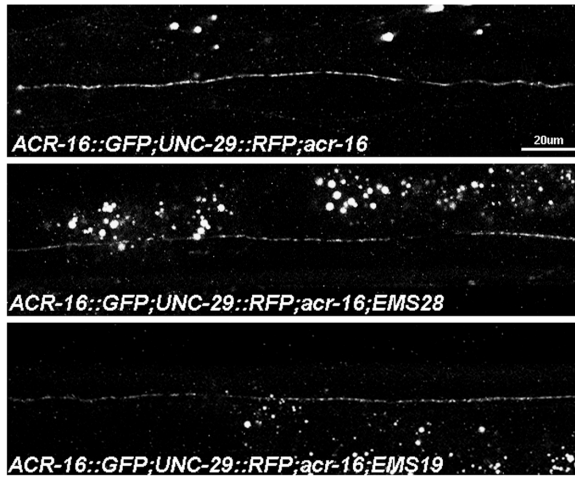
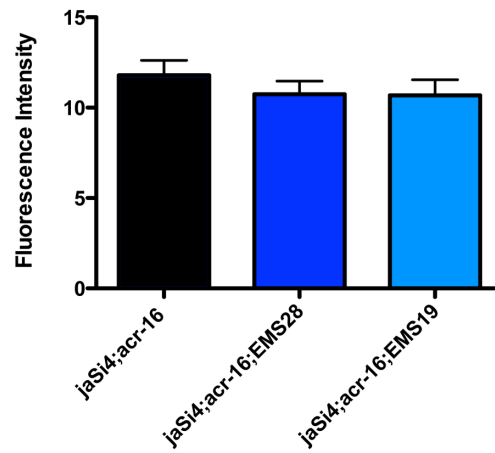
A**B**

Figure 13. Expression and localization of the LChRs was unchanged in the *EMS* mutants. A. Representative images of UNC-29::RFP fluorescence levels and localization in the *EMS* mutants. B. Quantification of UNC-29::RFP fluorescence in the *EMS* mutants demonstrated no change in UNC-29::RFP intensity as compared to the control (*EMS19*: 10.7 ± 9.6 n=10, 10.7 ± 3.7 n=6, *EMS28*: 11.8 ± 5.1 n=13).

The *EMS27* mutant could not be evaluated with the UNC-29::RFP construct because of the level of ACR-16::GFP reduction in the *EMS27* mutant background. Although the levels of ACR-16::GFP were significantly reduced, it was not as dramatic as in the other two *EMS* mutants. This made generating different lines, especially those with added fluorescence markers, difficult to confidently homozygous for the *EMS27* ACR-16::GFP reduction phenotype. Other ways of evaluating LACHR were used for this mutant line, discussed below.

II.c.5 Electrophysiological analysis of *EMS* mutants

Based on the changes in ACR-16 receptor expression at the NMJ and the increased locomotory deficits seen in the ACR-16 LACHR double mutants, a change in synaptic transmission **was** expected in the *EMS* mutant backgrounds. The effect of these mutations on evoked response levels in dissected animals *in vivo* was examined using whole cell patch clamp techniques. All three *EMS* mutations caused a significant reduction in postsynaptic evoked amplitude compared to the control responses (Fig. 14A,B) (*EMS28*: 812.7 ± 513.6 n=6, *EMS27*: 1230 ± 624.2 n=7, *EMS19*: 716.3 ± 417.5 n=6, control: 2452.6 ± 459.4 n=8). This **indicates** that the *EMS* mutations affect postsynaptic receptor function.

Pressure-ejecting specific agonists onto dissected *C. elegans* allows for the analysis of the response of each of the **two** specific cholinergic receptor types at the synapse. Levamisole was used to selectively activate the LACHRs in each of the *EMS* mutant backgrounds. If the **total** number of **muscle** LACHRs were reduced, then a reduction in the pressure-ejected response would be seen. The amplitude of the

response in each of the *EMS* mutant backgrounds was not significantly reduced as compared to the control (Fig. 14C,D) (*EMS28*: 198.6 ± 24.7 n=5, *EMS27*: 199.8 ± 39.6 n=5, *EMS19*: 261.6 ± 126.6 n=7, control: 238.7 ± 97.5 n=11). **These** data, as well as the fluorescence imaging which showed no change in UNC-29::RFP levels, demonstrates that the *EMS* mutants specifically affect the NACHR ACR-16 at the NMJ.

To further understand how the *EMS* mutants are affecting the ACR-16 receptor, nicotine was pressured-ejected onto **muscles of the** dissected *C. elegans* preparation. In the *EMS28* and *EMS19* mutants there was a significant reduction in **current** amplitude in response to pressure-ejected nicotine when compared to the control (*EMS28*: 420 ± 213.1 n=4, *EMS19*: 460.3 ± 331 n=4, control: 1130.8 ± 355.3 n=6). This suggests a defect in **either ACR-16** receptor trafficking or assembly, or an increase in receptor degradation. In the *EMS27* mutant background there was no change in the response amplitude when nicotine **was** pressure-ejected when compared to the control (Fig. 14E,F) (*EMS27*: 1336.8 ± 371.1 n=5, control: 1130.8 ± 355.3 n=6). This suggests that the receptors were present and functional **on the muscle membrane**, but may be dispersed and no longer localized to the synapse.

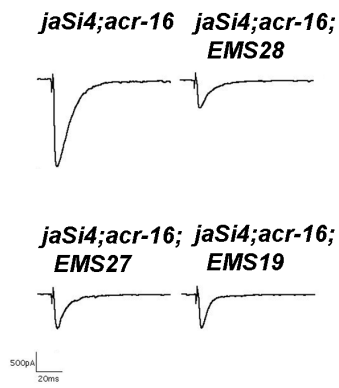
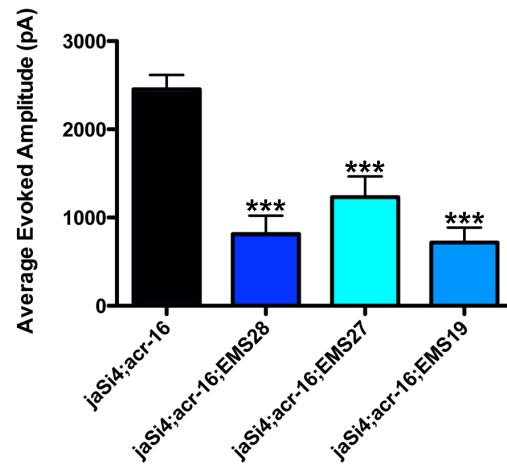
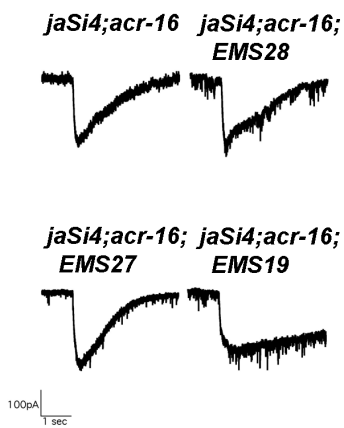
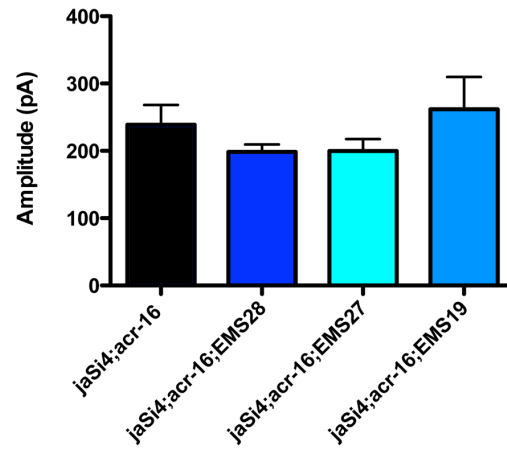
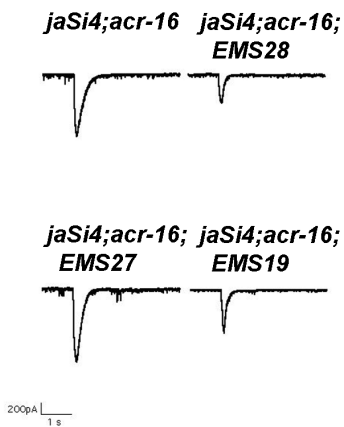
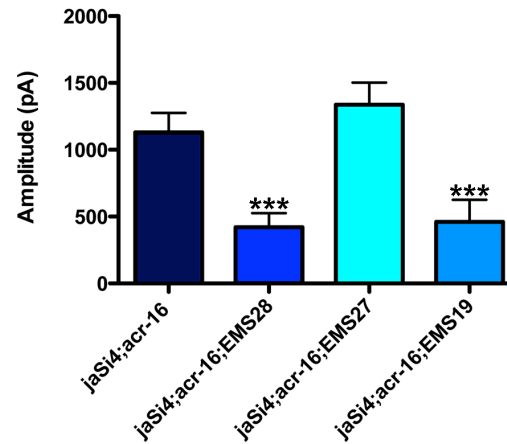
A**B****C****D****E****F**

Figure 14. Changes in synaptic transmission were observed in the *EMS* mutants. A. Representative traces of evoked postsynaptic amplitudes in the *EMS* mutants. B. Quantification of the evoked postsynaptic currents in the *EMS* mutants demonstrated that all three mutants have a significant decrease in average amplitude as compared to the control (*EMS28*: 812.7 ± 513.6 n=6, *EMS27*: 1230 ± 624.2 n=7, *EMS19*: 716.3 ± 417.5 n=6, control: 2452.6 ± 459.4 n=8). C. Representative traces of pressure-ejected levamisole amplitudes dissected *EMS* mutant worms. D. Quantification of pressure-ejected levamisole elicited amplitudes showed that there was no significant difference in amplitude size in the *EMS* mutants as compared to the control (*EMS28*: 198.6 ± 24.7 n=5, *EMS27*: 199.8 ± 39.6 n=5, *EMS19*: 261.6 ± 126.6 n=7, control: 238.7 ± 97.5 n=11). E. Representative traces of pressure-ejected nicotine amplitudes in *EMS* mutants. F. Quantification of the amplitudes elicited from pressure-ejected nicotine. *EMS28* and *EMS19* have significantly reduced amplitudes as compared to the control (*EMS28*: 420 ± 213.1 n=4, *EMS19*: 460.3 ± 331 n=4, control: 1130.8 ± 355.3 n=6). Amplitudes in *EMS27* mutants were unchanged as compared to the control (*EMS27*: 1336.8 ± 371.1 n=5, control: 1130.8 ± 355.3 n=6).

II.c.6 Whole genome sequencing to determine the identity of EMS mutants

In order to determine the identity of the genes that were perturbed in [the EMS28, EMS27 and EMS19 mutants](#), Whole Genome Sequencing was performed using the Variant Density Mapping approach (Fig. 15A). The CloudMap platform was used to subtract background mutations that were found in the original mutagenized strain and common mutations found in the three *EMS* mutant lines. This [narrowed down](#) the target mutation [to the following chromosomes](#): chromosome III for *EMS28* and chromosome II for *EMS27* (Fig. 15B). By evaluating the levels of ACR-16::GFP in heterozygous mutant males, it was determined that the target mutation was on the X chromosome in *EMS19* (Fig. 15B), as males with a single copy of the *EMS19* mutation still exhibited a significant reduction in ACR-16::GFP expression (data not shown).

From the data entered into and run using a CloudMap based algorithm, a list of possible gene candidates was generated. The location of these genes corresponded to the chromosome isolated in the original analysis, and were selected based on the presence of a mutation causing a non-synonymous amino acid change or a mutation in a regulatory region of a gene. The gene candidates for *EMS28* were *sca-1* and *ced-7*, the gene candidate for *EMS27* was *vab-1*, and the gene candidates for *EMS19* were *nrx-1*, *nlg-1*, *f59d12.1*, *f52g3.1*, *c04c11.1*, *pqn-36*, and *c44h4.4*.

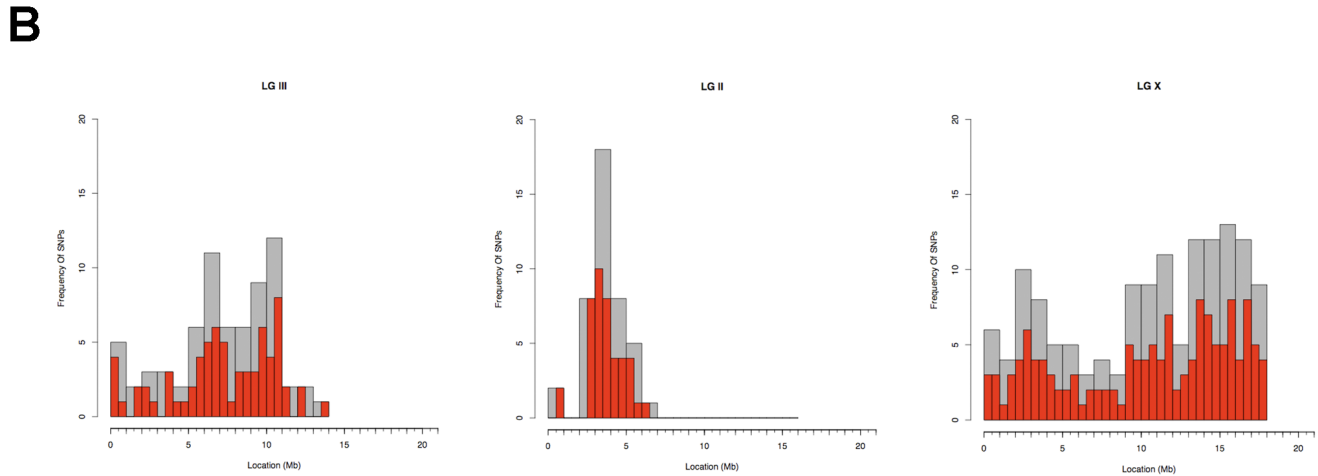
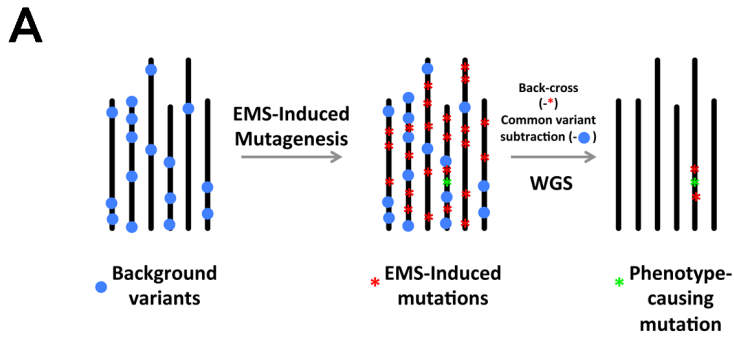


Figure 15. Whole genome sequencing and analysis with CloudMap was done to determine the mutated loci in the *EMS* mutants. A. Model of the variant density mapping approach, which was used to determine the mutated loci in the *EMS* mutants. B. After analysis of the whole genome sequencing results using the CloudMap platform, the chromosomes where the *EMS* mutations were located were determined. *EMS28* was located on chromosome II, *EMS27* was located on chromosome III, and *EMS19* was located on the X chromosome.

II.c.7 Quantification of ACR-16::GFP fluorescence intensity in candidate gene mutant backgrounds

Once the candidate genes had been identified, it was necessary to examine the effects of mutations in **each of** them on levels of ACR-16::GFP, as this was the original phenotype used in the gene identification. **When available, reference mutants** for each of the candidate genes were obtained, from either the Caenorhabditis Genetics Center (CGC) or the National BioResource Project (NBRP) and crossed into the *jaSi4;acr-16(ok789)* background. Levels of ACR-16::GFP fluorescence were then analyzed in these newly created **strains**.

The mutant alleles obtained for the *EMS28* gene candidates were *sca-1(tm5339)* and *ced-7(n1996)*. Fluorescence levels of ACR-16::GFP were examined in these mutant backgrounds and a significant reduction in fluorescence was **observed** in the *sca-1(tm5339)* mutant as compared to the control (*sca-1(tm5339)*: 17.7 ± 8.0 n=20, control: 26.7 ± 10.1 n=44) (Fig. 16A,B). However, there was no significant change in ACR-16::GFP fluorescence levels in the *ced-7(n1996)* mutant background (*ced-7(n1996)*: 28.1 ± 11.2 n=19, control: 26.7 ± 10.1 n=44). Based on **these results** *sca-1* was further evaluated as a regulator of ACR-16 and *ced-7* was no longer pursued.

vab-1 was the candidate gene identified from the Whole Genome Sequencing of *EMS27* and the mutant allele that was procured was *vab-1(ok1699)*. The mutant allele was crossed into *jaSi4;acr-16(ok789)*, and this new **strain** was used to evaluate the levels of ACR-16::GFP fluorescence. When compared to control levels of fluorescence, there was a significant reduction in the *vab-1(ok1699)* mutant (*vab-*

1(*ok1699*): 21.9 ± 7 n=21, control: 26.7 ± 10.1 n=44). (Fig. 16A,B) This reduction suggested that the *EMS27* mutation may be in the *vab-1* gene.

There were not many mutant alleles available for the gene candidates for *EMS19*, so RNAi was **used** to evaluate changes in ACR-16::GFP. First, mutant alleles *nrx-1(ok149)* and *nlg-1(ok259)* were crossed into *jaSi4;acr-16(ok789)*. These newly created lines were imaged to analyze levels of ACR-16::GFP **and** no significant change in fluorescence **was found when** compared to the control, **decreasing the likelihood that** these genes **are** possible **loci** for *EMS19* (*nrx-1(ok149)*: 28.0 ± 11.3 n=21, *nlg-1(ok259)*: 28.9 ± 9.6 n=20, control: 26.7 ± 10.1 n=44) (Fig. 16A,B). Next, using the feeding method, RNAi was **performed on** *jaSi4;acr-16(ok789)* animals **for** constructs against *f59d12.1*, *f52g3.1*, *c04c11.1*, *pqn-36*, and *c44h4.4*. A **RNAi** construct **against** *acr-16* was also included as a positive control. **When** compared to the control, **neither** the empty RNAi construct L4440, **nor the candidate gene constructs exhibited a** significant change in ACR-16::GFP fluorescence levels (*f59d12.1*: 25.9 ± 8.9 n=10, *f52g3.1*: 23.6 ± 8.1 n=9, *c04c11.1*: 23.2 ± 8.8 n=11, *pqn-36*: 22.8 ± 5.2 n=5, *c44h4.4*: 25.4 ± 5.6 n=5, and L4440: 23.5 ± 6.8 n=12), **whereas the *acr-16* RNAi eliminated ACR-16::GFP fluorescence** (*acr-16*: 6.9 ± 4.5 n=10, L4440: 23.5 ± 6.8 n=12) (Fig. 16C,D). This does not, however, rule out all of these genes, as it is possible that the RNAi library from which the constructs were obtained was compromised by age of the library, library storage conditions, or validity of the original constructs. Finally a mutant allele, *f59d12.1(gk1000)*, was obtained and crossed into *jaSi4;acr-16(ok780)* and ACR-16::GFP levels were evaluated. **A significant reduction in fluorescence levels was observed when** compared to the control, suggesting that the

EMS19 mutation is in the *f59d12.1* gene (*f59d12.1(gk1000)*): 12.8 ± 5.0 n=9, control: 29.1 ± 8.6 n=11) (Fig. 16E,F).

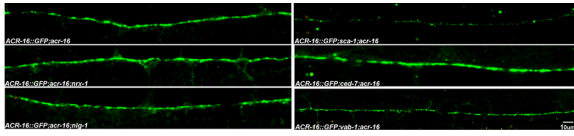
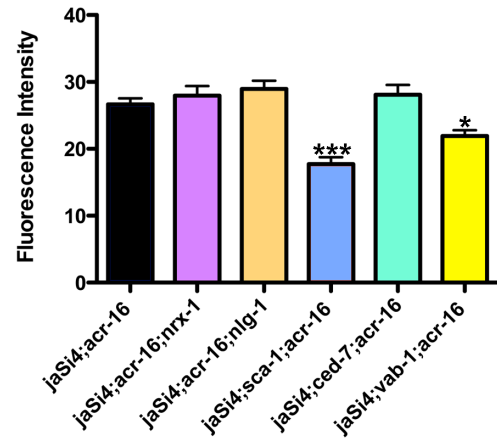
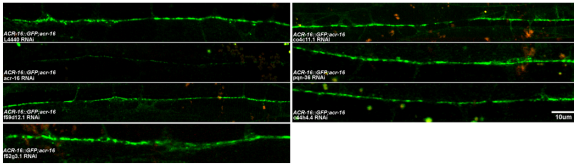
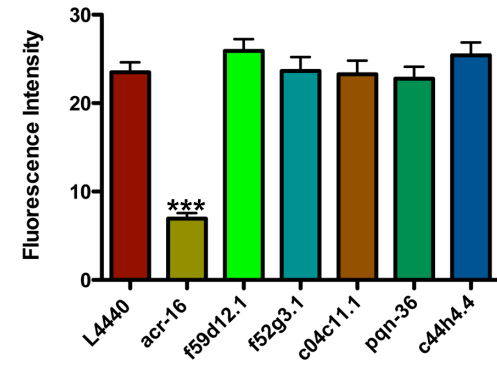
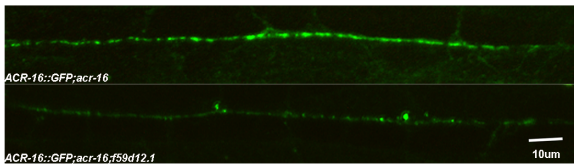
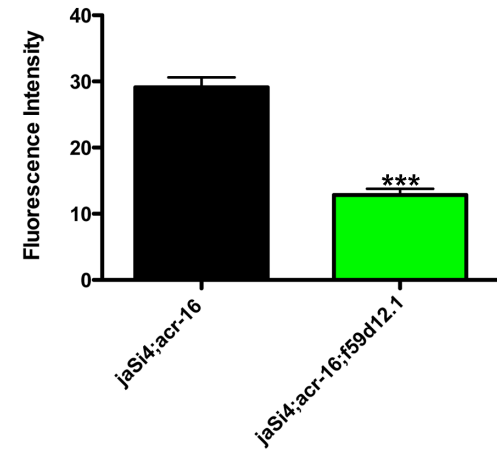
A**B****C****D****E****F**

Figure 16. Evaluation of ACR-16::GFP in candidate mutants. A. Representative images of ACR-16::GFP fluorescence levels in candidate mutants determined by whole genome sequencing. B. Quantification of ACR-16::GFP fluorescence levels demonstrated that *sca-1(tm5339)* and *vab-1(ok1699)* mutants caused a significant decrease in ACR-16::GFP at the NMJ as compared to the control, whereas the other mutants evaluated did not cause a significant change (*sca-1(tm5339)*: 17.7 ± 8.0 n=20, *ced-7(n1996)*: 28.1 ± 11.2 n=19, *vab-1(ok1699)*: 21.9 ± 7 n=21, *nrx-1(ok149)*: 28.0 ± 11.3 n=21, *nlg-1(ok259)*: 28.9 ± 9.6 n=20, control: 26.7 ± 10.1 n=44). C. Representative images of ACR-16::GFP fluorescence levels in *jaSi4;acr-16(ok789)* animals treated with RNAi constructs against *EMS19* candidate genes. D. Quantification of ACR-16::GFP fluorescence levels showed that none of the RNAi constructs caused any significant change in ACR-16::GFP fluorescence intensity as compared to the control (*f59d12.1*: 25.9 ± 8.9 n=10, *f52g3.1*: 23.6 ± 8.1 n=9, *c04c11.1*: 23.2 ± 8.8 n=11, *pqn-36*: 22.8 ± 5.2 n=5, *c44h4.4*: 25.4 ± 5.6 n=5, and L4440: 23.5 ± 6.8 n=12). E. Representative images of changes in ACR-16::GFP fluorescence in the *f59d12.(gk1000)* mutant. F. Quantification of ACR-16::GFP fluorescence levels in the *f59d12.1(gk1000)* mutant showed a significant reduction as compared to the control (*f59d12.1(gk1000)*: 12.8 ± 5.0 n=9, control: 29.1 ± 8.6 n=11).

II.c.8 Confirmation of candidate gene identity

Once genes that phenocopied the reduction in ACR-16::GFP were found, it was necessary to test if they were, in fact, the same genes that were perturbed in the *EMS* mutants. To do this complementation tests were done using the previously evaluated gene candidate mutant lines crossed into the appropriate *EMS* mutant males. F1 hermaphrodites from the cross were imaged and levels of ACR-16::GFP were evaluated. If the lesion was found in the same gene in each of the mutant lines, then a significant reduction in ACR-16::GFP should be seen in the F1 population. As the *EMS* mutants tended to have a higher reduction in ACR-16::GFP levels, males were generated using the *EMS* mutants through heat shock. Once imaged, F1 animals were genotyped for the candidate mutations and only images from worms that were heterozygous, implying they were the cross progeny, were analyzed.

Based on this [analysis](#), all three candidate genes that previously showed a significant reduction of ACR-16::GFP levels continued to show a significant reduction when crossed over their appropriate *EMS* mutation as compared to the control. This showed non-complementation of *sca-1(tm5339)* and *EMS28 (EMS28: 8.9±4.3 n=8, sca-1: 18.4±5.8 n=6, EMS28xsca-1:13.8±5.3 n=20, control: 27.7±9.5 n=9)* (Fig. 17A,B) *vab-1(ok1699)* and *EMS27 (EMS27: 19.5±5.6 n=19, vab-1: 22.6±6.1 n=13, EMS27xvab-1: 15.9±6.0 n=25, control: 24.7±8.7 n=16)* (Fig. 17C,D), and *f59d12.1(gk1000)* and *EMS19 (EMS19: 6.6±1.7 n=7, f59d12.1: 15.1±3.7 n=10, EMS19xf59d12.1: 11.9±3.3 n=15, control: 23.4±8.0 n=16)* (Fig. 17E,F), suggesting that the lesions are found in the same gene and confirming the identification of new regulators of ACR-16 receptors.

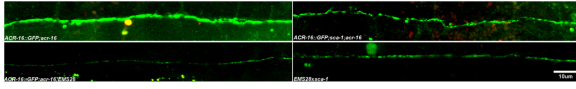
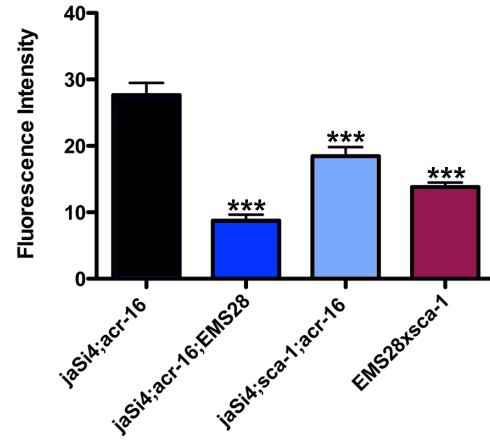
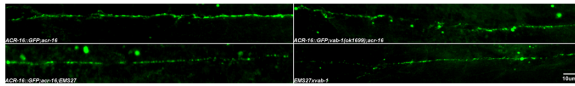
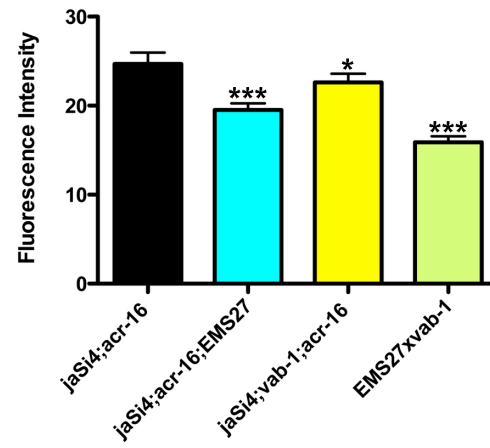
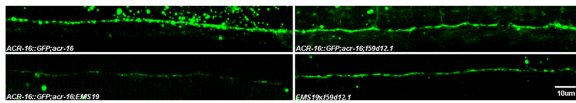
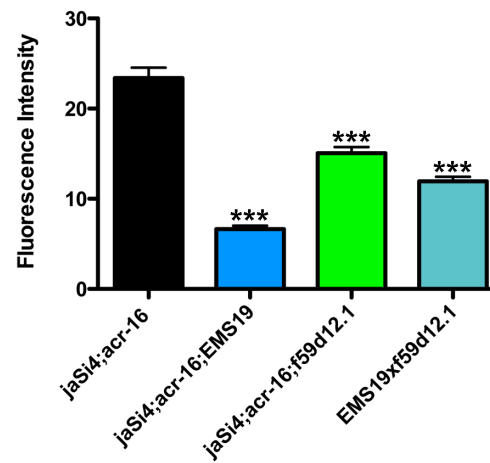
A**B****C****D****E****F**

Figure 17. EMS mutants and candidate genes are non-complimentary. A.

Representative images of ACR-16::GFP fluorescence in *EMS28*, *sca-1(tm5339)*, and *EMS28xsca-1* mutants. B. Quantification of ACR-16::GFP demonstrated a significant decrease in *EMS28* and *sca-1(tm5339)* mutants, and *EMS28xsca-1* mutants (*EMS28*: 8.9 ± 4.3 n=8, *sca-1*: 18.4 ± 5.8 n=6, *EMS28xsca-1*: 13.8 ± 5.3 n=20, control: 27.7 ± 9.5 n=9). C. Representative images of ACR-16::GFP fluorescence in *EMS27*, *vab-1(ok1699)*, and *EMS27xvab-1* mutants. D. Quantification of ACR-16::GFP fluorescence showed a significant decrease in *EMS27*, *vab-1(ok1699)* mutants, and the *EMS27xvab-1* mutants (*EMS27*: 19.5 ± 5.6 n=19, *vab-1*: 22.6 ± 6.1 n=13, *EMS27xvab-1*: 15.9 ± 6.0 n=25, control: 24.7 ± 8.7 n=16). E. Representative images of ACR-16::GFP fluorescence in *EMS19*, *f59d12.1(gk1000)*, and *EMS19xf59d12.1(gk1000)*. F. Quantification of ACR-16 fluorescence levels demonstrated a significant reduction in *EMS19*, *f59d12.1(gk1000)* mutants, and *EMS19xf59d12.1(gk1000)* mutants (*EMS19*: 6.6 ± 1.7 n=7, *f59d12.1*: 15.1 ± 3.7 n=10, *EMS19xf59d12.1*: 11.9 ± 3.3 n=15, control: 23.4 ± 8.0 n=16).

II.d Discussion

Using chemical [mutagenesis](#), [in a](#) forward genetic screen, three new regulators of the ACR-16 receptor were identified. When originally identified in the screen these mutants, referred to as *EMS28*, *EMS27*, and *EMS19*, all showed a significant reduction in ACR-16::GFP fluorescence levels and a significant reduction in evoked response amplitudes, suggesting that the NACHRs were affected. The effect of these *EMS* mutations on the second class of NMJ cholinergic receptor, LACHRs, was evaluated using fluorescence microscopy and electrophysiology, which demonstrated that the *EMS* mutations were acting [specifically](#) on the ACR-16 receptor. Whole genome sequencing was done to determine the genes perturbed in the screen. Using Variant Density Mapping, *sca-1*, *vab-1*, and *f59d12.1* were identified as gene candidates for *EMS28*, *EMS27*, and *EMS19*, respectively. Non-complementation between these mutants suggested [ed](#) that the lesions were in the [identified](#) genes.

Further characterization of these genes needs to be done to understand their role in affecting ACR-16 receptor function. It is possible, based on the widely different predicted functions of these genes, that novel [regulatory](#) pathways for NACHRs will be discovered. [Given the highly-conserved nature of these genes, it is plausible that these pathways will not only function at the C. elegans NMJ but also in the nervous systems of many organisms, given that both ACR-16 and its mammalian homolog \$\alpha 7\$ are expressed in a subset of neurons.](#)

III. The *C. elegans* sarcoplasmic reticulum calcium-ATPase regulates nicotinic acetylcholine receptor ACR-16 expression

III.a Introduction

Calcium is an important intracellular messenger, increases in internal calcium activating many processes including but not limited to neurotransmitter release, synaptic plasticity, and cell survival ⁽⁸⁰⁾. In vertebrate systems, nAChRs have been shown to mediate calcium entry by depolarizing the plasma membrane leading to voltage-gated calcium channel activation and/or through intrinsic nAChR calcium permeability. The homopentameric $\alpha 7$ receptors found in neurons are the most calcium permeable of nAChRs found in the central nervous system and have been implicated in a number of calcium mediated signaling cascades ^(81, 82, 2). Proteins that regulate the levels of nAChRs present at these synapses are therefore positioned to affect levels of calcium entry and in turn modulate the strength of calcium driven signaling mechanisms.

Internal pathways of calcium release and removal are well characterized. When calcium enters the cell through nicotinic acetylcholine receptors, it can cause calcium influx as well as calcium-induced calcium release (CICR) via ryanodine receptors and inositol (1,4,5)-triphosphate (IP3) receptors located on either the sarcoplasmic or endoplasmic reticulum ⁽⁸³⁾. The release of calcium from these two internal receptor types has different kinetics. The ryanodine receptors open rapidly upon membrane depolarization or calcium influx. The IP3 receptors are activated through a calcium triggered signaling cascade involving PIP₂ cleavage to produce IP3, and causes a slower wave of internal calcium release. This biphasic release

process can result in a large, transient increase in cytoplasmic calcium concentrations, at times as much as 100 fold [that of](#) resting calcium ^(80, 84). The termination of this calcium signal [involves the](#) sarco(endo)plasmic reticulum calcium ATPases (SERCA). SERCAs are P-type calcium pumps containing two calcium-binding sites, which are located in transmembrane helices (Periasamy, 2007). In vertebrates there are three SERCA genes and at least ten different isoforms, [specific](#) genes and isoforms functioning in different cell types (Gehlert, 2015). SERCA pumps work together with plasma membrane calcium ATPases and Na⁺/Ca²⁺-K⁺ exchangers to maintain resting internal calcium levels, in mammalian muscles SERCA pumps being the primary calcium clearance mechanism into the sarcoplasmic reticulum ⁽⁸⁵⁾.

The single *C. elegans* SERCA gene, encoded by *sca-1*, was recently identified in a genetic screen looking for regulators of *C. elegans* ACR-16 NACHRs, which are homologous to vertebrate $\alpha 7$ [receptors](#) (56, ⁸⁶). Little is known about the function of SCA-1 in *C. elegans*, or its potential role in the regulation of synaptic transmission. To gain further insights, a viable hypomorphic allele of *sca-1* was characterized.

III.b Materials and Methods

Strains and Culturing Conditions: The genotypes of nematode strains used in this study are: the wild-type Bristol isolate N2, *jaSi4[Pmyo-3::ACR-16::GFP]* SY1407, *jaSi4;acr-16(ok789)* SY1422, *sca-1(tm5339)*, *jaSi4; sca-1(tm5339)*; *acr-16(ok789)* SY1615, *ACR-16::RFP(kr305)*, *sca-1(tm5339);ACR-16::RFP(kr305)* SY1641, *jaSi4;acr-16(ok789);UNC-29::RFP (kr208)* SY1568, *sca-1(tm5339);UNC-*

29::RFP(kr208) SY1619, *oxIs22[Punc-47::UNC-47::GFP]*, *sca-1(tm5339)*; *oxIs22* SY, *unc-63(x37)*; *sca-1(tm5339)* SY1626, *acr-16(ok789)*, *unc-63(x37)*, *unc-63(x37)*; *acr-16(ok789)*, *jaIs1103[Pacr-2::mCherry::RAB-3]*, *sca-1(tm5339)*; *jaIs1103* SY1616, *raIs5[Pmyo-3-3::GFP::MYO-3]*, *sca-1(tm5339)*; *raIs5[pMYO-3::GFP::MYO-3]* SY1630, , *jaSi4*; *sca-1(tm5339)*; *acr-16(ok789)*; *jaEx1064[Pmyo-3::SCA-1::mCherry]* SY, *zxIs1481[zxIs6{Punc17::chop-2(H134R)::yfp,lin-15(+)};Pmyo3::RCaMP35]*, *sca-1(tm5339)*; *zxIs1481* SY1627. Animals were grown at 15-20° C on OP50-seeded NGM plates. For electrophysiological recordings, *zxIs6* and mutants crossed into *zxIs6* were cultured in the dark at 20°C on OP50-seeded NGM plates supplemented with all-*trans* retinal at a final concentration of 500uM.

Cloning: The multisite gateway three-fragment vector construction protocol (Invitrogen, Carlsbad, California, United States) was used to generate the *sca-1* expression vector *jaEx1064[Pmyo-3::SCA-1::Mcherry::unc-54::3'UTR]*. Primers 5'GGGGACCACTTTGTACAAGAAAGCTGGGTGGTAACTTGTCTGGGCGTGA and 5'GGGGACAAGTTTGTACAAAAAAGCAGGCTGGCGCCAGTGTGTGCCATATC were used to amplify the coding region of *sca-1*, omitting the stop codon, from adult hermaphrodite genomic DNA using Phusion High-Fidelity DNA Polymerase (NEB, Ipswich, Massachusetts, United States). The PCR product was then cloned into pDONR221. A 2500bp sequence from the MYO-3 promoter region was amplified using primers 5'GGGGACAACCTTTGTATAGAAAAGTTGGGAGTGATTATAGTCTCTGTTTTTC and 5'GGGGACTGCTTTTTTGTACAACTTGGTTCTAGATGGATCTAGTGGTC, again from

adult hermaphrodite genomic DNA using Phusion High-Fidelity DNA Polymerase (NEB, Ipswich, Massachusetts, United States). This PCR product was then cloned into pDONOR P4-P1r. The pDONOR P2R-P3 vector including Mcherry and an *UNC-54::3'UTR* was graciously gifted from Marc Hammarlund. A ligation reaction was then performed to build all three donor vectors into the final gateway destination vector, pDEST R4-R3 Vector II, producing a C-terminally mCherry-tagged SCA-1 under the *myo-3* promoter.

Microscopy: Fluorescence images were obtained using an Olympus Fluoview™ FV10i laser-scanning confocal microscope with a 60x objective (oil-immersion) or a Fluoview™ laser-scanning confocal microscope with a 40x objective (oil-immersion). Worms were mounted on 2% agarose pads and immobilized with 20mM sodium azide (Sigma, St. Louis, Missouri, United States) in M9. For analysis of ACR-16::GFP, ACR-16::RFP, UNC-29::RFP, MYO-3::GFP, and UNC-47::GFP expression, maximum intensity Z-series stacks were made in the image analysis program ImageJ (imagej.nih.gov/ij). Fluorescence levels were then measured at three locations along the length of the ventral nerve cord, anterior to the vulva, using a rectangular region of interest **10µm in length**. For each measurement along the nerve cord, a corresponding measurement of background fluorescence level was taken. The background fluorescence level was then subtracted from the nerve cord fluorescence level to control for variations in illumination intensity. For analysis of synaptic puncta, maximum intensity Z-series

stacks were made in ImageJ and a 50 μ m region of the dorsal nerve cord was cropped out. The threshold of this image was set in ImageJ to include only the synaptic puncta present. The puncta analyzer tool in ImageJ was used to determine the number of puncta found per 50 μ m of nerve cord.

Behavioral Analysis: Behavioral analysis was conducted on N2, *acr-16(ok789)*, *unc-63(x37)*, *unc-63(x37);acr-16(ok789)*, *sca-1(tm5339)*, and *unc-63(x37);sca-1(tm5339)*. Body bend assays were **performed** on worms allowed to acclimate for one minute on unseeded agar plates. The number of full body bends completed by the worm in one minute was then counted. A body bend is counted when the head of the worm completes a full sinusoid.

Electrophysiology: The **worm** dissection and electrophysiological methods were done as previously described (50,74). Briefly, animals were immobilized with Histoacryl Blue glue, and a lateral cuticle incision was made with a borosilicate glass needle, exposing the ventral medial body wall muscles. Body wall muscle recordings were done in the whole-cell voltage-clamp configuration (holding potential, -60 mV) using an EPC-10 patch-clamp amplifier and digitized at 1 kHz. The 1 mM Ca²⁺ extracellular solution composed of 150 mM NaCl, 5 mM KCl, 1mM CaCl₂, 4 mM MgCl₂, 10 mM glucose, 5 mM sucrose, and 15 mM HEPES (pH 7.3, ~340 mOsm). The patch pipette was filled with 120 mM KCl, 20 mM KOH, 4 mM MgCl₂, 5 mM (N-tris[Hydroxymethyl] methyl-2-aminoethane-sulfonic acid), 0.25 mM CaCl₂, 4

mM Na²ATP, 36 mM sucrose, and 5 mM EGTA (pH 7.2, ~315 mOsm). Data were acquired using Pulse software (HEKA, Southboro, Massachusetts, United States) run on a Dell computer. Analysis and graphing was performed using Pulsefit (HEKA), Mini analysis (Synptosoft Inc., Decatur, Georgia, United States) and Igor Pro (Wavemetrics, Lake Oswego, Oregon, United States).

Quantitative RT-PCR: Total mRNA was isolated from 10 worms per strain using TRIzol (Invitrogen, Carlsbad, California, United States) extraction. Purified mRNA concentration was calibrated and reverse transcription was done using the SuperScript III First-Strand Synthesis System (Invitrogen, Carlsbad, California, United States) with oligo(dT) primers. qRT-PCR was performed using fluorescent detection and quantification of SYBR green-labeled PCR product using an MJResearch Opticon2 real-time thermocycler. The cycle threshold [C(t)] value for *acr-16* was normalized to that of an actin control using the equation:
$$\Delta C(t)_{\text{sample}} = C(t)_{\text{acr-16}} - C(t)_{\text{act-1}}$$
Normalized C(t) values for *acr-16* samples were then referenced to the wild type (calibrator) to determine the relative amount of *acr-16* mRNA using the equation: $\Delta \Delta C(t)_{\text{sample}} = \Delta C(t)_{\text{sample}} - \Delta C(t)_{\text{calibrator}}$. Primers for RT-PCR for Acr-16 were: 5'- CACGTAACCTCCTTCTCTATTGG and 5'- GATCAATGATTCCGAGTGACGA. Primers for RT-PCR for Act-1 were: 5'- GCTGGACGTGATCTTACTGATTACC and 5'- GTAGCAGAGCTTCTCCTTGATGTC

Calcium Imaging: To prepare worms for imaging, *zx1481* and *sca-1(tm5339);zx1481* animals were glued down and dissected to expose the muscles in an extracellular solution of 1mM Ca²⁺ composed of 150 mM NaCl, 5 mM KCl, 1 mM CaCl₂, 4 mM MgCl₂, 10 mM glucose, 5 mM sucrose, and 15 mM HEPES (pH 7.3, ~340 mOsm). RCaMP fluorescence imaging was done with a CMOS PCO-EDGE system (Cooke, Leicester, United Kingdom) mounted onto a compound microscope (Olympus BX50WI; Olympus, Tokyo, Japan) using a 60x water immersion objective. RCaMP was excited at a peak of 594nm with an LED, channel rhodopsin was activated with a brief pulse (10ms) with an LED with a peak emission of 470nm. Both diodes were coilluminated and transmitted to the same optical path through a dichroic beam combiner. Acquisition was done using μ Manager software (micro-manager.org). First, a baseline level of fluorescence was obtained over 10s. After allowing the prep to rest for two minutes, a train of ten, 10ms blue light stimulations with 50ms in between pulses was delivered. The animal again was allowed to recover for two minutes and then another train was delivered. Images were analyzed in ImageJ and Igor Pro (Wavemetrics, Lake Oswego, Oregon, United States).

Statistical Analysis: Graphed data were plotted as mean and S.E.M, and significance was assessed using either the Mann-Whitney test or a ONE-way ANOVA with a Tukey post test correction. Statistically significant values were as follows: no significant $p > 0.05$, * $p \leq 0.05$, ** $p \leq 0.01$, *** $p \leq 0.001$. Sample sizes for each experiment

were determined using a type two error rate of 0.80 and a type one error rate of 0.05.

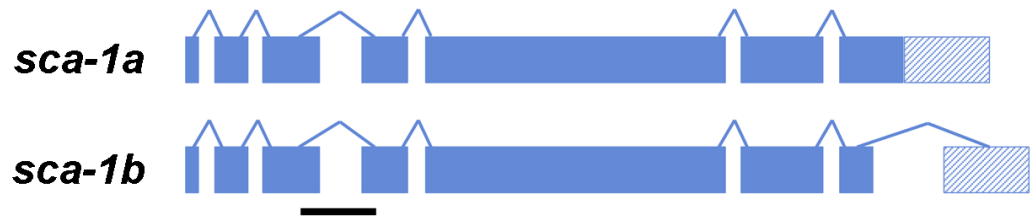
III.c Results

III.c.1 SCA-1 is a SERCA present in *C. elegans*

There is one sarco(endo)plasmic reticulum Ca²⁺ ATPase (SERCA) homologue found in *C. elegans*, referred to as *sca-1*. This homologue is thought to be differentially spliced at the C terminal, resulting in 2 possible isoforms. The predicted isoform SER-1A encodes 1059 amino acids, consisting of 7 exons, and the predicted isoform SER-1B encodes 1004 amino acids consisting of 8 exons (Fig. 18A). The amino acid sequences in both isoforms have approximately 70% identity (80% similarity) with human SERCA1, 2, and 3 proteins, indicating that *C. elegans* SCA-1 is highly conserved (^{87, 88}).

A previous study determined that SCA-1 is expressed in *C. elegans*. Specifically a transcriptional fusion of the promoter region of *sca-1* tagged to GFP (*P_{sca-1}::GFP*) demonstrated that *sca-1* was expressed in all muscles (body wall muscle, pharyngeal muscle, vulval and uterine muscle, and sphincter and anal depression muscles) (Fig. 18B). *P_{sca-1}::GFP* expression was also observed in non-muscle tissue, including gonadal sheath cells, somatic spermatheca and uterine sheath cells, and neurons along the ventral nerve cord and excretory cells. *sca-1* null mutants arrest at the L1 larval stage (^{87, 88}). Therefore, a hypomorphic mutant strain, *sca-1(tm5339)*, was obtained from NBRP which has a 205 base pair deletion in the intronic region between exons three and four (Fig. 18A). This mutant hypomorph produced healthy, viable animals with no obvious phenotypes. However since *acr-16* null mutants also lack apparent locomotory defects, the lack of phenotype in *sca-1* mutants was not unexpected.

A



B

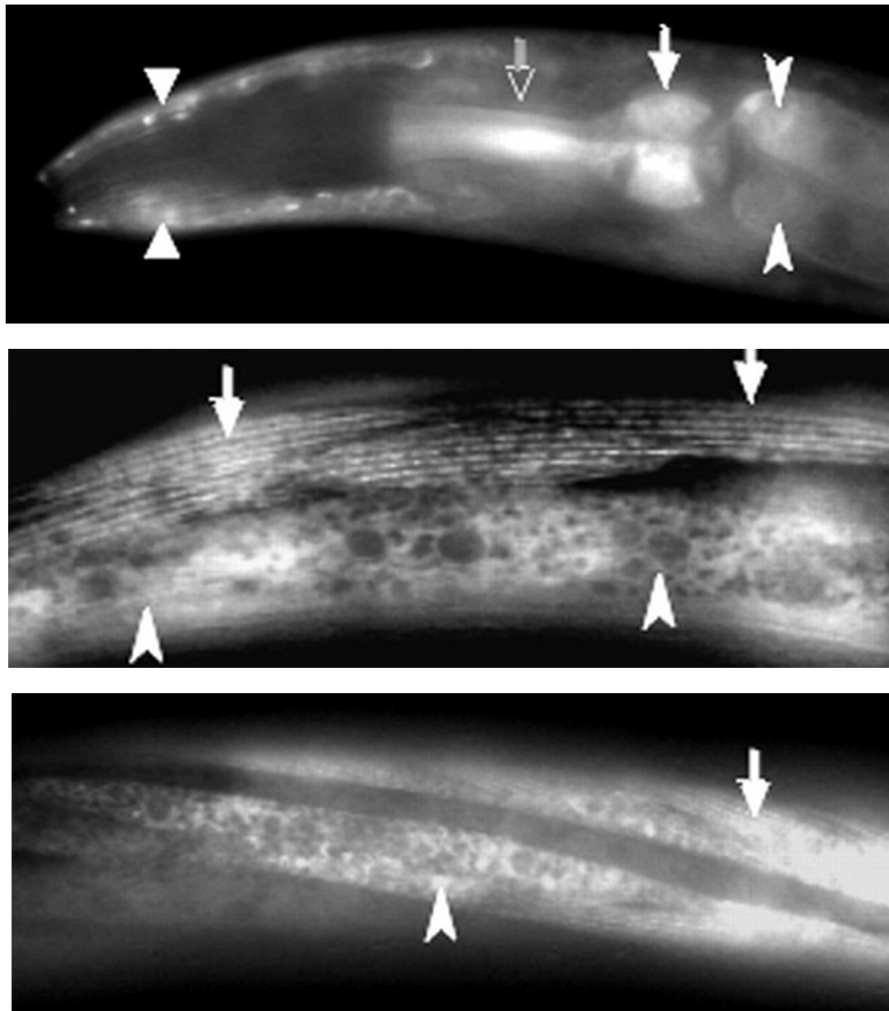


Figure 18. Gene structure and expression pattern of *sca-1*. A. *sca-1* is predicted to encode two isoforms with a differential splice site at the C-terminal. The exons are depicted as boxes and the introns are depicted as lines, with the patterned boxes representing the 3' UTR region. The location of the *sca-1(tm5339)* mutation is denoted by a black bar. B. Examples of expression of *P_{sca-1}::GFP* seen in pharynx (open arrow is the isthmus, closed arrow is the terminal bulb, triangles are head muscles and arrow heads are intestine), and body wall muscles (arrowheads are membranous structures and arrows are dense bodies). Adapted from ⁽⁸⁸⁾.

III.c.2 *sca-1* causes a reduction in ACR-16 levels

The gene locus covering *sca-1* was identified through whole genome sequencing on isolated mutants defective in ACR-16::GFP expression at the NMJ. To further explore the possible role of *sca-1* in ACR-16 regulation a single copy insert of ACR-16::GFP referred to as *jaSi4* (79) was crossed into *sca-1(tm5339)*. This cross was kept in an *acr-16* null background to prevent dilution of the ACR-16::GFP signal by endogenous untagged ACR-16 receptors. In *jaSi4;sca-1(tm5339);acr-16(ok789)* mutants, the levels of ACR-16::GFP expression was significantly decreased as compared to the control, *jaSi4;acr-16(ok789)* (17.6 ± 8.0 n=20 and 24.5 ± 9.7 n=15, respectively) (Fig. 19A,B). This suggests that SCA-1 is involved in the regulation of ACR-16 receptors at the NMJ.

In *jaSi4* the ACR-16::GFP transgene is driven under the muscle specific promoter *Pmyo-3*. This raises the possibility that the observed reduction in ACR-16::GFP expression is an indirect consequence of *sca-1(tm5339)* misregulating the *myo-3* promoter. To examine this possibility *sca-1(tm5339)* was crossed into a *Pmyo-3::GFP::MYO-3* expressing line, referred to as *rals5*. The quantification of MYO-3::GFP levels were unaltered in the *sca-1(tm5339)* mutants suggesting that misregulation of the *myo-3* promoter was not the reason for the ACR-16::GFP reduced expression (*sca-1(tm5339)*: 18.6 ± 2.2 n=11, control: 16.0 ± 5.0 n=10) (Fig. 22C,D). A second line of evidence supporting this conclusion was obtained by crossing *sca-1(tm5339)* into a single copy ACR-16::RFP line expressed under its own promoter. ACR-16::RFP was generated through homologous recombination. In the *sca-1(tm5339)* mutant background, ACR-16::RFP fluorescence levels were

significantly decreased as compared to the control (*sca-1(tm5339)*): 6.4 ± 2.9 n=11, control: 11.0 ± 4.4 n=19) (Fig. 19C,D). Together these data suggest that the *sca-1* mutation affects ACR-16 expression at the NMJ.

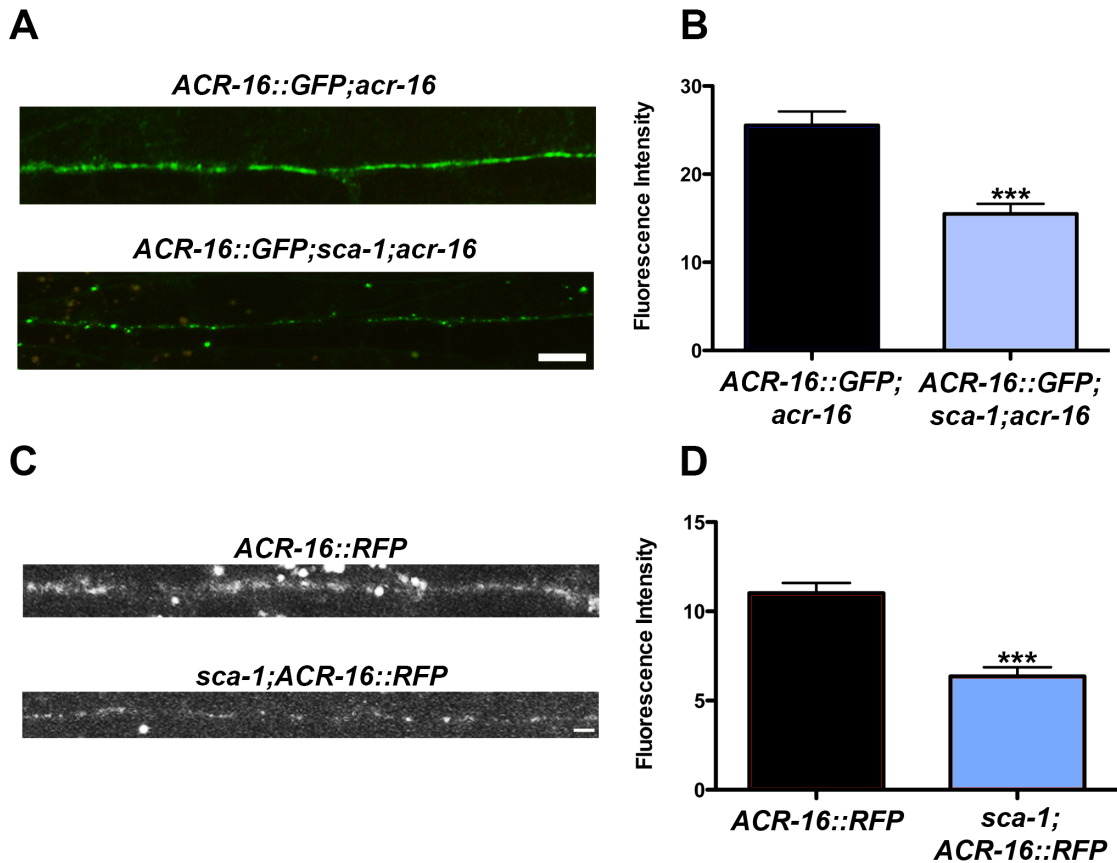


Figure 19. The mutant *sca-1(tm5339)* causes a reduction in ACR-16 receptor levels at the NMJ. A. Representative image of ACR-16::GFP fluorescence in the *sca-1(tm5339)* mutant. B. Quantification of ACR-16::GFP fluorescence in the *sca-1(tm5339)* mutant was significantly reduced as compared to the control (17.6 ± 8.0 n=20 and 24.5 ± 9.7 n=15, respectively). C. Representative image of ACR-16::RFP fluorescence in the *sca-1(tm5339)* mutant. D. Quantification of ACR-16::RFP in the *sca-1(tm5339)* mutant was significantly reduced (*sca-1(tm5339)*: 6.4 ± 2.9 n=11, control: 11.0 ± 4.4 n=19).

III.c.3 Localization and levels of the two other *C. elegans* NMJ receptor types are unchanged in *sca-1* mutants

C. elegans NMJs express two classes of cholinergic receptors, the homopentameric nicotine-sensitive ACR-16 receptors and the heteropentameric levamisole-sensitive LAChRs. To determine if *sca-1* regulates both NAChRs and LAChRs, *sca-1(tm5339)* mutants were crossed into a line expressing RFP-tagged UNC-29, one of the LAChR subunits. There was no significant difference in levels of UNC-29::RFP fluorescence as compared to the control (*sca-1(tm5339)*: 12.8 ± 3.7 n=7, control: 13.1 ± 4.0 n=11) and no obvious difference in localization of the RFP at the NMJ (Fig. 20A,B).

C. elegans NMJs also expressed inhibitory GABA receptors composed of UNC-49 subunits (Bamber et. al, 1999). In order to determine if *sca-1* affects the GABA receptor expression, fluorescence levels and localization of a GFP-tagged UNC-49 reporter were examined. In the *sca-1(tm5339)* mutant background there was no significant difference in either the levels or localization of UNC-49::GFP as compared to the control (*sca-1(tm5339)*: 23.0 ± 8.1 n=17, control: 25.3 ± 10.5 n=13) (Fig. 20C,D). This suggests that *sca-1* specifically regulates ACR-16 receptors. Furthermore the normal appearance of both LAChRs and GABA receptors in the NMJs indicates that *sca-1(tm5339)* mutants do not impact overall post-synaptic structure and patterning.

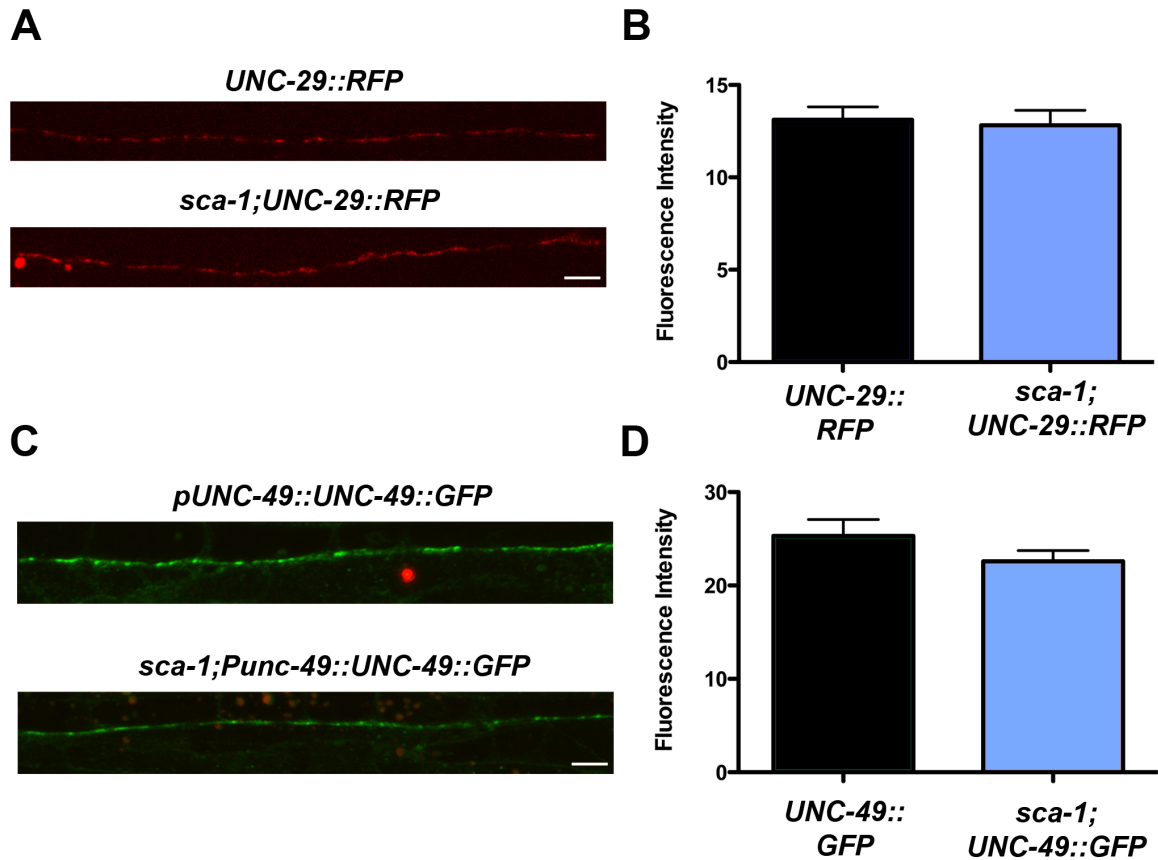


Figure 20. The LACHR and GABA receptor levels and localization are unchanged in a *sca-1* mutant. A. Representative image of LACHR reporter *UNC-29::RFP* in *sca-1(tm5339)* mutants. B. Quantification of *UNC-29::RFP* fluorescence levels in *sca-1(tm5339)* mutants demonstrated no significant difference as compared to the control (*sca-1(tm5339)*: 12.8±3.7 n=7, control: 13.1±4.0 n=11). C. Representative image of GABA receptor reporter *UNC-49::GFP* in *sca-1(tm5339)* mutants. D. Quantification of *UNC-49::GFP* in *sca-1(tm5339)* mutants showed no significant difference as compared to the control (*sca-1(tm5339)*: 23.0±8.1 n=17, control: 25.3±10.5 n=13).

III.c.4 Behavioral analysis of *sca-1* mutants

Previously published studies have shown that *acr-16* mutants alone have no obvious locomotory defects, but in the presence of a LAChR mutant background, there is a significant reduction in motility. The virtually immobilized phenotype of the ACR-16 and LAChR mutant doubles is much more severe than the characteristic uncoordinated, loopy phenotype seen in LAChR mutants alone (Touroutine et. al, 2005). Given the reduction of ACR-16 expression in *sca-1(tm5339)*, an additive locomotory phenotype should be seen in a *sca-1(tm5339)* and LAChR double mutant. To evaluate this *sca-1(tm5339)* and LAChR mutant *unc-63(x37)* double mutants were generated and a body bend assay was performed. As predicted there was no significant difference in the number of body bends in *sca-1(tm5339)* mutants alone when compared to the *acr-16(ok789)* null mutant or to the corresponding N2 control (*sca-1(tm5339)*: 16.1 ± 5.1 n=10, *acr-16(ok789)*: 16.2 ± 4.5 n=10, N2: 14.2 ± 3.4 n=10). However, the *unc-63(x37);sca-1(tm5339)* double mutants exhibited a significant decrease in the number of body bends as compared to the *unc-63(x37)* mutant alone (*unc-63(x37);sca-1(tm5339)*: 3.4 ± 1.3 n=10, *unc-63(x37)*: 8 ± 1.9 n=10). This decrease was similar to the *unc-63(x37);acr-16(ok789)* double mutant (2.9 ± 2 n=10), suggesting that *sca-1* mutants have functional defects consistent with loss of ACR-16 receptors at the NMJ.

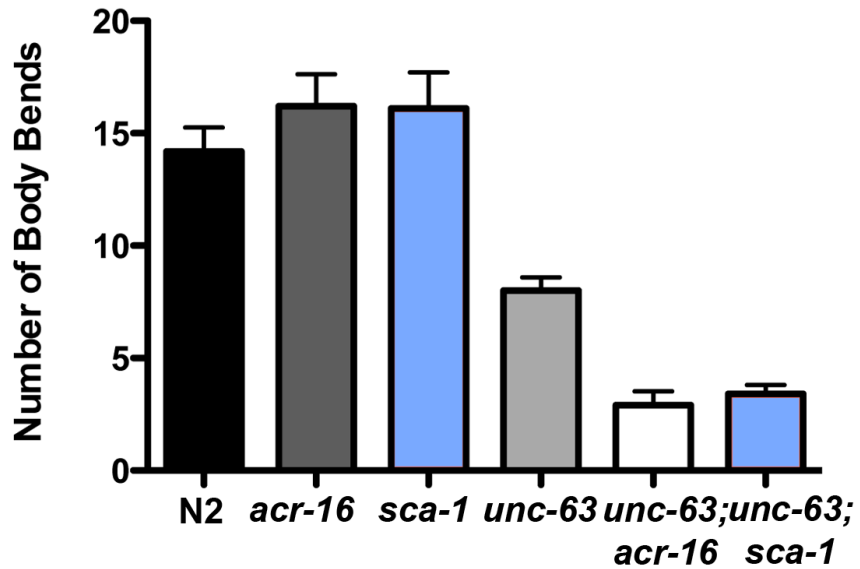


Figure 21. Similar to *acr-16* mutants, *sca-1* worsens the motility deficits of LChR mutants. *sca-1* mutants alone do not demonstrate any change in the number of body bends as compared to wild-type (N2) or the *acr-16* mutant (*sca-1(tm5339)*): 16.1 ± 5.1 n=10, *acr-16(ok789)*: 16.2 ± 4.5 n=10, N2: 14.2 ± 3.4 n=10. LChR (*unc-63(x37)*) and *sca-1(tm5339)* double mutants have a significantly reduced number of body bends, as compared to the already uncoordinated *unc-63(x37)* control (*unc-63(x37);sca-1(tm5339)*): 3.4 ± 1.3 n=10, *unc-63(x37)*: 8 ± 1.9 n=10). This reduction is similar to the reduction seen in the *acr-16;unc-63(x37)* double mutant (2.9 ± 2 n=10).

III.c.5 Synapse abundance and muscle integrity appear unaltered in *sca-1* mutants

It is possible that the functional defects of *sca-1* mutants on ACR-16 receptor levels and **behavioral** motility **are** due to defects in the number of cholinergic synapses. To address this possibility *sca-1(tm5339)* was crossed into a reporter strain expressing a mCherry-tagged cholinergic vesicle marker, RAB-3, under the cholinergic **neuron** specific promoter *Pacr-2*. In the *sca-1(tm5339)* mutant background there was no significant difference in the number of RAB-3::mCherry puncta as compared to the control (*sca-1(tm5339)*: 15.9±4.4 n=10, control: 17.0±4.0 n=9). This suggests that the change in ACR-16::GFP fluorescence intensity and the behavioral phenotypes seen in the *sca-1* mutant are not due to a synaptogenesis or presynaptic maintenance defect.

Muscle structure was **also** examined in the *sca-1(tm5339)* mutants expressing GFP tagged MYO-3 under the MYO-3 promoter. This allowed for the evaluation of both levels of MYO-3 expression and organization of the protein in the body wall muscle structure. As previously indicated levels of MYO-3::GFP **were** unchanged as compared to the control (*sca-1(tm5339)*: 18.6±2.2 n=11, control: 16.0±5.0 n=10). This suggests that there is no change in the level of MYO-3 expression in the body wall muscles. There were **also** no apparent differences in the body wall muscle organization or myosin localization.

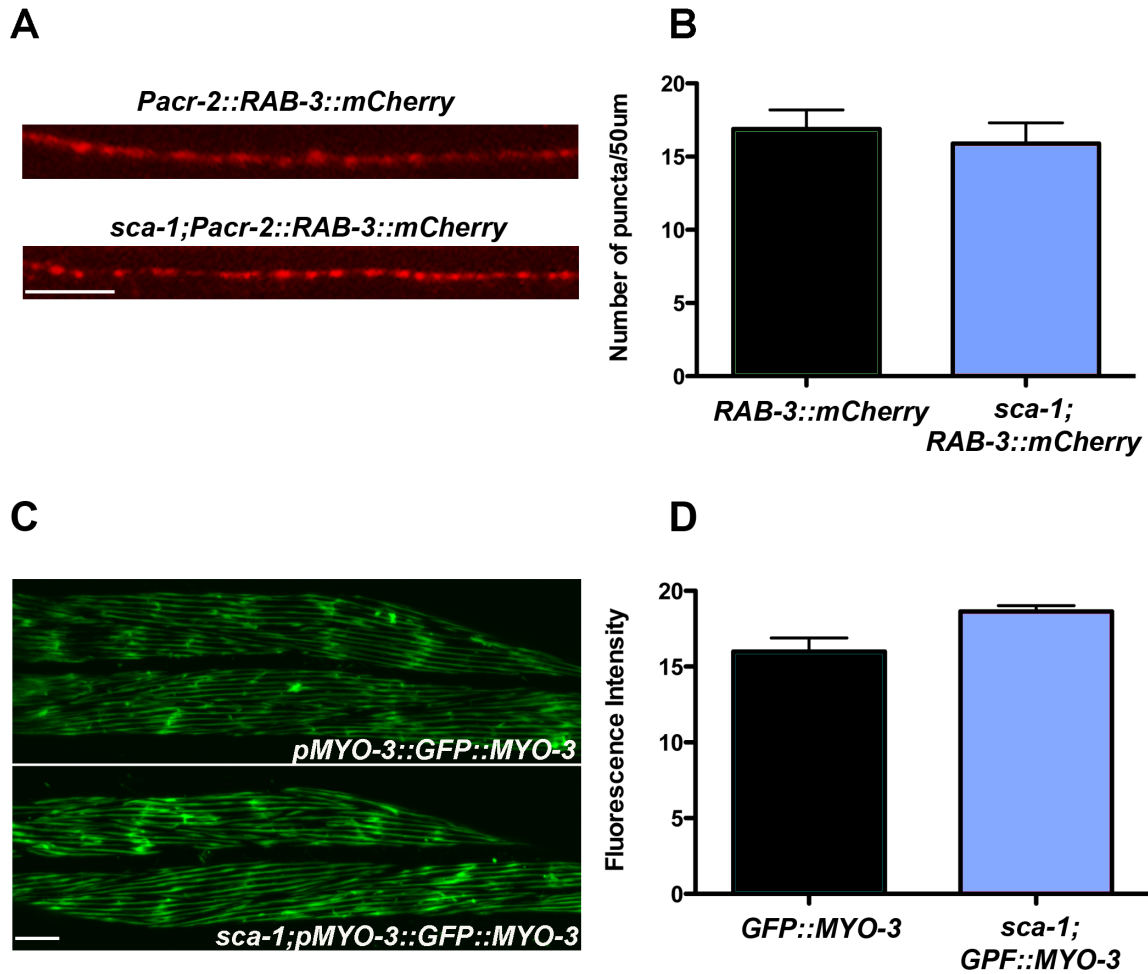


Figure 22. ACR-16 deficits in *sca-1* mutants are not due to a mispatterning of the NMJ. A. Representative image of cholinergic vesicular marker RAB-3::mCherry in *sca-1(tm5339)* mutants. B. Quantification of number of synaptic puncta in *sca-1(tm5339)* mutants showed no significant difference as compared to control (*sca-1(tm5339)*: 15.9 ± 4.4 n=10, control: 17.0 ± 4.0 n=9). C. Representative images of myosin reporter MYO-3::GFP in body wall muscles in *sca-1(tm5339)* mutants. D. Quantification of MYO-3::GFP in *sca-1(tm5339)* mutants was not significantly different as compared to the control (*sca-1(tm5339)*: 18.6 ± 2.2 n=11, control: 16.0 ± 5.0 n=10).

III.c.6 A mutation in *sca-1* does not affect levels of *acr-16* mRNA

The reduction in ACR-16::GFP fluorescence could be the result of altered transcription through a *sca-1* mediated mechanism. To evaluate the level of *acr-16* transcript total mRNA was isolated from both *sca-1(tm5339)* and the control, reverse transcribed and then measured using quantitative Real Time-PCR (qRT-PCR), using actin transcript levels as an internal control for samples. When the relative levels of *acr-16* mRNA in the *jaSi4;sca-1(tm5339)acr-16(ok789)* mutant background were compared to a normalized control there was no significant difference in the amount of mRNA present (*sca-1(tm5339)*: 1.3 ± 0.4 n=5, control: 1 ± 0 n=5) (Fig. 23). This suggests that *sca-1* does not regulate the transcription of *acr-16*.

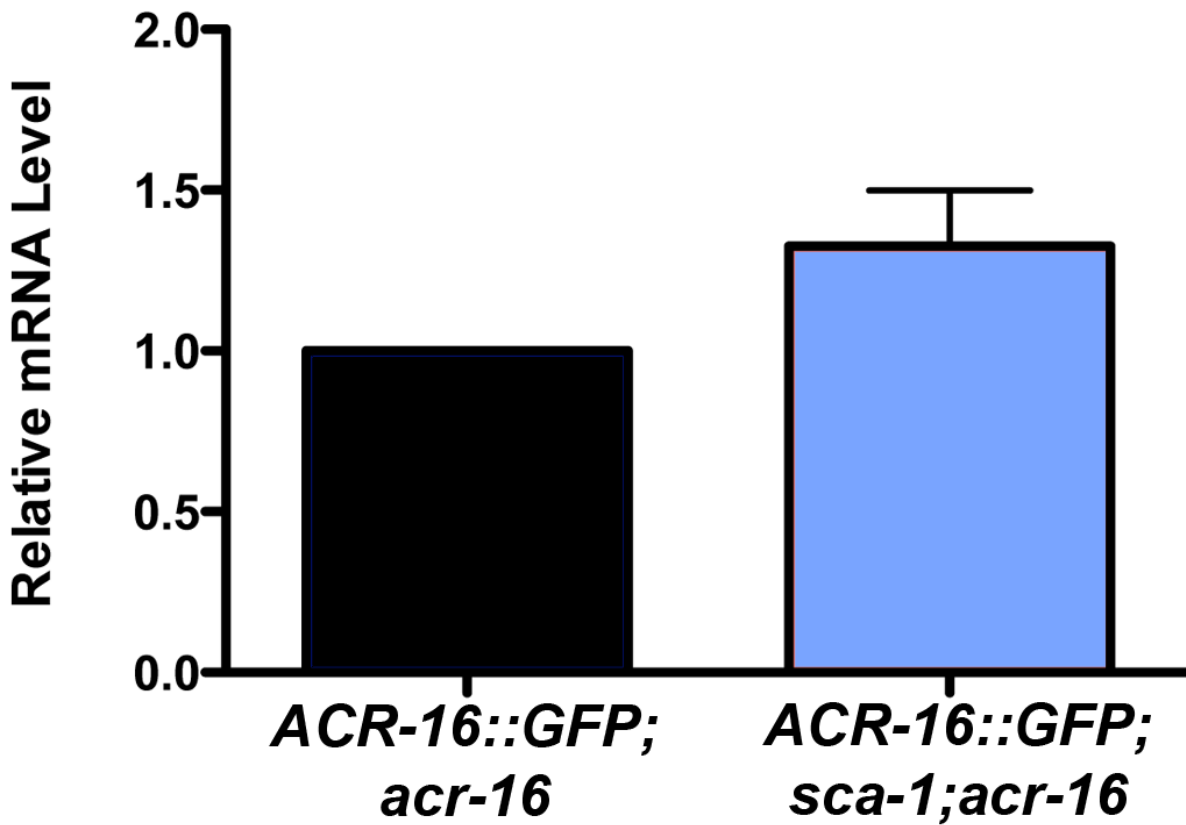


Figure 23. *sca-1* mutants do not affect transcription of *acr-16*. Relative levels of *acr-16* mRNA were unchanged in a *sca-1(tm5339)* mutants (*sca-1(tm5339)*: 1.3 ± 0.4 $n=5$, control: 1 ± 0 $n=5$).

III.c.7 *sca-1* mutants have a significant reduction in evoked response amplitude

The observed reduction in ACR-16::GFP expression in *sca-1(tm5339)* at the NMJ should impact postsynaptic responses to endogenous ACh release. To test this prediction whole cell patch clamp recordings of evoked NMJ responses were obtained in 1mM Ca²⁺ from dissected worms. Initially the evoked current amplitudes were recorded from *jaSi4;sca-1(tm5339);acr-16(ok789)* mutants and were found to be significantly decreased as compared to the *jaSi4;acr-16(ok789)* control (*jaSi4;sca-1(tm5339);acr-16(ok789)*: 512.2±361.6 n=6, *jaSi4;acr-16(ok789)*: 1919.3±753.3 n=6) (Fig. 24A,B). To ensure this result could be recapitulated with endogenous untagged ACR-16 receptors, currents were then recorded from *sca-1(tm5339)* mutants alone. Again there was a significant decrease in evoked response amplitudes as compared to the wild-type control N2 (*sca-1(tm5339)*: 1319±503.1 n=12, N2: 1875.1±420.4 n=15) (Fig. 24C,D). These data agree with the reduced levels of fluorescence of ACR-16::GFP receptors at NMJs.

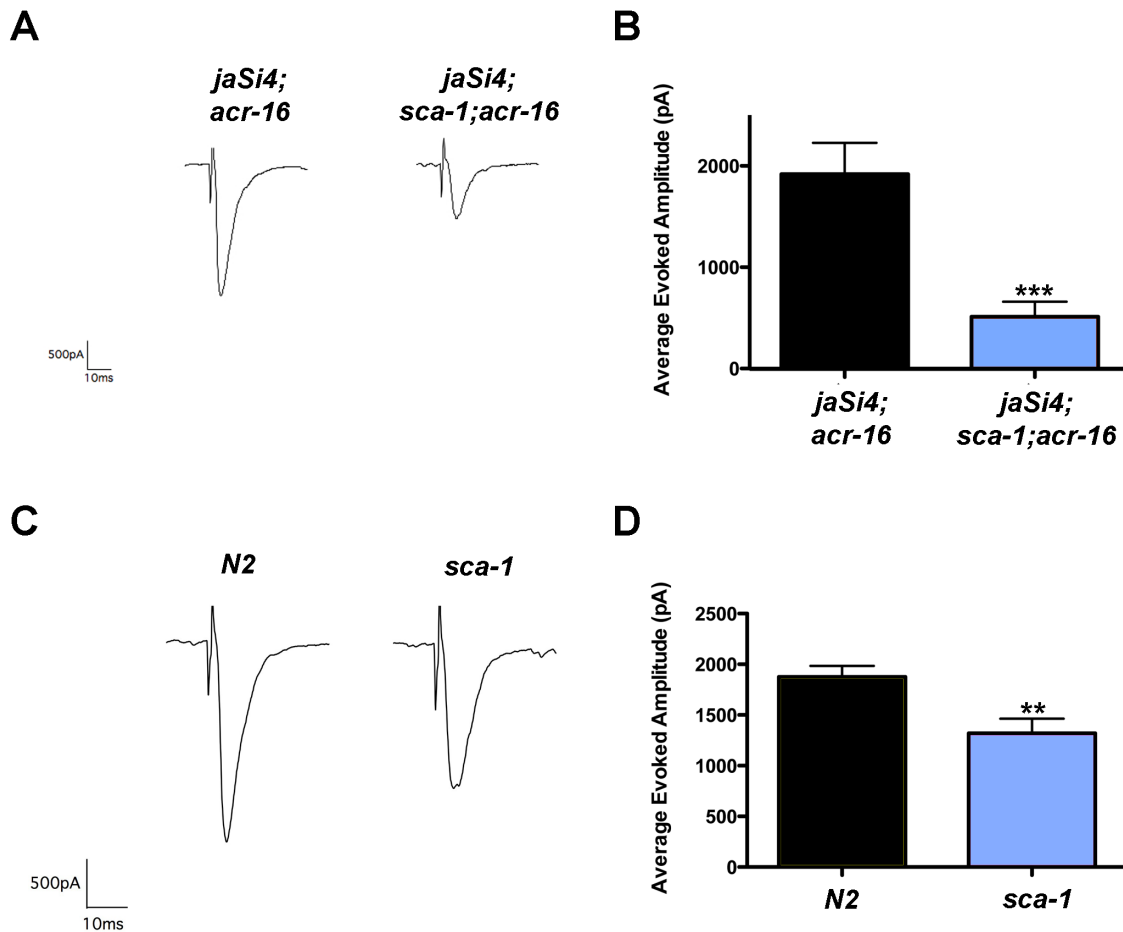


Figure 24. Evoked response amplitudes are decreased in *sca-1* mutants. A. Representative traces of postsynaptic evoked current amplitudes in *jaSi4;sca-1(tm5339);acr-16* mutants. B. Quantification of evoked current amplitudes demonstrated a significant reduction in *sca-1* mutants as compared to the control (*jaSi4;sca-1(tm5339);acr-16(ok789)*: 512.2 ± 361.6 n=6, *jaSi4;acr-16(ok789)*: 1919.3 ± 753.3 n=6). C. Representative traces of postsynaptic evoked current amplitudes in *sca-1(tm5339)* mutants. D. Quantification of evoked current amplitudes demonstrated a significant reduction in current amplitudes in *sca-1* mutants.

The reduction in evoked postsynaptic response amplitude could be due to a decrease in overall receptor levels or reflect dispersal of functional receptors away from the NMJ. To differentiate between these two possibilities, exogenous nicotine was pressure-ejected onto dissected animals that were whole cell patch clamped. Nicotine is a specific agonist of the ACR-16 receptors in *C. elegans*, thus the response amplitudes elicited by pressure-ejection reflect ACR-16 receptor-mediated currents. In the *jaSi4;sca-1(tm5339);acr-16(ok789)* mutant background there was no significant change in pressure-ejected nicotine response amplitude as compared to the *jaSi4;acr-16(ok789)* control (*sca-1(tm5339)*: 2007.2±318.1 n=6, *jaSi4;acr-16(ok789)*: 2068.6±248.5 n=7) (Fig. 25A,b). Similar results were observed when nicotine was applied to *sca-1(tm5339)* alone when compared to wild-type (N2) (*sca-1(tm5339)*: 1420.3±101.8 n=4, N2:1149.5±166.9 N=4) (Fig. 25C,D). This suggests that while the overall number of ACR-16 receptors at the NMJ is unchanged, the receptors present are declustered from the synapse.

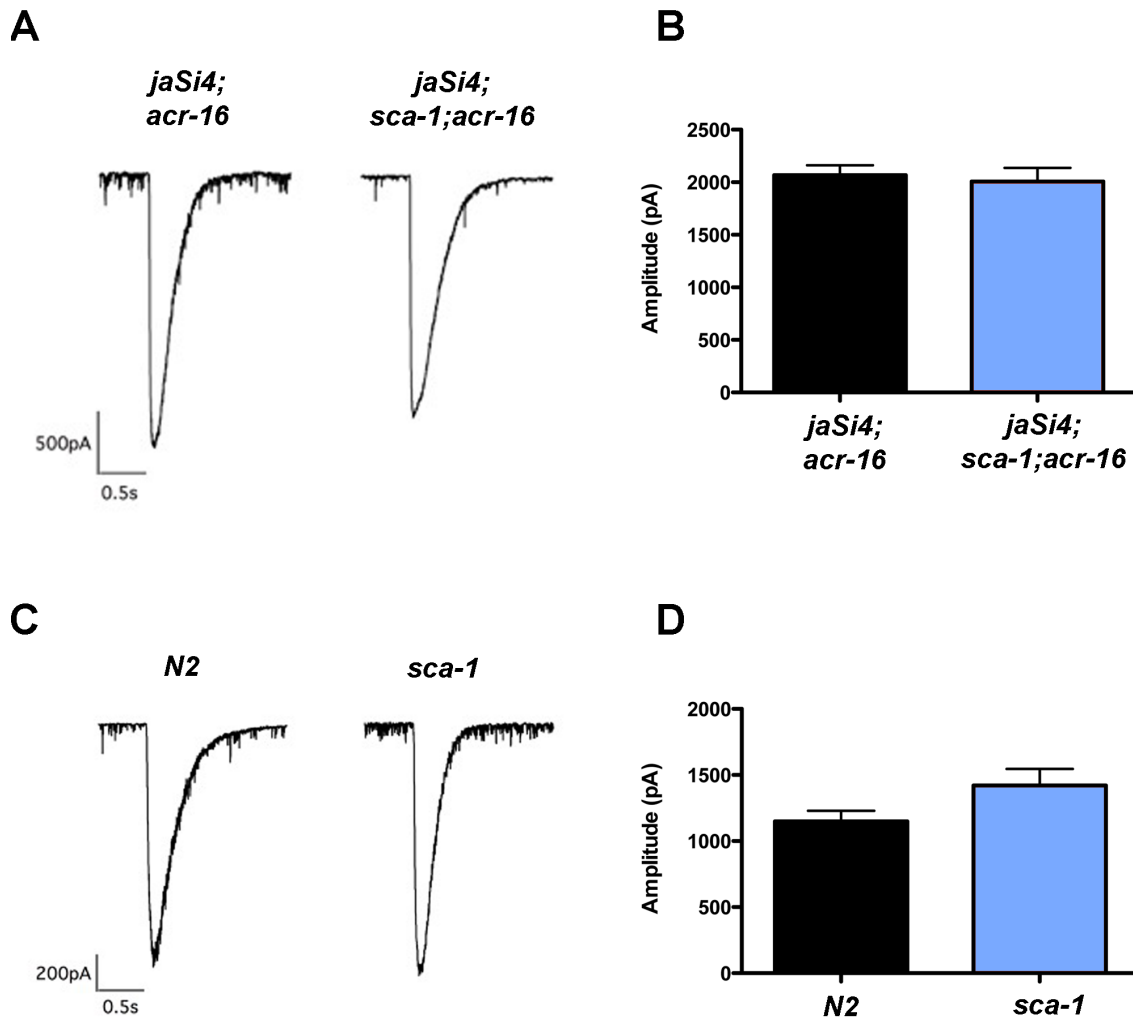


Figure 25. Pressure-ejected nicotine responses are unchanged in the *sca-1* mutant. A. Representative traces of nicotine pressure-ejection response amplitudes in *jaSi4;sca-1;acr-16* mutants. B. Quantification of pressure-ejected nicotine amplitudes demonstrated no difference in the *jaSi4;sca-1;acr-16* mutants as compared to the control (*sca-1(tm5339)*: 2007.2 ± 318.1 n=6, *jaSi4;acr-16(ok789)*: 2068.6 ± 248.5 n=7). C. Representative traces of nicotine pressure-ejected response amplitudes in *sca-1* mutants. D. Quantification of nicotine pressure-ejected response amplitudes showed no significant difference between *sca-1* mutants and the control (*sca-1(tm5339)*: 1420.3 ± 101.8 n=4, *N2*: 1149.5 ± 166.9 N=4).

III.c.8 Expression of *Pmyo-3::SCA-1::mCherry* in *sca-1* mutants rescues ACR-16::GFP reduction

To determine if the defects seen in ACR-16 function in *sca-1(tm5339)* hypomorph mutants is specifically due to loss of SCA-1 in body wall muscles, an extrachromosomally expressed mCherry tagged genomic *sca-1* transgene was expressed under the body wall muscle specific promoter *Pmyo-3*, in *sca-1* mutants (Fig. 26A). The *Pmyo-3::SCA-1::Mcherry* significantly rescued the reduction in ACR-16::GFP, however not to wild type levels (*jaSi4;sca-1(tm5339);acr-16(ok789)*: 21.1±7.5 n=19, *jaSi4;sca-1(tm5339);acr-16(ok789);jaEx1064*: 25.8±6.8 n=11, *jaSi4;acr-16(ok789)*: 28.7±6.1 n=21) (Fig. 26B,C). This **partial rescue could** be the result of **the** mosaic expression **of** **SCA-1** as this construct was an extrachromosomal array. To address this possibility regions of the nerve cord juxtaposed to muscle cells with and without the *Pmyo-3::SCA-1::Mcherry* transgene expression were **separately** analyzed from the same worms. ACR-16::GFP expression **at NMJs** in muscle cells expressing SCA-1 was significantly increased over regions without SCA-1 expression, **and** showed a significant increase over the control **expression levels** (+SCA-1 muscle: 37.2±13.9, n=8 -SCA-1 muscle: 24.2±5.8 n=8, *jaSi4;acr-16(ok789)*: 28.7±6.1 n=21) (Fig. 26D). The ability of the ***sca-1*** transgene to rescue the **ACR-16 clustering** defect indicates that the reduction in ACR-16::GFP is due to the *sca-1* gene knockdown and not a background mutation. Furthermore the enhanced ACR-16::GFP expression in muscle **NMJs** enriched for SCA-1 is consistent with a **cell autonomous** dose-dependent regulation of **ACR-16** receptor **localization**.

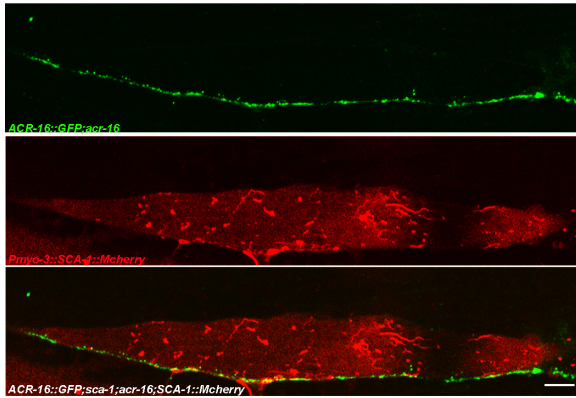
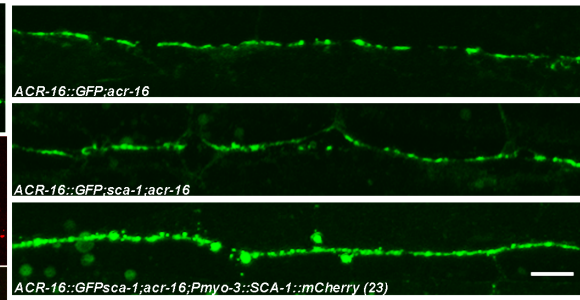
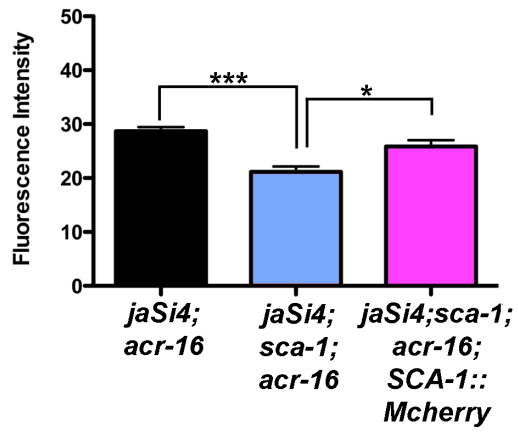
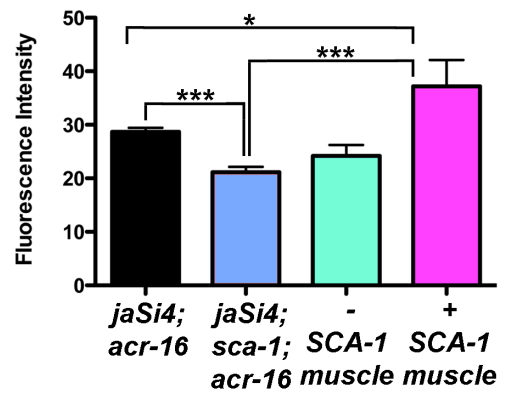
A**B****C****D**

Figure 26. Rescue of ACR-16::GFP expression by *Pmyo-3::SCA-1::mCherry* is cell autonomous and dose dependent. A. Representative image of *Pmyo-3::SCA-1::mCherry* expression in body wall muscles. B. Representative images of ACR-16::GFP in *sca-1* mutant worms with and without the *Pmyo-3::SCA-1::Mcherry* rescue construct. C. Quantification of ACR-16::GFP fluorescence in *sca-1;Pmyo-3::SCA-1::Mcherry* expressing animals showed a rescue of fluorescence levels as compared to the *sca-1* mutants alone (*jaSi4;sca-1(tm5339);acr-16(ok789)*: 21.1±7.5 n=19, *jaSi4;sca-1(tm5339);acr-16(ok789);jaEx1064*: 25.8±6.8 n=11, *jaSi4;acr-16(ok789)*: 28.7±6.1 n=21). D. Quantification of ACR-16::GFP fluorescence at the NMJ with muscles cells expressing SCA-1::mCherry (+SCA-1 muscle) showed a significant increase in fluorescence as compared to both *sca-1* mutants and the *jaSi4;acr-16* control. This increase was not seen in regions of the NMJ without muscles expressing SCA-1::mCherry (-SCA-1 muscle) (+SCA-1 muscle: 37.2±13.9, n=8 -SCA-1 muscle: 24.2±5.8 n=8, *jaSi4;acr-16(ok789)*: 28.7±6.1 n=21).

III.d Discussion and Future Directions

This study presents evidence implicating the *C. elegans* SERCA protein, SCA-1 in the regulation of NACHR of the alpha 7 family. Specifically *sca-1* mutants exhibit a significant reduction in ACR-16::GFP clustering at the NMJ while the two other cysteine loop ionotropic receptors present were unaffected. Consistent with a specific targeting of a receptor class, neither synaptic density nor muscle architecture were altered in the *sca-1* hypomorph. Therefore the *sca-1* phenotype is unlikely to be due to a developmental defect. Electrophysiological analysis showed a significant reduction in evoked cholinergic response amplitudes, which accounts for the locomotory defect uncovered in the *sca-1*;LACHR double mutant. Rescue of the *sca-1* mutant phenotype using a muscle specific MYO-3 promoter indicates that the change in ACR-16 regulation is a cell autonomous muscle specific function of *sca-1*.

There are many possible mechanisms through which calcium may be regulating the synaptic localization of the ACR-16 receptors. One possibility is through transcriptional regulation of the *acr-16* gene. There is evidence of activity dependent calcium mediated gene transcription of vertebrate nAChRs. For example, in chicken myotubes increases in cytosolic calcium led to a decrease in the number of surface nAChRs as well as a decrease in nAChR mRNA levels. This inhibition was mediated through protein kinase C signaling (89, 90). In rat myotubes nAChR RNA levels were also observed to decrease when cytosolic calcium levels were increased, and this decrease was regulated through the calcium/calmodulin-dependent protein kinase II (CaMKII) (91, 92). However, when relative levels of *acr-16* mRNA in the *sca-1* mutant background were examined there was no significant change from the

control consistent with normal nicotine-induced ACR-16 currents in *C. elegans* muscles. This evidence suggests that if calcium regulation of transcription is involved in the *sca-1* mutant phenotype, it must be acting downstream of *acr-16* transcription.

_____ In vertebrates there is a large family of CAMKs that play various roles in CREB mediated signal transduction. A similar, although simpler, pathway has been shown to function in *C. elegans*. CKK-1, the CaMKK homologue, phosphorylates CMK-1, the CaMKI/IV homologue. CMK-1 acts as both the cytonuclear transporter and the kinase that phosphorylates CRH-1, a CREB homologue, which activates gene transcription (93). Whether this pathway impacts ACR-16 clustering at the NMJ remains to be evaluated.

The next possible mechanism is through regulation of ACR-16 protein levels at the neuromuscular junction. It is possible that the ACR-16 receptors are declustered and thus no longer directly opposed to areas of neurotransmitter release. Postsynaptic responses elicited using pressure-ejected nicotine showed no significant changes in amplitude in the *sca-1(tm5339)* mutants as compared to the control. This indicates that the overall number of ACR-16 receptors at the NMJ is unchanged; however the receptors are no longer properly clustered at the synapse.

Regulation of ACR-16 receptors by *sca-1* is most likely mediated through a calcium homeostasis-dependent pathway. Identification of proteins involved in this mechanism will be essential in understanding modulation of ACR-16 receptors by internal calcium levels. A potential candidate in this process is the calcium-activated serine-threonine phosphatase, calcineurin. Previous work has shown that *C. elegans*

has a single homologue of the vertebrate calcineurin A, referred to as TAX-6. This protein has a catalytic domain and a regulatory domain. The regulatory domain contains a calcineurin B subunit binding site, a calmodulin binding site, and an autoinhibitory binding site. When both the B subunit and [calcium](#)/calmodulin bind to the TAX-6 regulatory domain, there is an increase in its phosphatase activity, due to loss of autoinhibition (94). TAX-6 is expressed in *C. elegans* muscle cells and has been shown to directly associate with NACHR through tandem affinity purification experiments (94, 95). The activity of TAX-6 is regulated by calcium/calmodulin binding in several calcium signaling pathways. In particular calcineurins directly modulate calcium release through the regulation of IP3 receptors, ryanodine receptors, and calcium pumps to help maintain internal calcium levels (96). Analysis of *tax-6* mutants in *C. elegans* suggests it is a negative regulator of olfactory adaption. When TAX-6 is activated by calcium, it blocks the continued activation of the calcium permeable channels found in the sensory neurons (94). It has also been observed that *tax-6* mutants are hypersensitive to nicotine application, implying that normally *tax-6* inhibits either the number or activation of NACHRs, or the affects of NACHRs on downstream targets (95). It is possible that in the *sca-1* mutants, altered levels of cytoplasmic calcium may increase or decrease TAX-6, activity, changing the phosphorylation state of ACR-16 receptors or their regulators.

To evaluate possible changes in intracellular calcium levels in *sca-1(tm5339)* mutants, extrachromosomally expressed RCaMP fluorescence in body wall muscles was measured. In preliminary experiments, the levels of RCaMP fluorescence appeared to be enhanced (data not shown). Neuronal activation was induced

through an integrated channel rhodopsin driven under the neuronal promoter *Punc-17* in the RCaMP line. Preliminary analysis of these data demonstrated a slight trend towards an increased tau for the recovery time constant following depolarization induced calcium spikes in *sca-(tm5339)* mutants, however this was not significant (*sca-1(tm5339)*: 4.1 ± 1.1 n=7, control: 3.7 ± 1.0 n=11). However, because the RCaMP line was not integrated the variable levels of RCaMP expression between muscle cells was observed. The RCaMP mosaicism made it difficult to accurately measure changes in calcium or calibrate the system. While these results demonstrate the feasibility of this experiment, the analysis of calcium dynamics in the *sca-1* mutant will be pursued in an integrated RCaMP line that has been ordered. Future experiments will also focus on examining ACR-16 receptor expression and function in a *tax-6* mutant background and continued characterization of this calcium-regulated pathway.

IV. *C. elegans* VAB-1 and F59D12.1 regulate nicotinic acetylcholine receptor ACR-16 expression

IV.a Introduction

To identify possible regulators of nAChRs, a forward genetic screen was performed in *C. elegans* targeting modifiers of the $\alpha 7$ nAChR homologue ACR-16. From this screen two genes were identified: *vab-1*, which encodes a protein homologue of the vertebrate ephrin tyrosine kinase receptor (Eph) and *f59d12.1*, which shares homology with the rhodopsin G-protein coupled receptor (GPCR) cholecystokinin type B (CCK-5/CCK2R).

The model organism *C. elegans* contains only a single Eph receptor, *vab-1*, and four ephrin ligands, *efn1-4* (97, 98). In vertebrates there are two classes of Eph receptors, EphA and EphB. Both of these receptor classes have a multidomain extracellular region where the ephrin ligands bind, one transmembrane segment, and an intracellular kinase domain. There are also two classes of ephrin ligands in vertebrates, ephrin A and ephrin B. Ephrin A ligands are characterized by attaching to the cell surface through a glycosylphosphatidylinositol (GPI) anchor and ephrin B ligands are characterized by a transmembrane region. What is unique about Eph receptors as tyrosine kinases is they tend to associate with surface expressed ligands, allowing for both forward and reverse signaling cascades that can affect both the cells expressing the Eph receptor and the cells containing the ligand (99).

Another gene that was identified through the ACR-16 regulator screen was the rhodopsin G-protein coupled receptor (GPCR) cholecystokinin type B (CCK-B/CCK2R) vertebrate homologue *f59d12.1*. CCK2R receptors are reported to be

expressed in the mammalian brain in high levels. The CCK2R gene encodes a protein with seven transmembrane domains and structural features similar to GPCRs in the rhodopsin family. CCK2Rs are activated through the cholecystokinin ligands CCK-8 and CCK-4. Ligand activation of the CCK2Rs has been demonstrated to cause an increase in cytosolic calcium, potentially from intracellular sources through the activation of the phospholipase C (PLC) and protein kinase C (PKC) pathway (100). Studies have shown that CCK2R activation in hippocampal slices obtained from rats, increased NMDA receptor mediated currents in a PLC and PKC dependent manner (101), separately previously published results have shown that activation of the CCK2R causes an increase in GABA release in GABAergic interneurons through the inhibition of calcium activated potassium currents (102). Using the poorly characterized *C. elegans* homologue *f59d12.1*, a better understanding of these GPCRs ability to regulate calcium-mediated current can be achieved.

Preliminary experiments have determined that both *vab-1* and *f59d12.1* are involved in the regulation of ACR-16 function, although most likely through unique mechanisms. Further examination of these proteins' role in the modulation of ACR-16 will be necessary to tease out the pathways at work. Future directions for these experiments will be addressed in the discussion.

IV.b Materials and Methods

Strains and Culturing Conditions: The genotypes of nematode strains used in this study are: the wild-type Bristol isolate N2, *acr-16(ok789)*, *unc-63(x37)*, *unc-63(x37);acr-16(ok789)*, *jaSi4[pMYO-3::ACR-16::GFP]* SY1407, *jaSi4;acr-16(ok789)* SY1422, *unc-63(x37);jaSi4;acr-16(ok789)* SY1423, *vab-1(ok1699)*, *vab-1(e2027)*, *vab-1(ju8)*, *jaSi4;vab-1(ok1699);acr-16(ok789)* SY1597, *jaSi4;vab-1(e2027);acr-16(ok789)* SY1604, *jaSi4;vab-1(ju8);acr-16(ok789)* SY1609, *f59d12.1(gk1000)*, *jaSi4;acr-16(ok789);f59d12.1(gk1000)* SY1620, *jaIs1103[Pacr-2::mCherry::RAB-3]*, *UNC-29::RFP(kr208)*, *vab-1(e2027);UNC-29::RFP(kr208)* SY1608, *vab-1(e2027);jaIs1103* SY1606, *vab-1(ju8);jaIs1103* SY 1607, *rals5[Pmyo-3-3::GFP::MYO-3]*, *vab-1(ok1699);rals5* SY1632, *unc-63(x37);jaSi4;vab-1(ok1699);acr-16(ok789)* SY, *unc-63(x37);jaSi4;acr-16(ok789);f59d12.1(gk1000)* SY, *f59d12.1(gk1000);UNC-29::RFP(kr208)* SY, *f59d12.1(gk1000);rals5* SY1633, *f59d12.1(gk1000);jaIs1103* SY1628, *ACR-16::RFP(kr305)*, *f59d12.1(gk1000);ACR-16::RFP(kr305)* SY1639, *vab-1(ok1699);ACR-16::RFP(kr305)* SY1646. Animals were grown at 15-20° C on OP50-seeded NGM plates.

Microscopy: Fluorescence images were obtained as described in Chapter III.

Behavior Analysis: Behavioral analysis was conducted on *jaSi4;acr-16(ok789)*, *unc-63(x37);jaSi4;acr-16(ok789)*, *jaSi4;acr-16(ok789);f59d12.1(gk1000)*, *jaSi4;vab-1(ok1699);acr-16(ok789)*, *unc-63(x37);jaSi4;acr-*

16(ok789);f59d12.1(gk1000), unc-63(x37);jaSi4;vab-1(ok1699);acr-16(ok789).

Thrashing motility for worms placed in M9 buffer was measured per minute for three minutes total. Body bend assays were done on worms allowed to acclimate for one minute on unseeded agar plates. The number of full body bends completed by the worm in one minute was then counted as described in Chapter III.

Electrophysiology: The dissection and electrophysiological methods were as previously described (Chapter III, Richmond, 1999, 2005).

Quantitative RT-PCR: As described in Chapter III.

Statistical Analysis: Graphed data were plotted as mean and S.E.M, and significance was calculated using either the Mann-Whitney test or a ONE-way ANOVA with a Tukey post test correction. Statistically significant values were as follows: not significant $p > 0.05$, * $p \leq 0.05$, ** $p \leq 0.01$, *** $p \leq 0.001$. Sample sizes for each experiment were determined using a type two error rate of 0.80 and a type one error rate of 0.05.

IV.c Results

IV.c.1 *C. elegans* VAB-1 is an ephrin RTK and F59D12.1 is a GPCR-like protein

There is a single ephrin receptor tyrosine kinase homolog in *C. elegans*, *vab-1*. This gene was originally identified in a screen performed to look for novel *C. elegans* mutants, and was [isolated based on](#) variable abnormalities, including a notched head and tail abnormalities (46). [The *vab-1* gene](#) produces a 4kb transcript of approximately 1120 amino acids, and has equal sequence similarity to both the vertebrate EphA and EphB receptors. The *C. elegans* [VAB-1 protein](#) contains an extracellular domain that has a N-terminal globular domain, a cysteine rich domain, and two fibronectin type III repeats (Fig. 25A). The domain with the most similarity to human ephrin receptors is the intracellular tyrosine kinase catalytic domain. Previous work has demonstrated that mutations in various domains of the *vab-1* gene can have different effects on the mutant phenotypes produced. Strong phenotypes are seen when the extracellular domain components are affected and weak phenotypes occur when there is a mutation in the kinase domain. A previous study demonstrated the expression pattern of VAB-1 using a VAB-1::GFP translational fusion construct driven by endogenous VAB-1 promoter. VAB-1 expression is seen throughout development in neuroblasts and epidermal precursors. In adult worms expression is seen in neurons and axons suggesting a role in neuronal and epidermal morphogenesis (97) (Fig. 25B).

[In order to study the possible role of VAB-1 in ACR-16 function](#), three mutant alleles of *vab-1* were obtained from the CGC for [preliminary characterization](#). The

allele *vab-1(ok1699)* has no noticeable phenotypes and contains a 1016 base pair deletion, eliminating the fifth coding exon (Fig. 27A). The allele *vab-1(e2027)* has a more penetrant notched head phenotype and over half of embryos arrest. It contains a 74 base pair deletion removing the first seven base pairs of the fifth exon (Fig. 27A). This exon contains the sequences that encode domains of the extracellular domain. The final allele was *vab-1(ju8)*, **which also** has a penetrant notched head phenotype and over half of the embryos arrest. This allele contains a single G to A base pair change, causing an amino acid in the N-terminal globular domain (Fig. 27A).

In contrast to *vab-1*, little is known about the *C. elegans* gene *f59d12.1*. It is predicted to have seven trans-membrane domains, similar to a member of the Rhodopsin family of G-protein coupled receptors (SMART, ExPaSy) (Fig. 27C). The closest human ortholog is an isoform of the Gastrin/cholecystokinin type B receptor (**CCKR**), which is expressed in the brain and central nervous system of mammals (103). To further study the role of *f59d12.1* in ACR-16 regulation, a mutant allele was obtained from the CGC. The allele *f59d12.1(gk1000)* contains a 198 base pair deletion which removes approximately half of the fourth exon and most of the fifth exon (Fig. 27C).

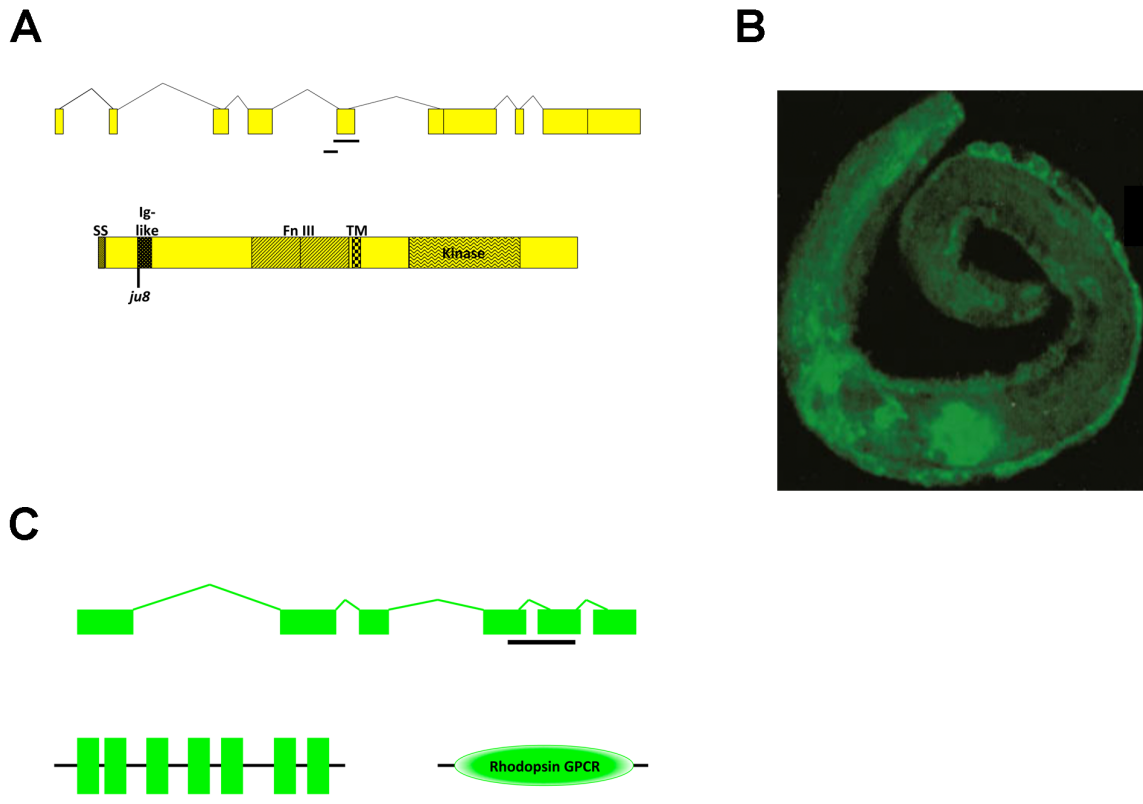


Figure 27. Gene structure and expression of *vab-1* and *f59d12.1*. A. Schematic of *vab-1* exons and introns as well as predicted protein domains. SS is signal sequence and TM is transmembrane domain. The location of the mutant alleles *ok1699* and *e2027* are denoted by black bars, and the location of *ju8* is noted in the protein domain structure. Adapted from (97). B. Example of VAB-1::GFP expression in a L1 animal with GFP present in the nerve ring and ventral nerve cord. Adapted from (97). C. Schematic of *f59d12.1* exons and introns as well as the predicted seven transmembrane domains and predicted rhodopsin GPCR like protein domain (SMART, ExPaSy).

IV.c.2 *vab-1* and *f59d12.1* cause a reduction in ACR-16::GFP and ACR-16::RFP levels

Both *vab-1* and *f59d12.1* were identified through whole genome sequencing based on their ability to affect expression of the ACR-16 receptor at the NMJ. Further evaluation of this modulation of ACR-16 receptors was examined by crossing these mutants into [a](#) line with a single copy insertion of ACR-16::GFP under the muscle specific promoter *Pmyo-3*, referred to as *jaSi4* (79). *jaSi4* was kept in an *acr-16* null background to prevent endogenous untagged ACR-16 receptor from diluting the ACR-16::GFP signal. [The three different *vab-1* mutant alleles described above](#) were crossed into *jaSi4;acr-16(ok789):vab-1(ok1699)*, *vab-1(e2027)*, and *vab-1(ju8)*. All three mutations caused a significant reduction in levels of ACR-16::GFP as compared to control, *jaSi4;acr-16(ok789)* (*(ok1699)*: 22.6±6.9 n=20, *(e2027)*: 24.7±6.4 n=10, *(ju8)*: 19.8±6.2 n=8, control: 28.3±9.2 n=35) (Fig. 28A,B). When *f59d12.1(gk1000)* was crossed into *jaSi4;acr-16(ok789)* and levels of ACR-16::GFP evaluated, again there was a significant reduction in fluorescence levels (*f59d12.1(gk1000)*: 12.8±5 n=9, control: 29.1±8.6 n=11) (Fig. 28C,D). This suggests that both [genes are involved in the regulation of](#) ACR-16 receptor expression at the NMJ.

It is possible that the reduction of ACR-16::GFP seen at the NMJ is not due to *vab-1(ok1699)* or *f59d12.1(gk1000)* affecting ACR-16 expression, but instead [regulation of](#) the *myo-3* promoter region. To assay this *vab-1(ok1699)* and *f59d12.1(gk1000)* were crossed into a line expressing a single copy of ACR-16::RFP driven under the endogenous *acr-16* promoter. *vab-1(ok1699)* and

f59d12.1(gk1000) mutants both caused a significant reduction in levels of ACR-16::RFP as compared to control (*vab-1(ok1699)*: 5.9 ± 3.4 n=7, *f59d12.1(gk1000)*: 5.9 ± 2.7 n=10, control: 11 ± 4.4 n=19) (Fig. 28.E,F). Additionally if these mutants were affecting regulation of the *myo-3* promoter region, a change in expression levels of MYO-3 would be expected. To explore this *vab-1(ok1699)* and *f59d12.1(gk1000)* were crossed into a line expressing the construct *Pmyo-3::GFP::MYO-3*, referred to as *rais5*. When levels of MYO-3::GFP were evaluated in the *vab-1(ok1699)* mutant background there was a slightly significant increase in fluorescence levels as compared to the control (*vab-1(ok1699)*: 23 ± 3.7 n=11, control: 15.8 ± 5 n=5) (Fig. 30E,F). In the *f59d12.1(gk1000)* mutant background there was no significant difference in levels of MYO-3::GFP as compared to the control (*f59d12.1(gk1000)*: 18.2 ± 3.2 n=11, control: 15.8 ± 3 n=5) (Fig. 30E,F). Together these two separate assays suggest that both *vab-1* and *f59d12.1* affect ACR-16 receptors in a way that is not dependent on promoter the used to express ACR-16.

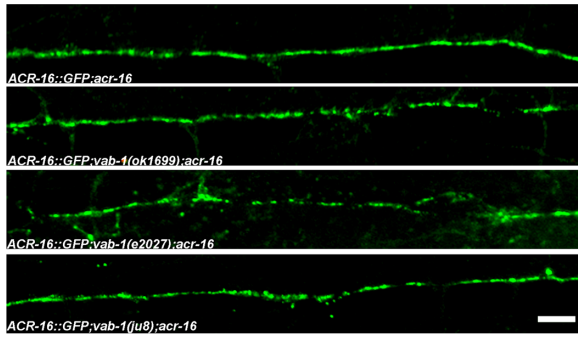
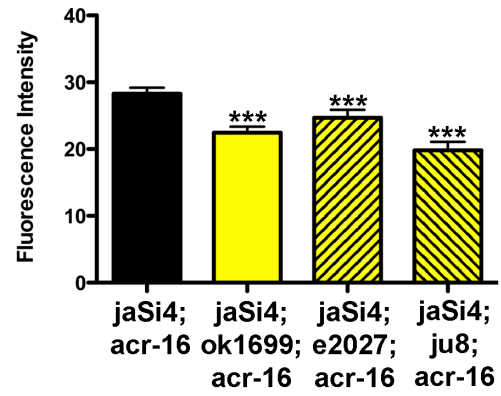
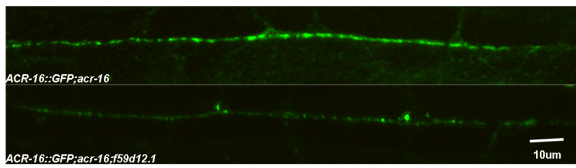
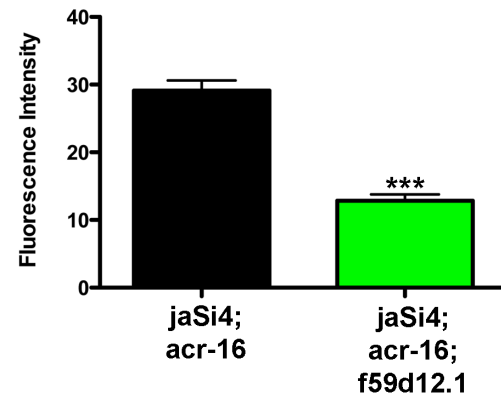
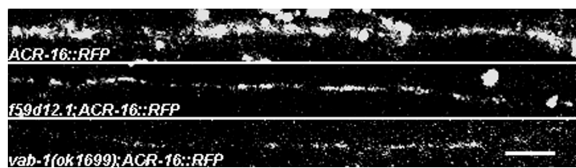
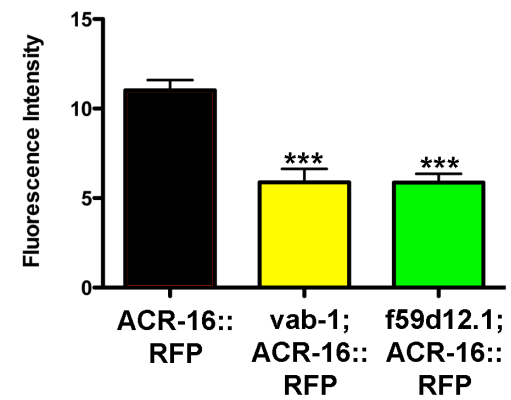
A**B****C****D****E****F**

Figure 28. Both *vab-1* and *f59d12.1* mutants decrease expression levels of ACR-16 receptors at the NMJ. A. Representative images of ACR-16::GFP in three different *vab-1* mutant alleles. B. Quantification of ACR-16::GFP fluorescence levels showed a significant decrease in all three *vab-1* mutants alleles as compared to the control (*ok1699*: 22.6 ± 6.9 n=20, *e2027*: 24.7 ± 6.4 n=10, *ju8*: 19.8 ± 6.2 n=8, control: 28.3 ± 9.2 n=35). C. Representative images of ACR-16::GFP in the *f59d12.1(gk1000)* mutant. D. Quantification of ACR-16::GFP fluorescence levels showed a significant decrease in the *f59d12.1* mutant background as compared to the control (*f59d12.1(gk1000)*: 12.8 ± 5 n=9, control: 29.1 ± 8.6 n=11). E. Representative images of ACR-16::RFP expression in *vab-1(ok1699)* and *f59d12.1(gk1000)* mutants. F. Quantification of ACR-16::GFP fluorescence showed a significant decrease in both the *vab-1(ok1699)* and *f59d12.1(gk1000)* mutants as compared to the control (*vab-1(ok1699)*: 5.9 ± 3.4 n=7, *f59d12.1(gk1000)*: 5.9 ± 2.7 n=10, control: 11 ± 4.4 n=19).

IV.c.3 Behavioral analysis of *vab-1* and *f59d12.1* mutants

Previous work by Touroutine et. al, (56) demonstrated that *acr-16* mutants alone do not have any significant behavioral phenotypes. However when *acr-16* mutants are crossed in to a LChR mutant background, the double mutant, lacking both AChR types, exhibit extreme levels of uncoordination. Thus the LChR mutant background was used to evaluate if *vab-1(ok1699)* and *f59d12.1(gk1000)* mutants were functionally affecting ACR-16 receptors.

In both a thrashing assay and a body bend assay there was no significant difference between *jaSi4;acr-16(ok789)* and *jaSi4;vab-1(ok1699);acr-16(ok789)*, as was expected (*jaSi4;vab-1(ok1699);acr-16(ok789)*: 22.1±6.1 n=10, *jaSi4;acr-16(ok789)*:22.9±4.1 n=10) (Fig. 29A,B). However, when *jaSi4;vab-1(ok1699);acr-16(ok789)* was crossed into the LChR mutant background, a significant reduction in number of thrashes and number of body bends was seen as compared the *unc-63(x37);jaSi4;acr-16(ok789)* control (*unc-63(x37);jaSi4;vab-1(ok1699);acr-16(ok789)*: 3.7±2.4 n=10, *unc-63(x37);jaSi4;acr-16(ok789)*: 10.7±2.6 n=10) (Fig. 29A,B). This suggests that the *vab-1* mutation is causing a deficit in ACR-16 receptor function.

In both a thrashing assay and a body bend assay there was no significant difference between *jaSi4;acr-16(ok789)* and *jaSi4;acr-16(ok789);f59d12.1(gk1000)*, again as was expected (*jaSi4;acr-16(ok789);f59d12.1(gk1000)*: 19.1±4.3 n=20, *jaSi4;acr-16(ok789)*: 19.7±4.5 n=20) (Fig. 29C,D). When *jaSi4;acr-16(ok789);f59d12.1(gk1000)* was crossed into a LChR mutant background, creating a double mutant, a reduction in number of thrashes and number of body bends was

observed, but it was not significant when compared to the *unc-63(x37);jaSi4;acr-16(ok789)* control (*unc-63(x37);jaSi4;acr-16(ok789);f59d12.1(gk1000)*: 7.8 ± 3 n=20, *unc-63(x37);jaSi4;acr-16(ok789)*: 10.1 ± 3.2 n=10) (Fig. 29C,D). Thus, although it seems that the *f59d12.1* mutation is having some functional affect on ACR-16 receptors, the impact is not as severe.

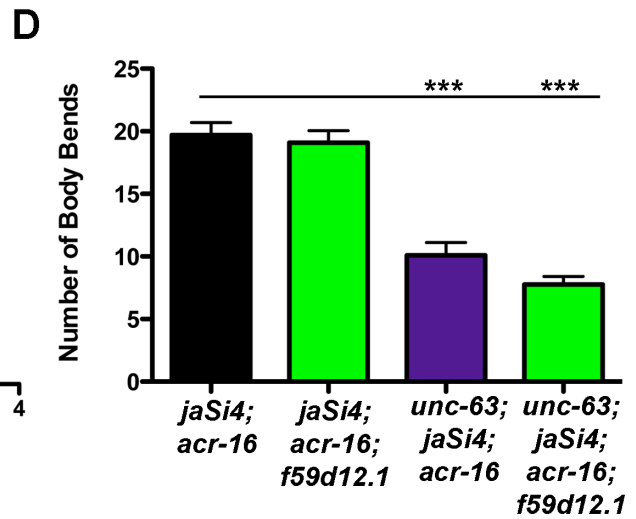
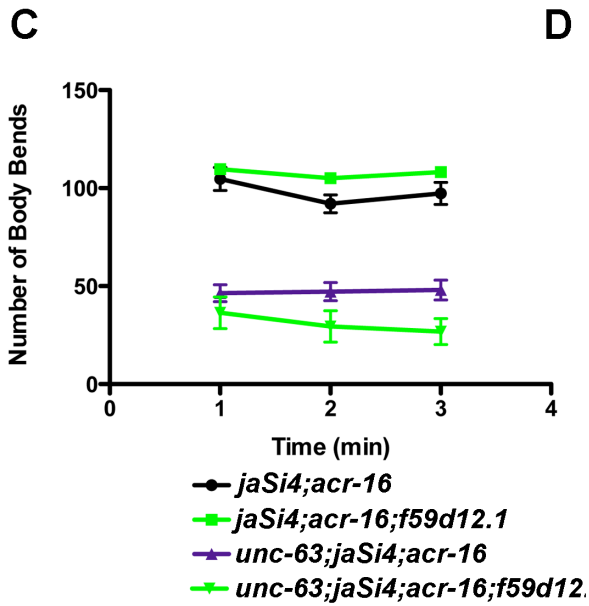
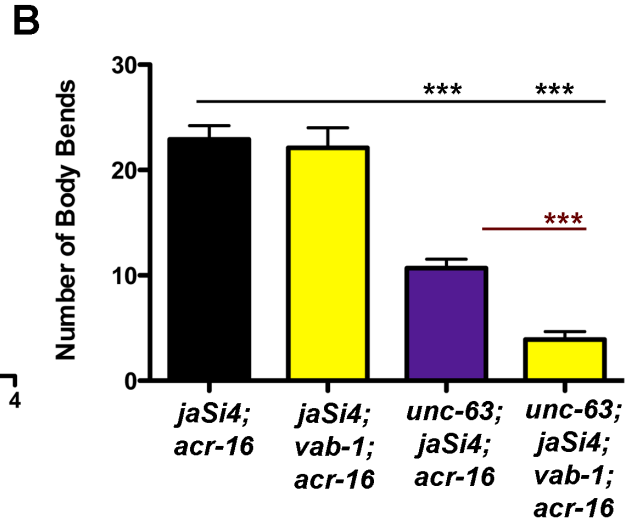
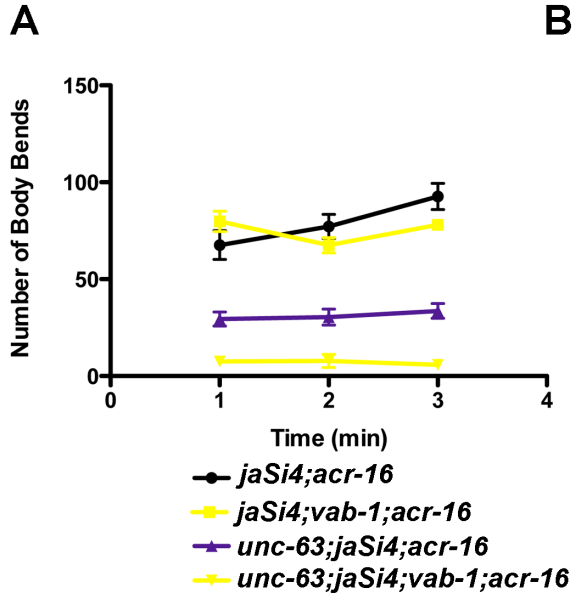


Figure 29. *vab-1* and *f59d12.1* mutants cause an increase in locomotory deficits in a LACHR mutant background. A. In *vab-1* mutants alone there is no significant change in number of thrashes as compared to the control; however when *vab-1* mutants are crossed into a LACHR mutant background there is a significant reduction in number of thrashes as compared to the uncoordinated LACHR mutants alone. B. In *vab-1* mutants alone there is no change in number of body bends as compared to the control (*jaSi4;vab-1(ok1699);acr-16(ok789)*: 22.1±6.1 n=10, *jaSi4;acr-16(ok789)*:22.9±4.1 n=10); however when crossed into a LACHR mutant background a significant reduction in the number of body bends is seen as compared to the already reduced LACHR mutant alone (*unc-63(x37);jaSi4;vab-1(ok1699);acr-16(ok789)*: 3.7±2.4 n=10, *unc-63(x37);jaSi4;acr-16(ok789)*: 10.7±2.6 n=10). C. There was no significant change in number of thrashes in *f59d12.1(gk1000)* mutants alone as compared to the control, however when crossed into an LACHR mutant background there is decreased number of thrashes as compared to the already uncoordinated LACHR mutant control, but it is not significant. D. There was no significant reduction in number of body bends in the *f59d12.1(gk1000)* mutants alone as compared to the control (*jaSi4;acr-16(ok789);f59d12.1(gk1000)*: 19.1±4.3 n=20, *jaSi4;acr-16(ok789)*: 19.7±4.5 n=20). However, when *f59d12.1(gk1000)* mutants were crossed into a LACHR mutant background there was a trend toward a reduction in body bends as compared to the already reduced LACHR mutant control (*unc-63(x37);jaSi4;acr-16(ok789);f59d12.1(gk1000)*: 7.8±3 n=20, *unc-63(x37);jaSi4;acr-16(ok789)*, however this was not significant.

IV.c.4 Synapse abundance and muscle integrity in *vab-1* and *f59d12.1* mutants

The ACR-16 receptor is found at the NMJ, thus it is important to address possible changes in presynaptic density as a cause for the reduction in expression level of postsynaptic ACR-16 in *vab-1(ok1699)* and *f59d12.1(gk1000)* mutants. To evaluate the number of cholinergic synapses, RAB-3, a cholinergic vesicular marker, was tagged with mCherry and expressed under the cholinergic neuron specific promoter *Pacr-2*. The *vab-1* mutants used to examine synapse number were: *vab-1(e2027)* and *vab-1(ju8)*. The number of RAB-3::mCherry puncta in these mutants was unchanged when compared with the control (*e2027*: 15.7±2.9 n=13, *ju8*: 12.4±2 n=9, control: 13.3±4.7 n=15) (Fig. 30A,B). The *f59d12.1(gk1000)* mutant was also evaluated for changes in synapse number, and again, when compared to the control, no significant difference in puncta number was seen (*f59d12.1(gk1000)*: 12.8±2.2 n=11, control: 13±2.2 n=9) (Fig. 30C,D). This suggests that a synaptogenesis defect is not the cause of observed changes in ACR-16 receptor expression in either *vab-1* or *f59d12.1* mutants.

Muscle architecture was also examined using the previously discussed *rals5* in *vab-1(ok1699)* and *f59d12.1(gk1000)* mutant backgrounds. As previously discussed, the level of MYO-3::GFP fluorescence was measured in the *vab-1* mutant background and a slight increase in fluorescence was observed (*vab-1(ok1699)*: 23±3.7 n=11, control: 15.8±5 n=5) (Fig. 28E,F). A slight rippling of the MYO-3 organization in the muscle was also observed. This may be due to a previously described role for *vab-1* in proper patterning of epithelial morphogenesis (George,

1998). There were no significant differences in the level of MYO-3::GFP fluorescence between the *f59d12.1* mutants and the control (*f59d12.1(gk1000)*): 18.2 ± 3.2 n=11, control: 15.8 ± 3 n=5) (Fig. 30E,F). The organization of MYO-3 also looked to be the same in both backgrounds. Overall, it does not seem that muscle structural defects are causing the ACR-16 expression and locomotion defects seen in *vab-1* and *f59d12.1* mutants.

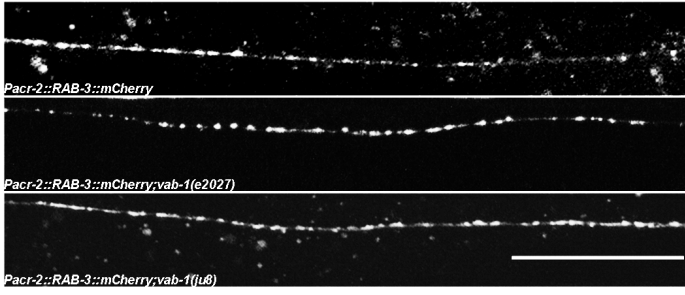
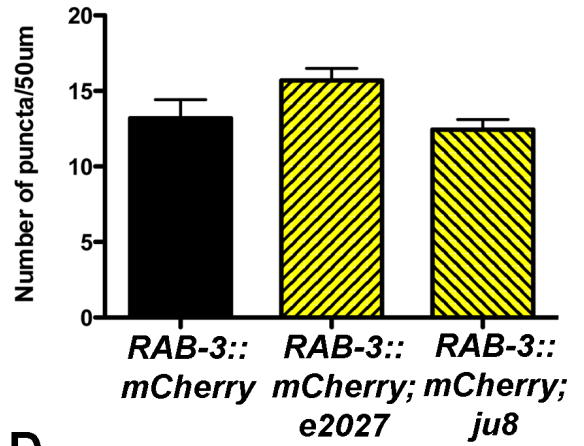
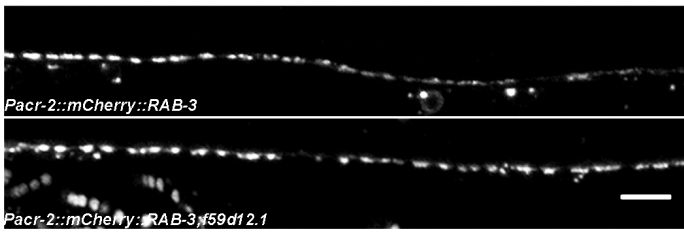
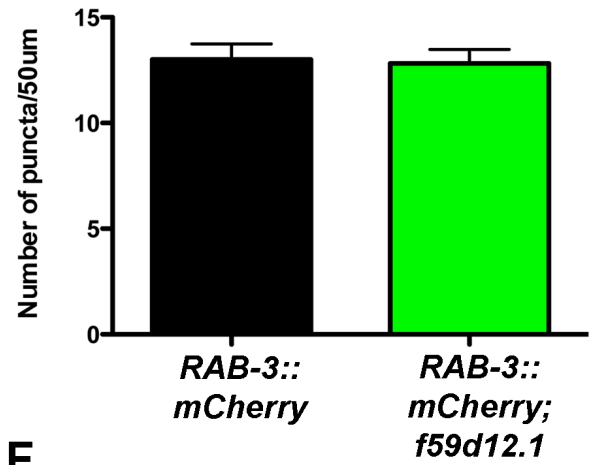
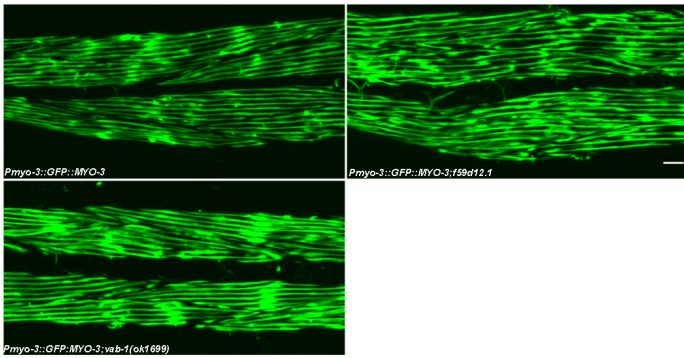
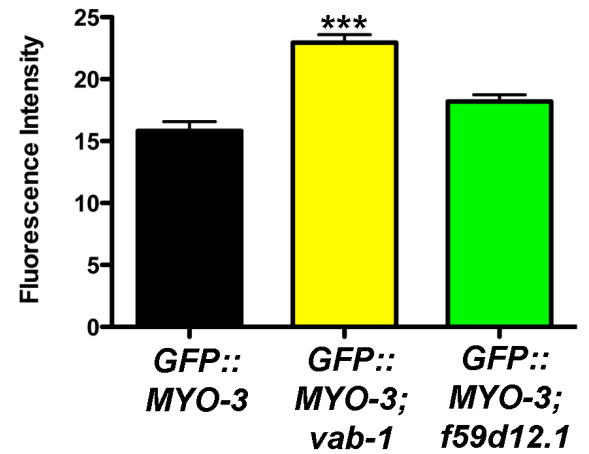
A**B****C****D****E****F**

Figure 30. Evaluation of *vab-1* and *f59d12.1* mutants roles in NMJ patterning.

A. Representative images of the cholinergic vesicular marker RAB-3::mCherry in multiple *vab-1* mutant alleles. B. Quantification of the number of cholinergic synaptic puncta showed no change in number in the *vab-1* mutant alleles as compared to the control (*e2027*: 15.7 ± 2.9 n=13, *ju8*: 12.4 ± 2 n=9, control: 13.3 ± 4.7 n=15). C. Representative images of the cholinergic synaptic marker RAB-3::mCherry in *f59d12.1* mutants. D. Quantification of the number of cholinergic synaptic puncta showed no change in number in the *f59d12.1(gk1000)* mutants as compared to the control (*f59d12.1(gk1000)*: 12.8 ± 2.2 n=11, control: 13 ± 2.2 n=9). E. Representative images of body wall muscle myosin marker MYO-3::GFP in *vab-1* and *f59d12.1* mutant backgrounds. F. Quantification of MYO-3::GFP in *vab-1* mutants showed a significant increase in GFP levels as compared to the control (*vab-1(ok1699)*: 23 ± 3.7 n=11, control: 15.8 ± 5 n=5). *f59d12.1* mutants showed no change in MYO-3::GFP levels as compared to the control (*f59d12.1(gk1000)*: 18.2 ± 3.2 n=11, control: 15.8 ± 3 n=5).

IV.c.5 Localization and levels of the LACHR in *vab-1* and *f59d12.1*

mutants

To determine whether *vab-1* and *f59d12.1* mutations were acting specifically on the ACR-16 receptor and not generally affecting NMJ receptors, the mutants were crossed into a strain expressing UNC-29::RFP. In the *vab-1(e2027)* mutant background there was no significant difference in UNC-29::RFP fluorescence levels as compared to the control (*vab-1(e2027)*: 15.6 ± 5.2 n=7, control: 14.5 ± 9.6 n=9) (Fig. 31A,B). The localization of the RFP signal along the nerve cord also did not have any distinctive changes in patterning when compared to the control. This data suggest that *vab-1* mutants act specifically on the ACR-16 receptors at the NMJ. In the *f59d12.1(gk1000)* mutant background there was also no significant difference in gross localization of the tagged receptors as compared to the control. However, there was a slightly significant increase in the levels of RFP fluorescence in the *f59d12.1(gk1000)* mutants as compared to the control, suggesting an increase in levels of LACHRs (*f59d12.1(gk1000)*: 18.5 ± 6.5 n=8, control: 14.5 ± 4.6 n=9) (Fig. 31C,D). This suggests that F59D12.1 may have opposing functions in regulating expression of the LACHRs at the NMJ.

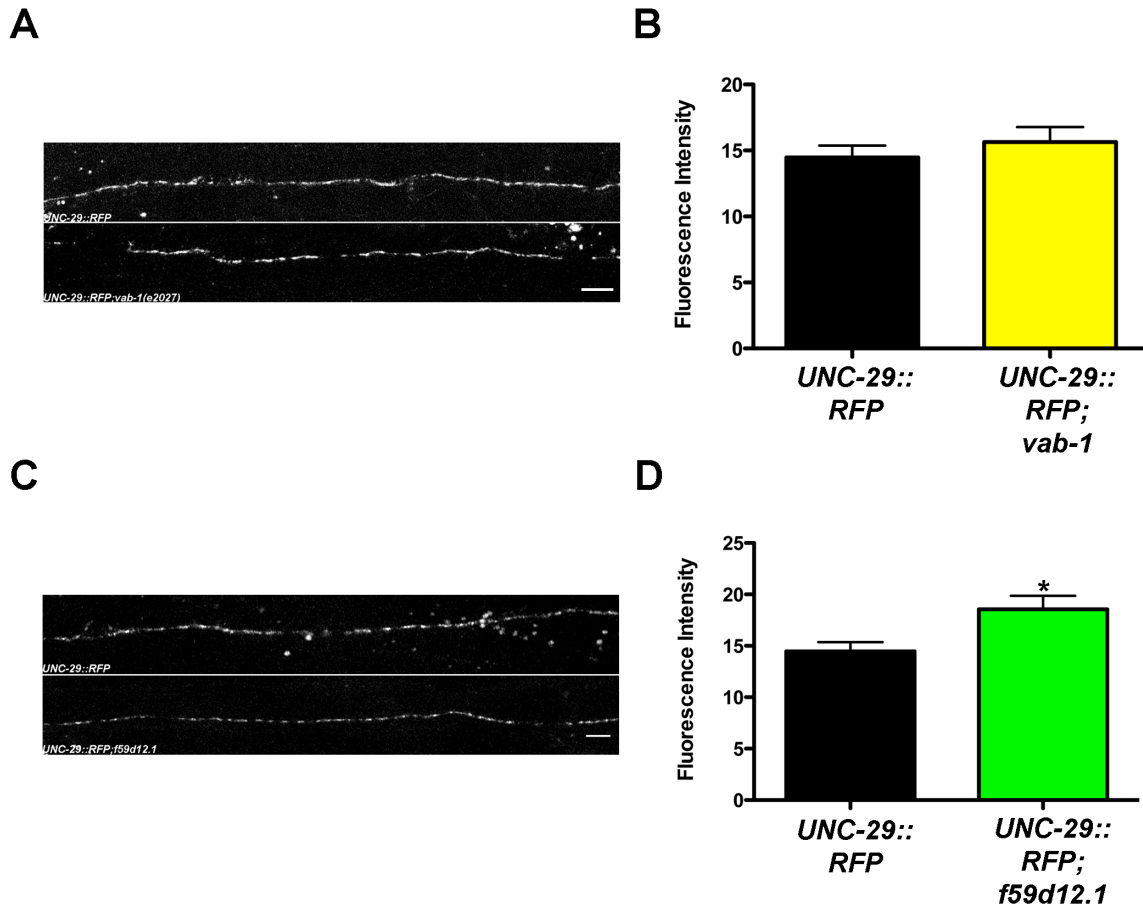


Figure 31. Change in LACHR levels and localization in *vab-1* and *f59d12.1*

mutants. A. Representative images of LACHR reporter UNC-29::RFP in *vab-1(e2027)* mutants. B. Quantification of UNC-29::RFP levels demonstrated no significant difference in fluorescence in *vab-1(e2027)* mutants as compared to the control (*vab-1(e2027)*): 15.6 ± 5.2 n=7, control: 14.5 ± 9.6 n=9). C. Representative images of LACHR reporter UNC-29::RFP in *f59d12.1(gk1000)* mutants. D. Quantification of UNC-29::RFP levels showed a significant increase in fluorescence levels in *f59d12.1* mutants as compared to the control (*f59d12.1(gk1000)*): 18.5 ± 6.5 n=8, control: 14.5 ± 4.6 n=9).

IV.c.6 Electrophysiological analysis of *vab-1* and *f59d12.1*

The changes observed in ACR-16 receptor expression and function in the *vab-1* and *f59d12.1* mutants suggest that there should also be an effect on postsynaptic responses to endogenous ACh release. This was evaluated performing whole cell patch clamp recordings of evoked NMJ responses, which were obtained in 1mM Ca²⁺ from dissected worms. The evoked current amplitudes were recorded from *vab-1(ok1699)* mutants and were **found to be** significantly increased as compared to the *N2* control (*vab-1(ok1699)*: 2445.2±650.9 n=6, *N2*: 1866.1±329.6 n=12) (Fig. 32A,B). This suggests that in addition to a postsynaptic change in ACR-16 receptor expression, there is also a presynaptic affect occurring, possibly a compensatory mechanism due to the reduction in receptor levels at the NMJ. The evoked current amplitudes were also recorded from *f59d12.1(gk1000)* mutants and a significant decrease was seen as compared to the wild-type control *N2* (*f59d12.1(gk1000)*: 1103.8±612.2 n=6, *N2*: 1866.1±329.6 n=12) (Fig. 32C,D). **This data** agrees with the **reduced** levels of fluorescence, and thus expression, of ACR-16::GFP receptors at NMJs see in *f59d12.1(gk1000)* mutants.

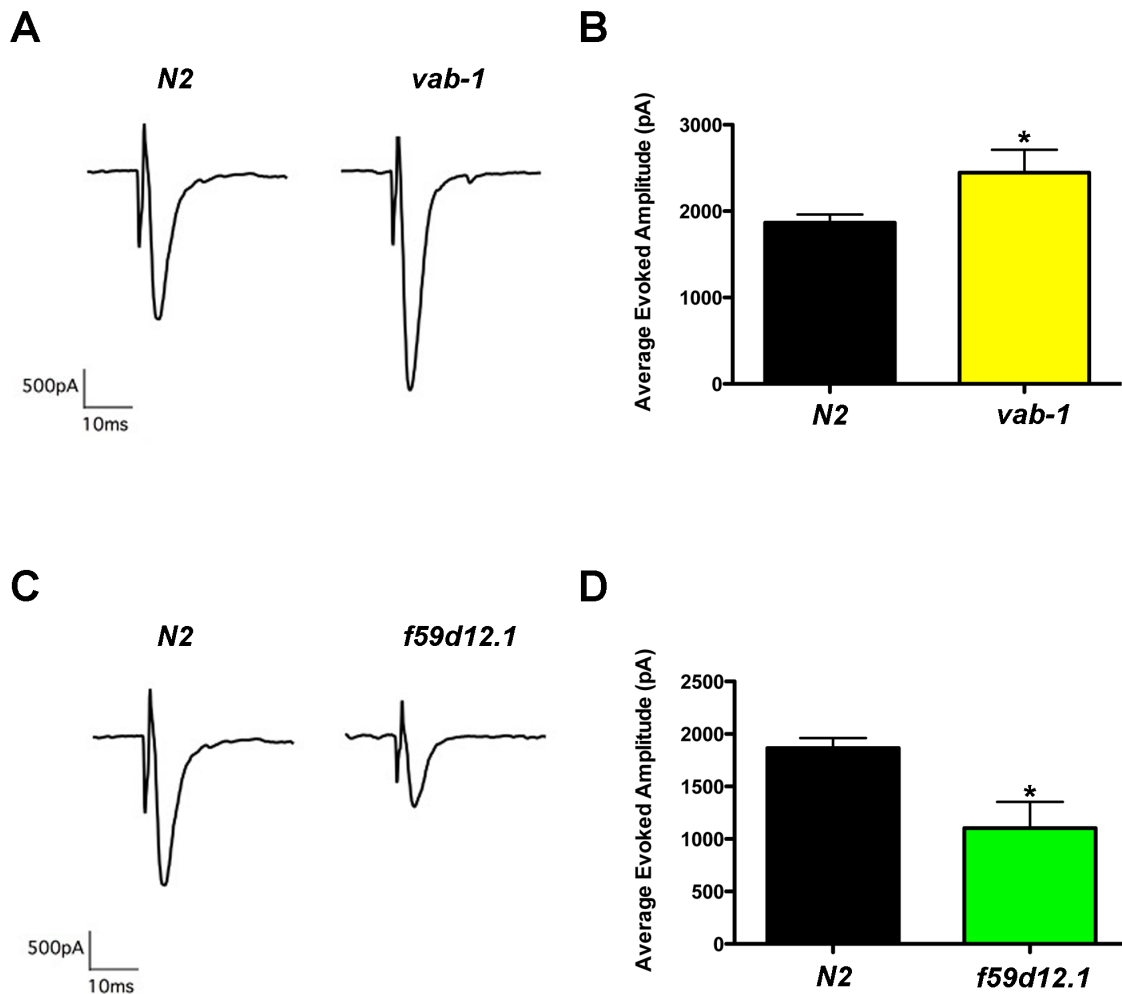


Figure 32. Electrophysiological evaluation of synaptic transmission in *vab-1* and *f59d12.1* mutants. A. Representative traces of postsynaptic evoked response amplitudes in *vab-1(ok1699)* mutants. B. Quantification of evoked response amplitudes in *vab-1(ok1699)* mutants showed a significant increase in amplitude size as compared to the control (*vab-1(ok1699)*: 2445.2 ± 650.9 n=6, *N2*: 1866.1 ± 329.6 n=12). C. Representative traces of postsynaptic evoked response amplitudes in *f59d12.1(gk1000)* mutants. D. Quantification of evoked response amplitudes in *f59d12.1(gk1000)* mutants showed a significant reduction in amplitude size as compared to the control (*f59d12.1(gk1000)*: 1103.8 ± 612.2 n=6, *N2*: 1866.1 ± 329.6 n=12)

IV.c.7 Relative *acr-16* mRNA levels in *vab-1* and *f59d12.1* mutants is increased

vab-1 and *f59d12.1* mutants could be causing the defects seen in ACR-16 expression and function through regulation of *acr-16* gene transcription. To address this possibility the relative mRNA levels of *acr-16* present in each of these mutant backgrounds was evaluated. Total mRNA was collected from *jaSi4;vab-1(ok1699);acr-16(ok789)* and *jaSi4;acr-16(ok789);f59d12.1(gk1000)* animals, reverse transcribed, and qRT-PCR was performed. Actin was used as an internal control for all samples. When the relative levels of *acr-16* mRNA were compared to the normalized control, obtained from *jaSi4;acr-16(ok789)* animals, a significant increase in both the *vab-1(ok1699)* and *f59d12.1(gk1000)* mutants was observed, suggesting an elevation of *acr-16* mRNA (*vab-1(ok1699)*: 1.7 ± 0.4 n=5, *f59d12.1(gk1000)*: 1.7 ± 0.5 n=5, control: 1 ± 0 n=5) (Fig. 33). This could be due to another regulatory pathway, compensating for the reduction in ACR-16 protein expression by increasing *acr-16* mRNA production.

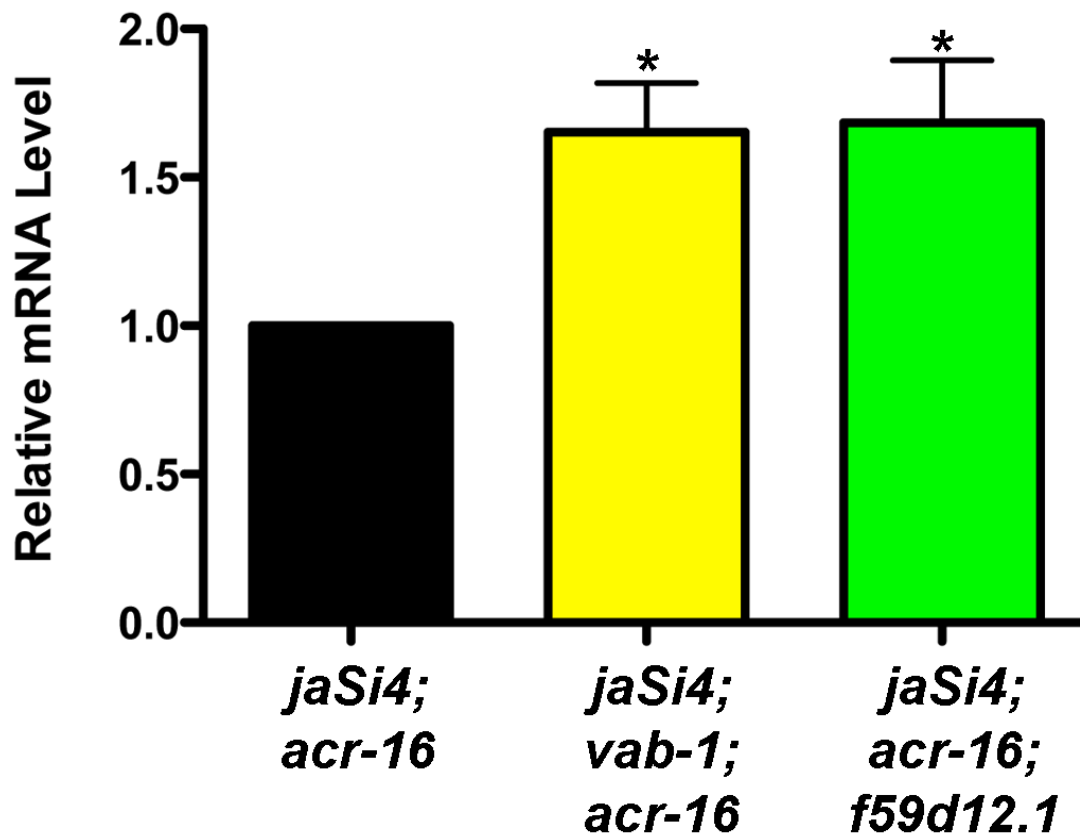


Figure 33. *vab-1* and *f59d12.1* mutants are affecting transcription of *acr-16*.

Relative levels of *acr-16* mRNA was increased in both *vab-1(ok1699)* and *f59d12.1(gk1000)* mutants (*vab-1(ok1699)*: 1.7 ± 0.4 n=5, *f59d12.1(gk1000)*: 1.7 ± 0.5 n=5, control: 1 ± 0 n=5).

IV.d Discussion and Future Directions

In this chapter evidence has been presented that show both *vab-1* and *f59d12.1* affect the expression of ACR-16 NACHRs. Mutants in each of these genes cause a reduction in levels of *Pmyo-3* driven ACR-16::GFP expression as well as ACR-16::RFP at the NMJ. Since ACR-16::RFP was expressed under the endogenous *acr-16* promoter together with the evidence that levels of MYO-3::GFP were not decreased in these mutant backgrounds, it appears that the changes in ACR-16 receptor fluorescence levels are not through the misregulation of the MYO-3 promoter region. There was no change in number of cholinergic synaptic puncta seen in either mutant background and the muscle architecture was unperturbed, demonstrating that the changes in ACR-16 receptor expression level are not due to a NMJ patterning defect. The behavioral assays displayed a functional defect in ACR-16 signaling based on the severely uncoordinated phenotype observed in *vab-1;unc-63* double mutants. Although the behavioral defects in the double mutant generated with *f59d12.1* were not statistically significant, there was a distinct trend towards the characteristic decreased motility. Interestingly, in both mutants there was an increase in relative levels of *acr-16* mRNA. This may suggest a role for these proteins in regulating transcription of *acr-16* or this may be indicative of a compensatory mechanism, suggesting targeted removal or degradation of the ACR-16 receptors.

How might VAB-1, an EphB homolog regulate *C. elegans* nAChR expression?

Studies have shown the interactions between EphB receptors, ephrin B ligands and AMPA and NMDA receptors at the synapses of vertebrates. Specifically, EphB4 receptor binding of the ephrinB2 ligand results in the stabilization of AMPA

receptors at the synapse. [Furthermore](#), in a mouse ephrinB2 [knockout](#), AMPA receptor internalization was seen along with a reduction in excitatory synaptic current (104). This implies that AMPA [receptor](#) stabilization is dependent on the ephrinB2 ligand. In a mouse knockout for the EphB receptor there was a significant difference in the function and distribution of NMDA receptors, causing a reduction in NMDA derived current. A significant decrease in post-synaptic density associated NMDA receptors was [also](#) seen, [although](#) the overall number of receptors was unchanged (105). [These](#) data, along with another study showing a post-synaptically located, direct interaction between EphB receptors and NMDA receptors, implies NMDA regulation is mediated through the EphB receptor (106). Other studies have identified roles for the EphA receptor and ephrin A ligand in stabilizing the NMJ in mammals. In ephrin A5 knockout mice, axon terminals were no longer properly coupled with post-synaptic machinery. This deficit illustrated the need for the interaction of the ligand, expressed in muscles, with the EphA4 receptor, expressed in motor neurons (107). A study examining the clustering mechanism of the second cholinergic receptor type present at the worm NMJ, LAChRs, demonstrated that LEV-10 was necessary for the localization of the LAChR. LEV-10 contains a domain most similar to vertebrate NETO2. NETO2, and its paralog NETO1, have been shown to be necessary for NMDA receptor stabilization, similar to that seen with EphB receptor interactions (71, 108). It is possible that these conserved clustering mechanisms may play a role in regulating the presence of the NAChR, ACR-16, at the *C. elegans* NMJ.

As the *C. elegans* Eph *vab-1* is similar to both vertebrate EphA and EphB and the 4 known ephrin ligands in the worm show strong similarities to ephrin B ligands, it will be interesting to examine mutants affecting other components of the ephrin pathway in *C. elegans*, on ACR-16 receptors (98). This is proposed with the caveat that based on these proteins known roles in gastrulation and endothelial development some combination may cause lethality.

How might the GPCR, F59D12.1 regulate *C. elegans* nAChR expression?

The role of GPCR regulation of ACR-16 receptors has not been previously explored in the worm. Further analysis addressing the function and localization *f59d12.1* should be investigated. Previous work has identified other CCKR2 homologues in *C. elegans*, referred to as *ckr-2*, which are expressed in both cholinergic and GABAergic motor neurons (109). In vertebrates, studies looking at the interactions between GPCRs and the $\alpha 7$ receptor have revealed that in regions of the mouse brain, $\alpha 7$ receptors associate with Gas, G α q, and G α i proteins. A G-protein binding motif within the M3-M4 loop of the $\alpha 7$ receptor was also identified. This coupling was shown to cause $\alpha 7$ mediated calcium release from internal stores in the endoplasmic reticulum, which is dependent on G α q binding to the $\alpha 7$ receptor (110). It is possible that F59D12.1 is working through a regulatory mechanism similar to this in *C. elegans*. Further examination of the potential G-protein binding site on ACR-16 and other components of the downstream signaling cascade should be pursued.

CITED LITERATURE

1. Shen J, Yakel JL. Nicotinic acetylcholine receptor-mediated calcium signaling in the nervous system. *Acta Pharmacol Sin.* 2009;30(6):673-680. doi:10.1038/aps.2009.64.
2. Fucile S. Ca²⁺ permeability of nicotinic acetylcholine receptors. *Cell Calcium.* 2004;35(1):1-8. doi:10.1016/j.ceca.2003.08.006.
3. Guerra-??lvarez M, Moreno-Ortega AJ, Navarro E, et al. Positive allosteric modulation of alpha-7 nicotinic receptors promotes cell death by inducing Ca²⁺ release from the endoplasmic reticulum. *J Neurochem.* 2015:309-319. doi:10.1111/jnc.13049.
4. Dineley KT, Pandya AA, Yakel JL. Nicotinic ACh Receptors as Therapeutic Targets in CNS Disorders. 2015;72(2):181-204. doi:10.1038/nature13314.A.
5. Steinlein OK, Bertrand D. Neuronal nicotinic acetylcholine receptors: From the genetic analysis to neurological diseases. *Biochem Pharmacol.* 2008;76(10):1175-1183. doi:10.1016/j.bcp.2008.07.012.
6. Kalamida D, Poulas K, Avramopoulou V, et al. Muscle and neuronal nicotinic acetylcholine receptors: Structure, function and pathogenicity. *FEBS J.* 2007;274(15):3799-3845. doi:10.1111/j.1742-4658.2007.05935.x.
7. Zouridakis M, Zisimopoulou P, Poulas K, Tzartos SJ. Recent advances in understanding the structure of nicotinic acetylcholine receptors. *IUBMB Life.* 2009;61(4):407-423. doi:10.1002/iub.170.

8. Dani JA, Bertrand D. Nicotinic acetylcholine receptors and nicotinic cholinergic mechanisms of the central nervous system. *Annu Rev Pharmacol Toxicol.* 2007;47:699-729.
doi:10.1146/annurev.pharmtox.47.120505.105214.
9. Gotti C, Clementi F. Neuronal nicotinic receptors: From structure to pathology. *Prog Neurobiol.* 2004;74(6):363-396. doi:10.1016/j.pneurobio.2004.09.006.
10. Oz M, Lorke DE, Yang KS, Petroianu G. On the Interaction of β -Amyloid Peptides and α 7-Nicotinic Acetylcholine Receptors in Alzheimer ' s Disease. *Curr Alzheimer Res.* 2013;10(6):618-630.
11. Wang H, Lee DHS, Andrea MRD, Peterson P a, Shank RP, Reitz AB. Amyloid 1 – 42 Binds to α 7 Nicotinic Acetylcholine Receptor with. *Biochemistry.* 2000;275(8):5626-5632.
12. Hernandez CM, Kaye R, Zheng H, Sweatt JD, Dineley KT. Loss of α 7 Nicotinic Receptors Enhances β -Amyloid Oligomer Accumulation , Exacerbating Early-Stage Cognitive Decline and Septohippocampal Pathology in a Mouse Model of Alzheimer ' s Disease. *Hippocampus.* 2010;30(7):2442-2453.
doi:10.1523/JNEUROSCI.5038-09.2010.
13. Puzzo D, Privitera L, Leznik E, et al. Picomolar amyloid-beta positively modulates synaptic plasticity and memory in hippocampus. *J Neurosci.* 2008;28(53):14537-14545. doi:10.1523/JNEUROSCI.2692-08.2008.
14. Quik M, Bordia T, Zhang D, Perez XA. *Nicotine and Nicotinic Receptor Drugs.*

Vol 124. 1st ed. Elsevier Inc.; 2015. doi:10.1016/bs.irn.2015.07.005.

15. Burghaus L, Schütz U, Krempel U, Lindstrom J, Schröder H. Loss of nicotinic acetylcholine receptor subunits $\alpha 4$ and $\alpha 7$ in the cerebral cortex of Parkinson patients. *Park Relat Disord*. 2003;9(5):243-246. doi:10.1016/S1353-8020(03)00028-2.
16. Lewis AS, Picciotto MR. High-affinity nicotinic acetylcholine receptor expression and trafficking abnormalities in psychiatric illness. *Psychopharmacology (Berl)*. 2013;229(3):477-485. doi:10.1007/s00213-013-3126-5.
17. Wing VC, Wass CE, Soh DW, George TP. A review of neurobiological vulnerability factors and treatment implications for comorbid tobacco dependence in schizophrenia. *Ann N Y Acad Sci*. 2012;1248(1):89-106. doi:10.1111/j.1749-6632.2011.06261.x.
18. Gautam M, Noakes PG, Moscoso L, et al. Defective neuromuscular synaptogenesis in agrin-deficient mutant mice. *Cell*. 1996;85(4):525-535. doi:10.1016/S0092-8674(00)81253-2.
19. Ferns MJ, Campanelli JT, Hoch W, Scheller RH, Hall Z. The ability of agrin to cluster AChRs depends on alternative splicing and on cell surface proteoglycans. *Neuron*. 1993;11(3):491-502. doi:10.1016/0896-6273(93)90153-I.
20. Zong Y, Jin R, Jolla L. Structural Mechanisms of the Agrin-LRP4-MuSK

- Signaling Pathway in Neuromuscular Junction Differentiation. 2015;70(17):0-20. doi:10.1007/s00018-012-1209-9.Structural.
21. Huh K-H, Fuhrer C. Clustering of nicotinic acetylcholine receptors: from the neuromuscular junction to interneuronal synapses. *Mol Neurobiol.* 2002;25(1):79-112. doi:10.1385/MN:25:1:079.
 22. Burden SJ. Building the vertebrate neuromuscular synapse. *J Neurobiol.* 2002;53(4):501-511. doi:10.1002/neu.10137.
 23. Messeant J, Dobbertin a., Girard E, et al. MuSK Frizzled-Like Domain Is Critical for Mammalian Neuromuscular Junction Formation and Maintenance. *J Neurosci.* 2015;35(12):4926-4941. doi:10.1523/JNEUROSCI.3381-14.2015.
 24. Glass DJ, Bowen DC, Stitt TN, et al. Agrin acts via a MuSK receptor complex. *Cell.* 1996;85(4):513-523. doi:10.1016/S0092-8674(00)81252-0.
 25. DeChiara TM, Bowen DC, Valenzuela DM, et al. The receptor tyrosine kinase MuSK is required for neuromuscular junction formation in vivo. *Cell.* 1996;85(4):501-512. doi:10.1016/S0092-8674(00)81251-9.
 26. Kim N, Stiegler AL, Cameron TO, et al. Lrp4 Is a Receptor for Agrin and Forms a Complex with MuSK. *Cell.* 2008;135(2):334-342. doi:10.1016/j.cell.2008.10.002.
 27. Weatherbee SD, Anderson K V, Niswander L a. LDL-receptor-related protein 4 is crucial for formation of the neuromuscular junction. *Development.* 2006;133(24):4993-5000. doi:10.1242/dev.02696.

28. Zhang W, Coldefy AS, Hubbard SR, Burden SJ. Agrin binds to the N-terminal region of Lrp4 protein and stimulates association between Lrp4 and the first immunoglobulin-like domain in muscle-specific kinase (MuSK). *J Biol Chem.* 2011;286(47):40624-40630. doi:10.1074/jbc.M111.279307.
29. Okada K. The Muscle Protein Dok-7 Is Essential for Neuromuscular Synaptogenesis. *Science (80-).* 2006;312(5781):1802-1805. doi:10.1126/science.1127142.
30. Inoue A, Setoguchi K, Matsubara Y, et al. Dok-7 activates the muscle receptor kinase MuSK and shapes synapse formation. *Sci Signal.* 2009;2(59):ra7. doi:10.1126/scisignal.2000113.
31. Yamanashi Y, Higuchi O, Beeson D. Dok-7/MuSK signaling and a congenital myasthenic syndrome. *Acta Myol.* 2008;27(JULY):25-29.
32. Bergamin E, Hallock PT, Burden SJ, Hubbard SR. The Cytoplasmic Adaptor Protein Dok7 Activates the Receptor Tyrosine Kinase MuSK via Dimerization. *Mol Cell.* 2010;39(1):100-109. doi:10.1016/j.molcel.2010.06.007.
33. Lu B, Garrido N, Spelbrink JN, Suzuki CK. Tid1 isoforms are mitochondrial DnaJ-like chaperones with unique carboxyl termini that determine cytosolic fate. *J Biol Chem.* 2006;281(19):13150-13158. doi:10.1074/jbc.M509179200.
34. Moransard M, Borges LS, Willmann R, et al. Agrin regulates rapsyn interaction with surface acetylcholine receptors, and this underlies cytoskeletal anchoring and clustering. *J Biol Chem.* 2003;278(9):7350-7359.

doi:10.1074/jbc.M210865200.

35. Apel ED, Glass DJ, Moscoso LM, Yancopoulos GD, Sanes JR. Rapsyn is required for MuSK signaling and recruits synaptic components to a MuSK-containing scaffold. *Neuron*. 1997;18(4):623-635. doi:10.1016/S0896-6273(00)80303-7.
36. Mihailovska E, Raith M, Valencia RG, et al. Neuromuscular synapse integrity requires linkage of acetylcholine receptors to postsynaptic intermediate filament networks via rapsyn-plectin 1f complexes. *Mol Biol Cell*. 2014;25(25):4130-4149. doi:10.1091/mbc.E14-06-1174.
37. Piguet J, Schreiter C, Segura JM, Vogel H, Hovius R. Acetylcholine receptor organization in membrane domains in muscle cells: Evidence for rapsyn-independent and rapsyn-dependent mechanisms. *J Biol Chem*. 2011;286(1):363-369. doi:10.1074/jbc.M110.139782.
38. Park J-Y, Ikeda H, Ikenaga T, Ono F. Acetylcholine receptors enable the transport of rapsyn from the Golgi complex to the plasma membrane. *October*. 2008;141(4):520-529. doi:10.1016/j.surg.2006.10.010.Use.
39. Godfrey EW. Comparison of agrin-like proteins from the extracellular matrix of chicken kidney and muscle with neural agrin, a synapse organizing protein. *Exp Cell Res*. 1991;195(1):99-109. doi:0014-4827(91)90504-N [pii].
40. Gingras J, Rassadi S, Cooper E, Ferns M. Agrin plays an organizing role in the formation of sympathetic synapses. *J Cell Biol*. 2002;158(6):1109-1118. doi:10.1083/jcb.200203012.

41. Ksiazek I, Burkhardt C, Lin S, et al. Synapse Loss in Cortex of Agrin-Deficient Mice after Genetic Rescue of Perinatal Death. *J Neurosci.* 2007;27(27):7183-7195. doi:10.1523/JNEUROSCI.1609-07.2007.
42. Garcia-Osta A, Tsokas P, Pollonini G, Landau EM, Blitzler R, Alberini CM. MuSK Expressed in the Brain Mediates Cholinergic Responses, Synaptic Plasticity, and Memory Formation. *J Neurosci.* 2006;26(30):7919-7932. doi:10.1523/JNEUROSCI.1674-06.2006.
43. Pohlkamp T, Durakoglugil M, Lane-Donovan C, et al. Lrp4 domains differentially regulate limb/brain development and synaptic plasticity. *PLoS One.* 2015;10(2):1-11. doi:10.1371/journal.pone.0116701.
44. Buzsáki G. Theta oscillations in the hippocampus. *Neuron.* 2002;33(3):325-340. doi:10.1016/S0896-6273(02)00586-X.
45. Daniels MP. The Role of Agrin in Synaptic Development, Plasticity, and Signaling in the Central Nervous System. 2011;72(2):181-204. doi:10.1038/nature13314.A.
46. Sulston JE, Brenner S. The DNA of *Caenorhabditis elegans*. *Genetics.* 1974;77(1):95-104.
47. The *C. elegans* Sequencing Consortium. Genome sequence of the nematode *C. elegans*: a platform for investigating biology. *Science.* 1998;282(5396):2012-2018. doi:10.1126/science.282.5396.2012.
48. Hobert O. Specification of the nervous system. *WormBook.* 2005:1-19.

doi:10.1895/wormbook.1.12.1.

49. Jones AK, Sattelle DB. Functional genomics of the nicotinic acetylcholine receptor gene family of the nematode, *Caenorhabditis elegans*. *BioEssays*. 2004;26(1):39-49. doi:10.1002/bies.10377.
50. Richmond JE, Jorgensen EM. One GABA and two acetylcholine receptors function at the. *America (NY)*. 1999:791-798.
51. Lewis A, Elmer S, Fleming J. Cholinergic elegans Receptor Mutants of the Nematode *Caenorhabditis*. *J Neurosci*. 1987;7(October):3059-3071.
52. Fleming JT, Squire MD, Barnes TM, et al. *Caenorhabditis elegans* levamisole resistance genes *lev-1*, *unc-29*, and *unc-38* encode functional nicotinic acetylcholine receptor subunits. *J Neurosci*. 1997;17(15):5843-5857.
53. Culetto E, Baylis H a, Richmond JE, et al. The *Caenorhabditis elegans* *unc-63* gene encodes a levamisole-sensitive nicotinic acetylcholine receptor alpha subunit. *J Biol Chem*. 2004;279(41):42476-42483.
doi:10.1074/jbc.M404370200.
54. Towers PR, Edwards B, Richmond JE, Sattelle DB. The *Caenorhabditis elegans* *lev-8* gene encodes a novel type of nicotinic acetylcholine receptor alpha subunit. *J Neurochem*. 2005;93(1):1-9. doi:10.1111/j.1471-4159.2004.02951.x.
55. Boulin T, Gielen M, Richmond JE, Williams DC, Paoletti P, Bessereau J-L. Eight genes are required for functional reconstitution of the *Caenorhabditis elegans*

- levamisole-sensitive acetylcholine receptor. *Proc Natl Acad Sci U S A*. 2008;105(47):18590-18595. doi:10.1073/pnas.0806933105.
56. Touroutine D, Fox RM, Von Stetina SE, Burdina A, Miller DM, Richmond JE. *acr-16* encodes an essential subunit of the levamisole-resistant nicotinic receptor at the *Caenorhabditis elegans* neuromuscular junction. *J Biol Chem*. 2005;280(29):27013-27021. doi:10.1074/jbc.M502818200.
57. Francis M, Evans S, Jensen M, et al. The Ror Receptor Tyrosine Kinase CAM-1 Is Required for ACR-16-Mediated Synaptic Transmission at the Neuromuscular Junction. *Neuron*. 2005;46(2):255-267.
58. Ballivet M, Alliod C, Bertrand S, Bertrand D. Nicotinic acetylcholine receptors in the nematode *Caenorhabditis elegans*. *J Mol Biol*. 1996;258(2):261-269. doi:10.1006/jmbi.1996.0248.
59. Nguyen M, Alfonso A, Johnson CD, Rand JB. *Caenorhabditis elegans* mutants resistant to inhibitors of acetylcholinesterase. *Genetics*. 1995;140(2):527-535.
60. Miller KG, Alfonso a, Nguyen M, Crowell J a, Johnson CD, Rand JB. A genetic selection for *Caenorhabditis elegans* synaptic transmission mutants. *Proc Natl Acad Sci U S A*. 1996;93(22):12593-12598. doi:10.1073/pnas.93.22.12593.
61. Bamber BA, Beg AA, Twyman RE, Jorgensen EM. The *Caenorhabditis elegans* *unc-49* locus encodes multiple subunits of a heteromultimeric GABA receptor. *J Neurosci*. 1999;19(13):5348-5359. doi:10.1006/dbio.1996.0240.
62. Halevi S, McKay J, Palfreyman M, et al. The *C. elegans* *ric-3* gene is required for

- maturation of nicotinic acetylcholine receptors. *EMBO J.* 2002;21(5):1012-1020. doi:10.1093/emboj/21.5.1012.
63. Shima DT, Scales SJ, Kreis TE, Pepperkok R. Segregation of COPI-rich and anterograde-cargo-rich domains in endoplasmic-reticulum-to-Golgi transport complexes. *Curr Biol.* 1999;9(15):821-824. doi:10.1016/S0960-9822(99)80365-0.
64. Garcia-Mata R, Szul T, Alvarez C, Sztul E. ADP-Ribosylation Factor/COPI-dependent Events at the Endoplasmic Reticulum-Golgi Interface Are Regulated by the Guanine Nucleotide Exchange Factor GBF1. *Mol Biol Cell.* 2003;14(February):2559-2569. doi:10.1091/mbc.E02.
65. Eimer S, Gottschalk A, Hengartner M, et al. Regulation of nicotinic receptor trafficking by the transmembrane Golgi protein UNC-50. *EMBO J.* 2007;26(August):4313-4323. doi:10.1038/sj.emboj.7601858.
66. Haugstetter J, Blicher T, Ellgaard L. Identification and characterization of a novel thioredoxin-related transmembrane protein of the endoplasmic reticulum. *J Biol Chem.* 2005;280(9):8371-8380. doi:10.1074/jbc.M413924200.
67. Martin RJ, Robertson AP, Buxton SK, Beech RN, Charvet CL, Neveu C. Levamisole receptors: A second awakening. *Trends Parasitol.* 2012;28(7):289-296. doi:10.1016/j.pt.2012.04.003.
68. Jensen M, Hoerndli FJ, Brockie PJ, et al. Wnt signaling regulates acetylcholine

- receptor translocation and synaptic plasticity in the adult nervous system. *Cell*. 2012;149(1):173-187. doi:10.1016/j.cell.2011.12.038.
69. Pinan-Lucarré B, Tu H, Pierron M, et al. *C. elegans* Punctin specifies cholinergic versus GABAergic identity of postsynaptic domains. *Nature*. 2014;511(7510):466-470. doi:10.1038/nature13313.
70. Copits BA, Robbins JS, Frausto S, Swanson GT. Synaptic targeting and functional modulation of GluK1 kainate receptors by the auxiliary NETO proteins. 2011;31(20):7334-7340. doi:10.1523/JNEUROSCI.0100-11.2011.Synaptic.
71. Gally C, Eimer S, Richmond JE, Bessereau J-L. A transmembrane protein required for acetylcholine receptor clustering in *C. elegans*. 2004;72(2):181-204. doi:10.1038/nature13314.A.
72. Gendrel M, Rapti G, Richmond JE, Bessereau J-L. A secreted complement-control-related protein ensures acetylcholine receptor clustering. *Nature*. 2009;461(7266):992-996. doi:10.1038/nature08430.
73. Rapti G, Richmond J, Bessereau J-L. A single immunoglobulin-domain protein required for clustering acetylcholine receptors in *C. elegans*. *EMBO J*. 2011;30(4):706-718. doi:10.1038/emboj.2010.355.
74. Richmond J. Synaptic function. *WormBook*. 2005:1-14. doi:10.1895/wormbook.1.69.1.
75. Zuryn S, Le Gras S, Jamet K, Jarriault S. A strategy for direct mapping and

- identification of mutations by whole-genome sequencing. *Genetics*. 2010;186(1):427-430. doi:10.1534/genetics.110.119230.
76. Minevich G, Park DS, Blankenberg D, Poole RJ, Hobert O. CloudMap: A cloud-based pipeline for analysis of mutant genome sequences. *Genetics*. 2012;192(4):1249-1269. doi:10.1534/genetics.112.144204.
77. Ahringer. Reverse genetics. *WormBook*. 2006:1-43. doi:10.1895/wormbook.1.47.1.
78. Flibotte S, Edgley ML, Chaudhry I, et al. Whole-genome profiling of mutagenesis in *Caenorhabditis elegans*. *Genetics*. 2010;185(2):431-441. doi:10.1534/genetics.110.116616.
79. Sancar F, Touroutine D, Gao S, et al. The dystrophin-associated protein complex maintains muscle excitability by regulating Ca²⁺-dependent K⁺ (BK) channel localization. *J Biol Chem*. 2011;286(38):33501-33510. doi:10.1074/jbc.M111.227678.
80. Clapham DE. Calcium Signaling. *Cell*. 2007;131(6):1047-1058. doi:10.1016/j.cell.2007.11.028.
81. Séguéla P, Wadiche J, Dineley-Miller K, Dani J a, Patrick JW. Molecular cloning, functional properties, and distribution of rat brain alpha 7: a nicotinic cation channel highly permeable to calcium. *J Neurosci*. 1993;13(2):596-604.
82. Broide RS, Leslie FM. The alpha7 nicotinic acetylcholine receptor in neuronal plasticity. *Mol Neurobiol*. 1999;20(1):1-16. doi:10.1007/BF02741361.

83. Seo MD, Enomoto M, Ishiyama N, Stathopoulos PB, Ikura M. Structural insights into endoplasmic reticulum stored calcium regulation by inositol 1,4,5-trisphosphate and ryanodine receptors. *Biochim Biophys Acta - Mol Cell Res.* 2014;1853(9):1980-1991. doi:10.1016/j.bbamcr.2014.11.023.
84. Gehlert S, Bloch W, Suhr F. Ca²⁺-dependent regulations and signaling in skeletal muscle: From electro-mechanical coupling to adaptation. *Int J Mol Sci.* 2015;16(1):1066-1095. doi:10.3390/ijms16011066.
85. Stammers AN, Susser SE, Hamm NC, et al. The regulation of sarco (endo) plasmic reticulum. 2015;12(January):1-12.
86. Francis MM, Evans SP, Jensen M, et al. The Ror receptor tyrosine kinase CAM-1 is required for ACR-16-mediated synaptic transmission at the C. elegans neuromuscular junction. *Neuron.* 2005;46(4):581-594. doi:10.1016/j.neuron.2005.04.010.
87. Hoon Cho J, Bandyopadhyay J, Lee J, Park CS, Ahnn J. Two isoforms of sarco/endoplasmic reticulum calcium ATPase (SERCA) are essential in Caenorhabditis elegans. *Gene.* 2000;261(2):211-219. doi:10.1016/S0378-1119(00)00536-9.
88. Zwaal RR, Van Baelen K, Groenen JT, et al. The sarco-endoplasmic reticulum Ca²⁺ ATPase is required for development and muscle function in Caenorhabditis elegans. *J Biol Chem.* 2001;276(47):43557-43563. doi:10.1074/jbc.M104693200.

89. Klarsfeld A, Laufer R, Fontaine B, Devillers-Thierry A, Dubreuil C, Changeux JP. Regulation of muscle AChR alpha subunit gene expression by electrical activity: involvement of protein kinase C and Ca²⁺. *Neuron*. 1989;2(3):1229-1236. doi:0896-6273(89)90307-3 [pii].
90. Altioek N, Changeux JP. Electrical activity regulates AChR gene expression via JNK, PKC?? and Sp1 in skeletal chick muscle. *FEBS Lett*. 2001;487(3):333-338. doi:10.1016/S0014-5793(00)02311-5.
91. Walke W, Staple J, Adams L, Gnegy M, Chahine K, Goldman D. Calcium-dependent regulation of rat and chick muscle nicotinic acetylcholine receptor (nAChR) gene expression. *J Biol Chem*. 1994;269(30):19447-19456.
92. Macpherson P. Protein Kinase C and Calcium/Calmodulin-activated Protein Kinase II (CaMK II) Suppress Nicotinic Acetylcholine Receptor Gene Expression in Mammalian Muscle. A SPECIFIC ROLE FOR CaMK II IN ACTIVITY-DEPENDENT GENE EXPRESSION. *J Biol Chem*. 2002;277(18):15638-15646. doi:10.1074/jbc.M109864200.
93. Cohen SM, Boxing L, Tsien RW, Huan M. Evolutionary and functional perspectives on signaling from neuronal surface to nucleus. 2015;73(4):389-400. doi:10.1530/ERC-14-0411.Persistent.
94. Kuhara A, Inada H, Katsura I, Mori I. Negative regulation and gain control of sensory neurons by the *C. elegans* calcineurin TAX-6. *Neuron*. 2002;33(5):751-763. doi:10.1016/S0896-6273(02)00607-4.

95. Gottschalk A, Almedom RB, Schedletzky T, Anderson SD, Yates JR, Schafer WR. Identification and characterization of novel nicotinic receptor-associated proteins in *Caenorhabditis elegans*. *EMBO J*. 2005;24(14):2566-2578. doi:10.1038/sj.emboj.7600741.
96. Bandyopadhyay J, Lee J, Bandyopadhyay A. Regulation of calcineurin, a calcium/calmodulin-dependent protein phosphatase, in *C. elegans*. *Mol Cells*. 2004;18(1):10-16. <http://www.ncbi.nlm.nih.gov/pubmed/15359118>.
97. George SE, Simokat K, Hardin J, Chisholm AD. The VAB-1 Eph receptor tyrosine kinase functions in neural and epithelial morphogenesis in *C. elegans*. *Cell*. 1998;92(5):633-643. doi:10.1016/S0092-8674(00)81131-9.
98. Wang X, Roy PJ, Holland SJ, Zhang LW, Culotti JG, Pawson T. Multiple ephrins control cell organization in *C. elegans* using kinase-dependent and -independent functions of the VAB-1 Eph receptor. *Mol Cell*. 1999;4(6):903-913. doi:10.1016/S1097-2765(00)80220-8.
99. Lisabeth EM, Falivelli G, Pasquale EB. Eph receptor signaling and ephrins. *Cold Spring Harb Perspect Biol*. 2013;5(9):1-20. doi:10.1101/cshperspect.a009159.
100. Lee YM, Beinborn M, McBride EW, Lu M, Kolakowski LF, Kopin AS. The human brain cholecystokinin-B/gastrin receptor: Cloning and characterization. *J Biol Chem*. 1993;268(11):8164-8169.
101. Xiao Z, Jaiswal MK, Deng PY, et al. Requirement of phospholipase C and protein kinase C in cholecystokinin-mediated facilitation of NMDA channel

- function and anxiety-like behavior. *Hippocampus*. 2012;22(6):1438-1450.
doi:10.1002/hipo.20984.
102. Deng P-Y, Lei S. Bidirectional modulation of GABAergic transmission by cholecystokinin in hippocampal dentate gyrus granule cells of juvenile rats. *J Physiol*. 2006;572(Pt 2):425-442. doi:10.1113/jphysiol.2005.104463.
103. Dufresne M, Seva C, Fourmy D. Cholecystokinin and gastrin receptors. *Physiol Rev*. 2006;86(3):805-847. doi:10.1152/physrev.00014.2005.
104. Essmann CL, Martinez E, Geiger JC, et al. Serine phosphorylation of ephrinB2 regulates trafficking of synaptic AMPA receptors. *Nat Neurosci*. 2008;11(9):1035-1043. doi:10.1038/nn.2171.
105. Henderson JT, Georgiou J, Jia Z, et al. The receptor tyrosine kinase EphB2 regulates NMDA-dependent synaptic function. *Neuron*. 2001;32(6):1041-1056. doi:10.1016/S0896-6273(01)00553-0.
106. Dalva MB, Takasu M a, Lin MZ, et al. EphB receptors interact with NMDA receptors and regulate excitatory synapse formation. *Cell*. 2000;103(6):945-956. doi:10.1016/S0092-8674(00)00197-5.
107. Yumoto N, Wakatsuki S, Kurisaki T, et al. Meltrin β /ADAM19 interacting with EphA4 in developing neural cells participates in formation of the neuromuscular junction. *PLoS One*. 2008;3(10).
doi:10.1371/journal.pone.0003322.
108. Ng D, Pitcher GM, Szilard RK, et al. Neto1 is a novel CUB-domain NMDA

receptor-interacting protein required for synaptic plasticity and learning.
PLoS Biol. 2009;7(2):0278-0300. doi:10.1371/journal.pbio.1000041.

109. Janssen T, Meelkop E, Lindemans M, et al. Discovery of a cholecystokinin-gastrin-like signaling system in nematodes. *Endocrinology*. 2008;149(6):2826-2839. doi:10.1210/en.2007-1772.

110. King JR, Nordman JC, Bridges SP, Lin M-K, Kabbani N. Identification and characterization of a G protein-binding cluster in $\alpha 7$ nicotinic acetylcholine receptors. *J Biol Chem*. 2015;290(33):jbc.M115.647040. doi:10.1074/jbc.M115.647040.

VITA

Ashley A. Martin

University of Illinois Chicago
Department of Biological Sciences
Molecular, Cellular, and Developmental Biology
840 W. Taylor Street, SEL 4311
Chicago, IL 60608
312-996-5190
Amarti7@uic.edu

Current Position

Doctoral Candidate, University of Illinois Chicago
Advisor: Dr. Janet Richmond

Education

B.S. Biology, Chemistry minor, 2008
University of Illinois Chicago

Honors, Awards

2015- Finalist, UIC Image of Research Competition
2012- Teaching Excellence Award
2008- University of Illinois Chicago Dean's List
2008- Awarded Athletic Academic Honor Roll
2005- Initiated as a member of Phi Eta Sigma National Honor Society at UIC
2004- University of Illinois Chicago Dean's List
2004- Received certificate for Outstanding Academic Performance from UIC
2004-2008 - Received Collegiate Full Scholarship for Volleyball at UIC

Publications

Szi-Chieh Yu, Susan M. Klosterman, **Ashley A. Martin**, Elena O. Gracheva, and Janet E. Richmond (2013). Differential roles for Snapin and Synaptotagmin in the synaptic vesicle cycle. **PLOS ONE** 2013;8,2.
Subei, O., Hunt, C., Kosalka, M., **Martin, A.**, Buhse Jr., H. E., Werlin, R., Hamilton, E., and Orias, E. (2008). Microarray Analysis of the Polymorphic Ciliate, *Tetrahymena vorax* (Ciliophora: Tetrahymenidae). **Transactions of the Illinois State Academy of Science Supplement** 101, 69.

Other Presentations and Posters

"Regulation of the nicotinic acetylcholine receptor ACR-16" 2015, Poster, 20th International *C. elegans* Meeting, Los Angeles, CA
"Regulation of the nicotinic acetylcholine receptor ACR-16" 2015, Poster, Michigan *C. elegans* Meeting, Grand Rapids, Michigan

Other Presentations and Posters (cont.)

“Regulation of the nicotinic acetylcholine receptor ACR-16” 2014, Poster, *C. elegans* Neuronal Development, Synaptic Function & Behavior Topic Meeting, Madison, Wisconsin

“Regulation of the nicotinic acetylcholine receptor ACR-16” 2013, Poster, 19th International *C. elegans* Meeting, Los Angeles, CA

“Screening for ACR-16 clustering mutants” 2011, Poster, 18th International *C. elegans* Meeting, Los Angeles, CA

“MOLO-1: a novel acetylcholine receptor-associated protein that modulates cholinergic transmission at neuromuscular junctions in *C. elegans*” 2010, Presentation, Neuronal Function, Synaptic Development, and Behavior *C. elegans* Topic Meeting, Madison, WI.

“Characterization of *C. elegans* snapin mutants” 2009. Poster, 17th International *C. elegans* Meeting, Los Angeles, CA and Neuroscience 2009, Chicago, IL.

“Microarray analysis of the polymorphic ciliate, *Tetrahymena vorax*” 2008, Poster, UIC Student Research Forum, Chicago, IL.

Teaching Positions

Teaching Assistant, University of Illinois Chicago

Biology of Cells and Organisms – 2008

Microbiology Laboratory – Spring 2011 through August 2014

Expertise

C. elegans genetics – creation of novel worm strains, forward genetic screens, reverse genetic screens

C. elegans behavioral assays – aldicarb/dylox sensitivity, thrashing assays, head tap assays, defecation assays, body bend assays

Confocal imaging

Gene cloning – creation of transgenic *C. elegans* strains using the Gateway system

Immunohistochemistry

Western blots

Microinjection

Microdissection of *C. elegans*

Undergraduate Mentorship

Dharati Desai – *C. elegans* strain maintenance, microinjection

Davis Bhagat – *C. elegans* strain maintenance

Yesha Patel – Behavioral assays, western blots, *C. elegans* genetics, confocal imaging

Nisha Patel – *C. elegans* strain maintenance

Sicha Chantaprasopsuk – Confocal imaging

Janki Majithia - Immunohistochemistry, confocal imaging, *C. elegans* genetics

Juan Jose Apiz-Saab – *C. elegans* genetics, behavioral assays, confocal imaging

Kourosh Yazdani – *C. elegans* genetics, behavioral assays, confocal imaging

Community Outreach

Chicago Brain Bee Laboratory Representative – February 2015

Science Fair judge for Lincoln Park High School, Chicago – December 2014

Member of UIC Green Labs Committee – May 2013 through May 2015

Volunteer at Expanding Your Horizons Conference, Chicago – March 2013

Science Fair judge for Lake Shore School, Chicago – February 2013

Undergraduate student mentor for Women in Science and Engineering, UIC Chapter
– Fall 2010

Professional Societies

Member- Genetics Society of America

Member- Society for Neuroscience

Member- Illinois State Academy of Science

Member– Association for Women In Science